Photocatalytic Reactions on Quantum-sized Semiconductor Colloids:

Photoinitiated Polymerization of Vinylic Monomers,

Formation of Hydrogen Peroxide and Organic Peroxides,

Oxidation of Carboxylic Acids, and Synthesis of Humic-like Material

Thesis by Amy Jo Hoffman

In Partial Fulfillment of the Requirements

for the Degree of

Doctor of Philosophy

Californial Institute of Technology

Pasadena, California

1993

(Defended April 2, 1993)

"Licht!" -Claudius Kormann
"Mehr Licht!" -Goethe

"Nature and Nature's laws lay hid in night: God said 'Let Photochemistry be!' and all was light." -Amy Hoffman, after Alexander Pope

"There prevails among men of letters an opinion that all appearance of science is particularly hateful to women." - Johnson (1709-1784)

"It is the great beauty of our science, CHEMISTRY, that advancement in it, whether in a degree great or small, instead of exhausting the subjects of research, opens the doors to further and more abundant knowledge..." -Faraday

Acknowledgements

I would like to express my deepest gratitude and sincere appreciation to all the people who have provided help and friendship to me over the years. First of all, I thank my parents, who have always offered their love and support and encouraged me to follow my dreams--no matter how far away I had to go to realize them. I am extremely grateful to my advisor, Michael Hoffmann, for his encouragement, advice, and guidance throughout these four and a half years of research at Caltech. I am grateful to German (Jimmy) Mills for starting me out on the right foot and teaching me about Q-sized semiconductors. I appreciate the enthusiasm and helpful discussions provided by the many members of the Hoffmann group.

I would also like to thank my co-advisor, Harry Gray, for his encouragement and insight, along with the other members of my examination committee: Nate Lewis and Robert Grubbs. I enjoyed the opportunity to learn about aquatic chemistry and transport from Jim Morgan and Norman Brooks.

Elaine Granger, Dian Buchness, Joe Fontana, Jess Miller, Louis Borbon, Gabor Faludi, Guy Duremberg, and Rayma Harrison deserve special thanks for both their expert abilities to get things done and for their friendly attitudes about doing it.

There are a number of students at Caltech who have provided not only terrific scientific insight and ideas, but also who have provided personal friendship and encouragement. I cannot begin to thank them enough, for they were the people who made my time at Caltech so memorable. They include Katherine Widdowson, Ann Miller, George Komatsoulis, Howell Yee, Ken Graham, Mike Youngquist, Mark Schlautman, and Beth Carraway. In particular, I am especially grateful for Bryan Balazs, who has shown

me the meaning of true friendship, and who literally kept me going by repairing my '73 Fiat Spider.

Other friends outside of Caltech are to be thanked for their assistance in opening my eyes to life besides science. They include Nick and Becky Dimmock, Darcy and Connie Stewart, Andrea Watts, and Mike Konigsberg. I offer special thanks to our "adopted" parents, Scotty and Muggins, who have extended such a warm welcome to their new neighbors.

Lastly, I am most grateful for the love and support of my husband and my best friend, Greg Kiefer. He has been a constant source of encouragement, faith, and understanding (not to mention the chocolate chip cookies and homemade bread.) Thank you, Greg, for putting the laughter in my life!

Abstract

Ultrasmall semiconductor particles (diameters 1-10 nm) of CdS, ZnO, and TiO_2 have been synthesized. These particles exhibit the quantum-size effect, which is characterized by a shift of the absorption onset (i.e., bandgap energy) from the visible region for the bulk material to the UV for ultrasmall diameters. The ability of these colloids to photocatalyze various chemical transformations was investigated.

Semiconductors were found to be efficient photoinitiators of polymerization of vinylic monomers. Q-sized colloids demonstrated significantly higher rates of photopolymerization than their bulk-sized counterparts. The semiconductor photoinitiation efficiencies were correlated to the reduction potentials of the conduction band electrons. The rates of polymerization were found to depend upon the solvent nature, the monomer and initiator concentrations, and the incident light intensity. The polymerization reaction proceeds via a mechanism involving anionic initiation by conduction band electrons. The valence band holes, which are formed upon illumination, are scavenged by the solvent. The observed rate of polymerization increased proportionally to the square root of the incident light intensity; this functional dependence arises from the second-order termination reactions of the free-radical intermediates.

Aqueous, oxygenated suspensions of quantum-sized ZnO particles with added hole scavengers produced steady-state H_2O_2 concentrations as high as 2 mM upon bandgap illumination. Isotopic labeling experiments demonstrated that H_2O_2 was produced via the reduction of adsorbed oxygen by conduction band electrons. The quantum yields followed an inverse square-root dependency on absorbed light intensity. Quantum yields as high as 30% were obtained. The quantum yield of H_2O_2 production increased as the Q-sized particle diameter decreased.

Q-sized ZnO particles also photocatalyzed the oxidation of acetate, formate, and glyoxylate. The observed product distributions were discussed regarding direct oxidation by the valence band holes or indirect oxidation by surface-bound hydroxyl radical intermediates. In illuminated semiconductor suspensions, radical intermediates react with the semiconductor surface, forming trapped species which are further oxidized either by semiconductor holes or by self-injection of a second electron into the conduction band.

In the final investigation of semiconductor photocatalyzed reactions, humic-like substances were formed in illuminated aqueous Q-sized suspensions containing catechol or gallic acid. Their formation was attributed to polymerization-type reactions initiated by $OH^{\bullet}$ radicals.

Table of Contents

Chapter 1

Prologue

Photoinduced reactions have been an area of growing interest over the last 22 years, due to the stimulus of the energy crisis and the promise of direct photoelectrochemical conversion of radiant energy into chemical energy (1). Some confusion exists in the literature as to the definition of these photoreactions as photocatalyzed or photosensitized. Figure 1 shows the energetic requirements for a photosensitized and a photocatalyzed reaction (2). In a photocatalyzed reaction, the overall reaction is exothermic and in principle only kinetically retarded. Semiconductor particles are considered photocatalysts for a desired reaction only if the products are formed with a high specificity and the semiconductor remains unchanged at the end of the reaction. In addition, electrons and/or holes generated by absorption of photons with an energy exceeding the semiconductor bandgap energy must be required for the process, and no net photon energy can be stored in the final products. In contrast, a photosensitized reaction is one in which the overall reaction is endothermic. This is the principle reaction type involved in solar energy storage.

While progress has been made in regards to the initial goal of solar energy storage (3), recently alternative uses of photocatalysis have also gained importance, i.e., in new synthetic routes and in the degradation of organic pollutants (4). For example, Fox et al. demonstrated the oxidation of 1,1diphenylethylene using TiO_2 as photocatalyst produces benzophenone as the sole product at complete conversion; whereas electrochemical oxidation of 1,1diphenylethylene at a Pt electrode produces as major product the cationic dimer, 1,1,4,4tetraphenylbutane (5). Pelizzetti et al. have demonstrated the complete photodegradation of 20 ppm of the herbicide atrazine in 30 minutes using 0.1 g/l TiO_2 and solar illumination (6). Although these studies have demonstrated the viabilty of using semiconductors as photocatalysts, little information has been obtained regarding the accurate efficiency and mechanism of the reactions. This is mainly due to the high degree of light scattering of the semiconductor.

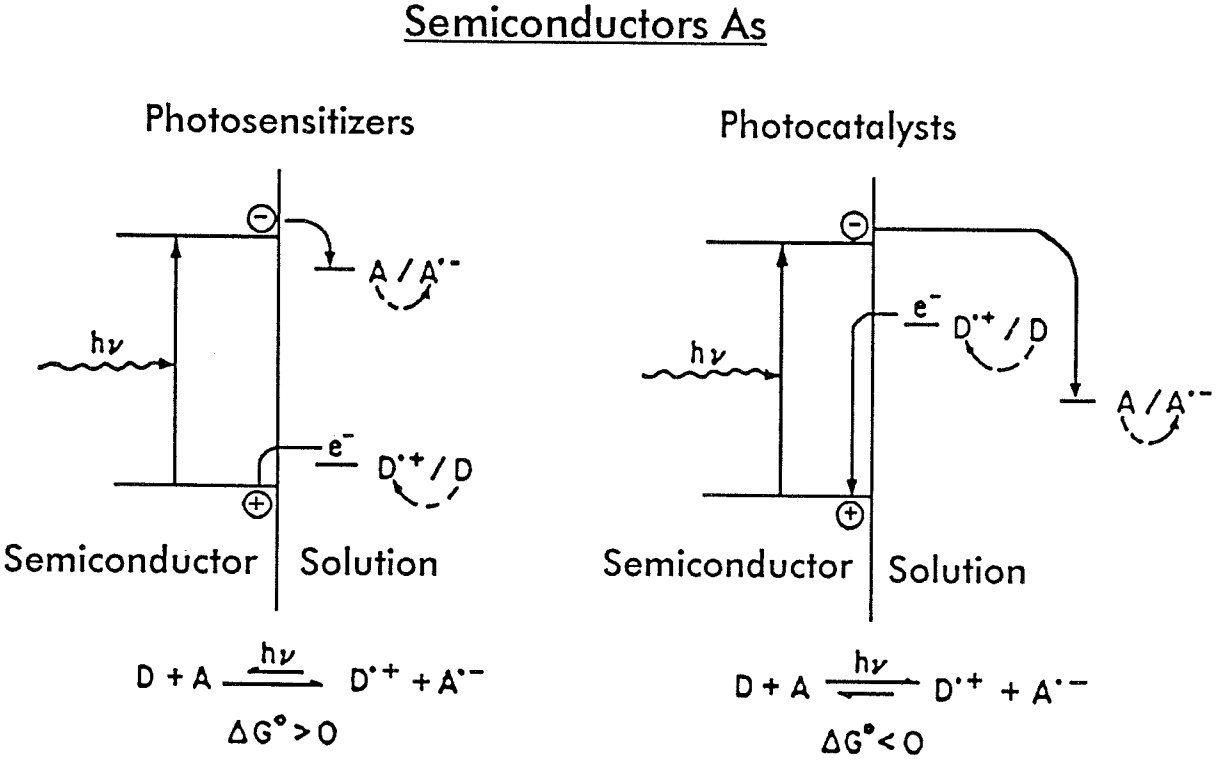

Figure 1: Energetic conditions for the definition of semiconductor colloids as photosensitizers or photocatalysts.

Recent advances in the synthesis of ultrasmall semiconductor particles has opened a new realm of exploration (7). These ultrasmall particles of 1-10 nm diameters exhibit the "quantum size" (Q-size) effect, which is defined as an increase in bandgap energy with decreasing particle size. While interesting in themselves from a solid state physics standpoint, the Q-sized particles have several advantages over their bulk-sized counterparts in regards to photocatalysis. Due to their small size, they exhibit negligible light scattering, which facilitates the measurements of accurate quantum yields. In addition, fast optical detection of intermediates is possible. Finally, the high surface area to volume ratios can enhance the rates of reactions which occur via surface states. Thus, the use of Q-sized semiconductors allows new insight into heterogeneous photochemistry. The overall goal of this thesis is to explore the efficiency of utilizing quantum-sized semiconductors as photocatalysts, to compare with bulk-sized semiconductors, and to determine the mechanism of their reactions. The reactions studied are in the category of the latter uses of photocatalysts, i.e., the development of new or alternative synthetic routes and the photodegradation of organic pollutants.

This thesis is organized into eight chapters, each of which may be read independently. This chapter introduces the concept of photocatalysis and its applications. The second chapter provides the necessary background information regarding the theory of quantum sized semiconductors, and their surface chemistry and reaction dynamics. The third chapter discusses the synthesis of Q-sized CdS, and its efficiency as a photoinitiator of polymerization of vinylic monomers. The fourth chapter examines the mechanism of the photoinitiation of polymerization of methyl methacrylate by Q-sized ZnO. The fifth chapter investigates the photocatalytic formation of peroxides, again using Q-sized ZnO. In compliment to the fifth chapter, the sixth chapter details the degradation of organic acids using Q-sized ZnO. The seventh chapter explores the possible formation of humic-like substances using Q-sized ZnO as a photocatalyst. The eighth chapter

summarizes the results of this research, discusses the practical viability of Q-sized semiconductor photocatalysis, and concludes with some suggestions for future research.

References

1. a) Norris, J. R., Jr.; Meisel, D. "Photochemical Energy Coversion: Proceedings of the 7th International Conference on Photochemical Conversion and Storage of Solar Energy," Elsevier Science Publishing Co.: New York, **1989**, 284. b) Boer, K. W., Ed. "Advances in Solar Energy," Plenum Press: New York, **1990**, Vol. 6, 394. c) Connolly, J. S., Ed. "Photochemical Conversion and Storage of Solar Energy," Academic Press: New York, **1981**, 131. d) Nozik, A. J. *Ann Rev. Phys. Chem.* **1978**, *29*, 189.

2. Pelizzetti, E.; Schiavello, M., Eds. "Proceedings of the 8th International Conference on Photochemical Conversion and Storage of Solar Energy," Elsevier Science Publishing Co.: New York, **1990,** 189.

3. O'Regan, B.; Gratzel, M. *Nature*, **1991**, *353*, 737.

4. a) Serpone, N.; Pelizzetti, E., Eds. "Photocatalysis: Fundamentals and Applications," Wiley & Sons: New York, **1989**, 603. b) Pelizzetti, E., Serpone, N., Eds. "Homogeneous and Heterogeneous Photocatalysis," Nato ASI Series C, Vol. 174, Reidel Publishing: Dordrecht, **1986**, 629. c) Ollis, D. F.; Pelizzetti, E.; Serpone, N. *Environ. Sci. Technol.*, **1991**, *25(9)*, 1523.

5. Fox, M. A. "Topics in Current Chem., Vol 142," Springer-Verlag: Berlin, **1987**, 71.

6. Pelizzetti, E. *Environ. Sci. Technol.*, **1990**, *24*, 1559.

7. Henglein, A. *Chem. Rev.*, **1989**, *89*, 1861.

Chapter 2

Background

In order to better understand the factors which influence the efficiency of Q-sized semiconductors in promoting photoreactions, some background knowledge regarding photocatalysis and semiconductors is presented in this chapter. First, the basic laws of photochemistry regarding the absorption of light and the calculation of quantum yields are reviewed. Then, the following relevant information is provided: 1) a summary of semiconductor band theory as it relates to molecular orbitals and Q-sized semiconductors; 2) a discussion of the thermodynamics of semiconductors, including a section on special considerations for Q-sized semiconductors; 3) a review of the dynamics of semiconductor processes such as the rate of electron-hole recombination and trapping in surface states; 4) a discussion of the surface chemistry of metal oxides in relation to colloid stability, surface complexation, and band edge shifts; 5) and derivations of generalized expressions for photo-induced heterogeneous reaction rates.

Laws of Photochemistry

Since only light which is absorbed by a photocatalytic system can cause chemical change, the rate of absorption is given by the well known Lambert-Beer law (1),

$$A = \log I_0/I = \varepsilon_v C l \qquad (1)$$

where A is the absorbance, I_0 is the incident light intensity, and I is the transmitted light intensity, ε is the molar extinction coefficient (M^{-1} cm^{-1}), C is the concentration in moles per liter, and l is the optical path length in cm. Since $I = I_0\ 10^{-\varepsilon_v C l}$, the amount of light absorbed by the system is given by the expression:

$$I_a = I_0 - I = I_0(1-10^{-\varepsilon_v C l}) \qquad (2)$$

Another useful rule is based on the Stark-Einstein law which states that one quantum of light is absorbed per molecule of absorbing and reacting substance that disappears. This law only applies to low light intensities, i.e., in the absence of lasers and biphotonic processes. To express the efficiency of a photochemical reaction, the quantum yield, Φ, is defined as:

$$\Phi = N_f / N_{abs} \tag{3}$$

where N_f = the number of moles of product formed and N_{abs} = number of moles of photons absorbed. Quantum yields can vary from 10^{-6} to 10^{6}.

Quantum-sized Semiconductor Theory

The physical chemistry of solid-state materials is often discussed in terms of band theory, which at first sight appears to be quite different from molecular orbital theory. However, as recently pointed out by Hoffmann (2), chemical intuition is fundamental to understanding the structures and properties of solid materials, and a "molecular" approach to solid materials can provide insight. As an example, consider a chain of equally spaced H atoms. Increasing the chain length increases the number and splitting of the orbitals in a well known manner as shown in Figure 1. Except for the lowest (and for even numbered chains, the highest) level, the orbitals come in degenerate pairs with the number of nodes increasing with increasing energy. The corresponding solid state approach is based on a process of symmetry adaption called formation of Bloch functions (3). On each lattice point is a basis function and the appropriate symmetry adapted linear combinations are given by:

$$\varphi_k = \Sigma\, e^{ikna}\, X_n \tag{4}$$

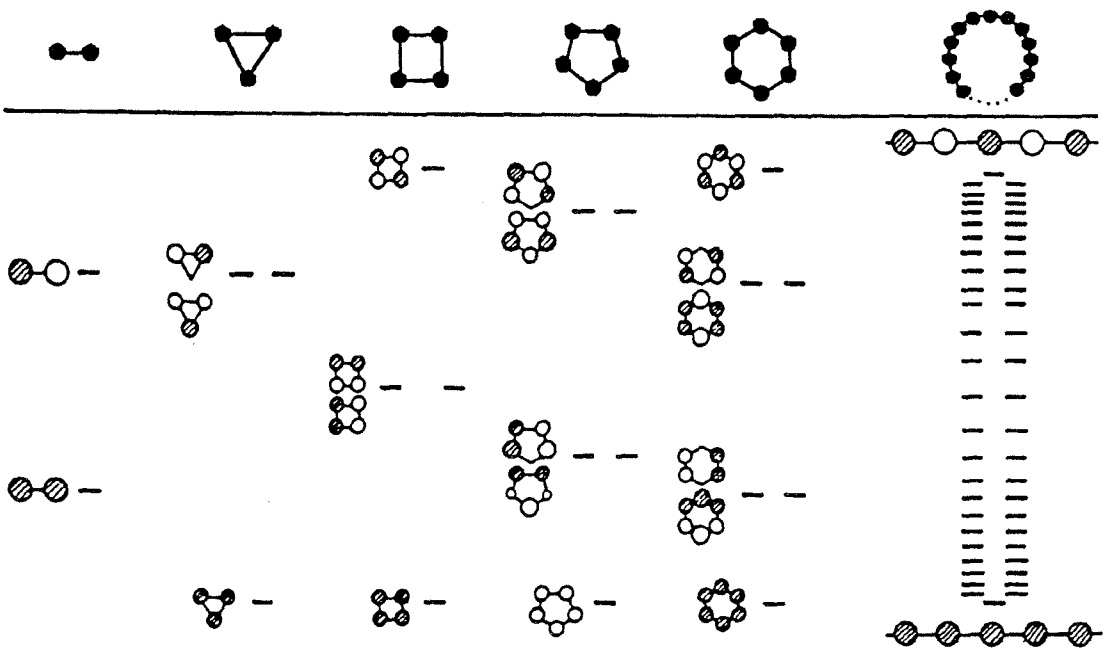

Figure 1: Evolution of molecular orbitals with increasing (hypothetical) H atom ring size.

where a is the lattice spacing and k is an index that labels the irreducible representation. φ_0 is the most bonding wavefunction and $\varphi_{\pi/a}$ is the top antibonding level. k has unique values between $-\pi/a$ and π/a. The total number of k values is identical to the number of translations or alternatively the number of microscopic unit cells in the macroscopic crystal. Thus an orbital diagram with N lines corresponds to an E(k) versus k diagram (Figure 2), which is called a band structure. Another useful diagram is that which shows the density of states, i.e., the number of levels between E and E + dE. The width of a band (the difference in energy between the highest and lowest levels) is determined by the overlap between the interacting orbitals. The flatter the slope of the E(k) versus k diagram, the sharper the "spike" of bands in the density of states diagram. For example, consider the density of states diagram for the rutile form of TiO_2 in Figure 3 (4). The strong Ti-O interaction splits the d metal orbitals into t_{2g} and e_g combinations. The corresponding density of state diagram shows well-separated bands which are essentially localized on either oxygen or titanium atoms, although a small amount of mixing occurs between the Ti e_g and the O(2s) and O(2p) and between the Ti t_{2g} and the O(2p). The O bands at lower energy are bonding and the metal Ti bands are antibonding. In general, semiconductors are characterized by two separated energy bands: a filled low energy valence band and an empty high energy conduction band. The difference in energy between the top of the valence band and the bottom of the conduction band is called the bandgap energy. Semiconductors typically have bandgap energies between 0.1 and 4.0 eV. Excitation of a semiconductor by light with energy greater than the bandgap energy promotes electrons from the valence to the conduction band and leaves a hole in the valence band. The existence of the band gap helps to prevent rapid deactivation of the excited electron hole pairs, which can disappear by recombination.

The electronic structure of very small isolated crystallites is comparible to a zero dimensional quantum well with infinite barriers. The band gap increases from that of the

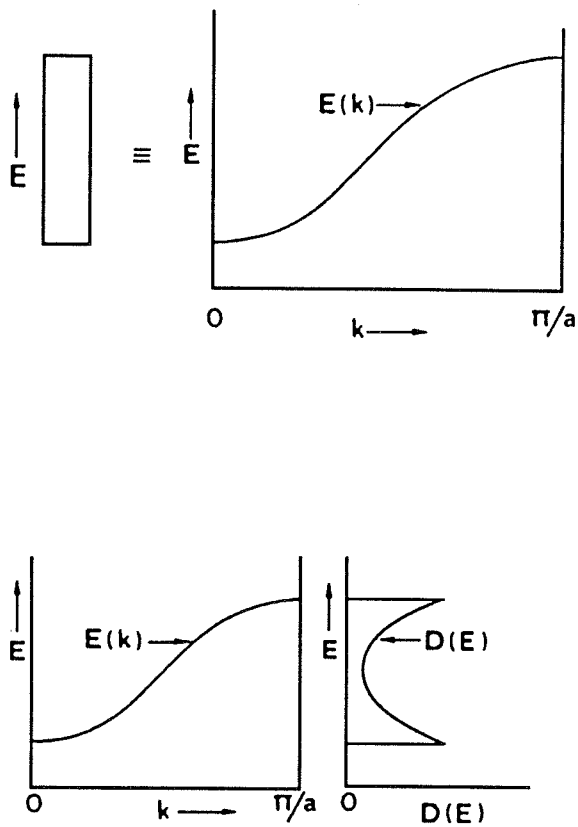

Figure 2: a) Relationship of molecular orbital diagram to band structure. The index k is defined in the preceding text b) Relationship of band structure to density of states diagram.

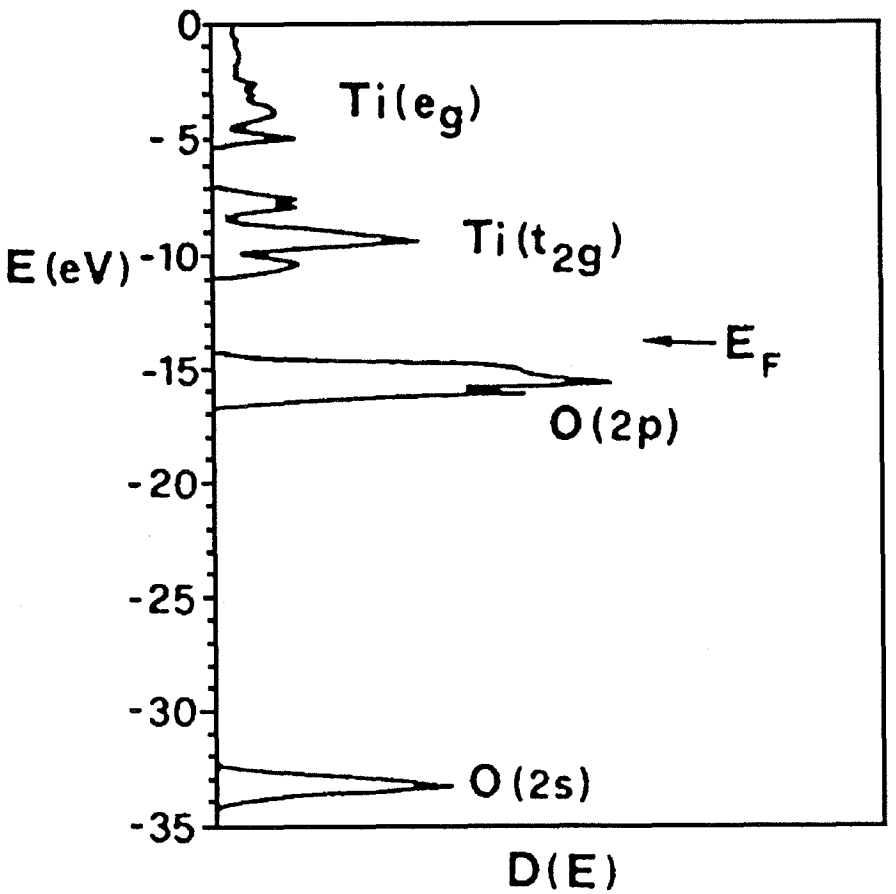

Figure 3: Density of states diagram for rutile-phase TiO_2.

bulk when the crystallite size decreases below a few hundred angstroms. Electrons and holes are confined to the crystallites; therefore, the binding energy of this electron-hole pair (exciton) is increased compared to the band gap of the bulk material. For a crystallite of radius R, the confinement energy becomes comparable to the gap energy for R<100Å. Brus (5) has described quantum mechanical calculations in which the energy for the lowest state can be approximated as

$$E = E_g + h^2/2R^2\,(1/\mu) - 1.8e^2/4\pi\varepsilon\varepsilon_0 R \qquad (5)$$

where E_g is the band gap energy, μ is the reduced mass of the exciton, and R is the radius of the particle, ε is the dielectric constant of the semiconductor, e is the constant of elementary charge, and h is Plank's constant. The first term in equation 5 is the band gap; the second term represents the ground state of a quantum well; and the third term represents a minor Coulomb correction due to small screening in the crystallite. Figure 4 shows the computed energy of the lowest excited state as a function of the radius of the particle. This equation predicts that the energy level of the first excited state increases as the cluster size decreases. Since the quantum size effects are expected to occur when the Bohr radius of the first exciton in the semiconductor becomes commensurate with or larger than that of the particle, the Q-size regime occurs at different particle size ranges for different types of semiconductors. The Bohr radius depends on the dielectric constant and the effective mass of the charge carrier. The most striking example occurs in HgSe particles, where due to the very low effective electron mass, the band gap is strongly dependent on particle size. The band gap energy shifts from 0.3 eV in the bulk-sized material (500 Å diameters) to 3.2 eV in the 30 Å Q-sized particles (6).

An alternative qualitative molecular orbital picture as shown in Figure 5 may also be used to account for the shift in the bandgap (7). The energetic levels split into a filled

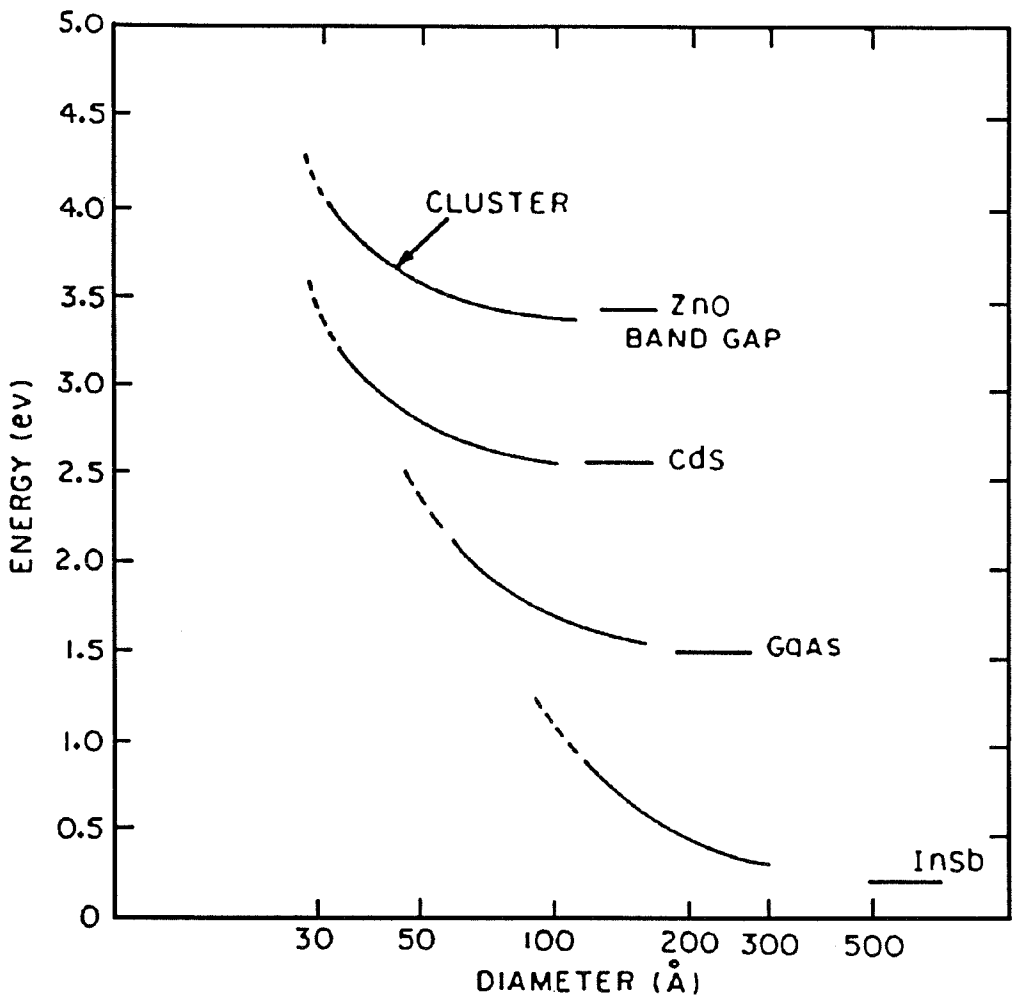

Figure 4: Apparent band gap energy of a semiconductor particle as a function of particle diameter. Energy calculation based on the Brus equation given in preceding text.

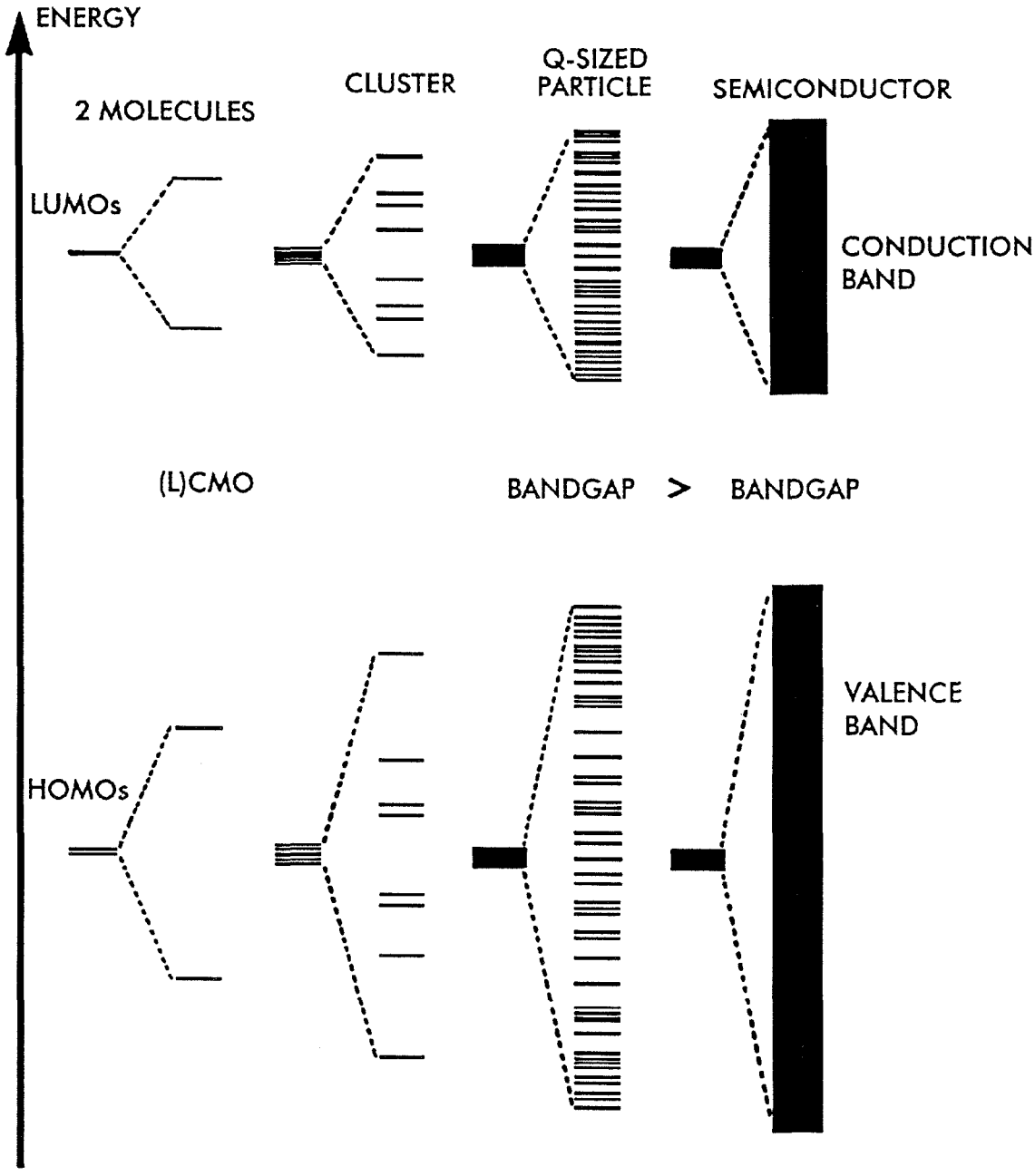

Figure 5: Molecular orbital model of particle growth showing decrease of band gap energy with increasing particle size. LUMOs = Lowest Unoccupied Molecular Orbitals, HOMOs = Highest Unoccupied Molecular Orbitals, (L)CMO = (Linear) Combination of Molecular Orbitals.

and empty region. As the number of contributing MO's increases, the ensemble of energetic levels becomes more dense, leading to the valence and conductance bands in bulk semiconductors. Electronic transitions from the HOMO's to the LUMO's yield the observed absorption spectrum, which is blue shifted for the Q-sized particles.

The absorption spectrum of ZnO during synthesis and particle growth is shown in Figure 6. As the colloid ages, the absorption onset exhibits a bathochromic shift. The fluorescence spectrum also exhibits a red shift with particle growth. The ZnO particles must be smaller than 50 Å before the bandgap shift becomes obvious. Transition probabilities between the MO's are governed by symmetry selection rules, which become increasingly important as the total number of orbitals decreases. This explains the pronounced maximum structure observed in the absorption spectra of very small ZnO clusters, indicating that transitions of narrow energy distribution and high probability occur. An alternate explanation is that the structure is due to higher concentrations of colloids of a given size, due to magic agglomeration numbers. The luminescence maximum at 365 nm closely coincides with the onset of absorption and is assigned as bandgap fluorescence caused by a transition from the lower edge of the conduction band to the upper edge of the valence band. The visible fluorescence is due to trapped electrons tunneling to trapped holes. The intensity of the UV emission increases in the absence of molecular oxygen, while the intensity of the visible emission decreases. The oxygen increases the ratio of visible emission to UV emission by acting as a shuttle to aid conduction band electrons into surface traps (7). The visible fluorescence then results from the tunneling of these trapped electrons into preexisting trapped holes.

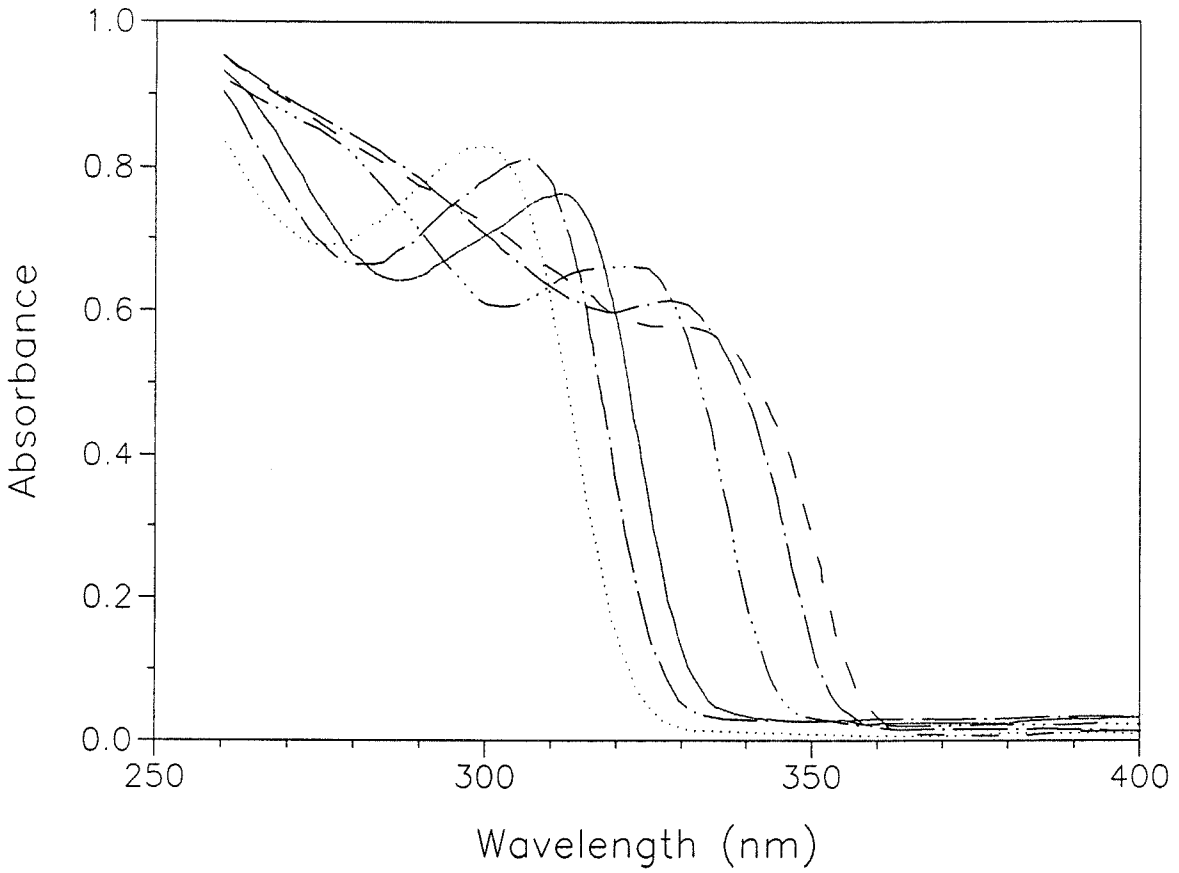

Figure 6: Absorption spectrum of ZnO immediately after synthesis and during particle growth. Isopropanol solvent, 1mM ZnO.

Thermodynamics of Semiconductors

Figure 7 gives the band gaps and band edge positions for a number of semiconductors (8). By comparison of the band edge position with the standard potentials for redox couples on the same energy scale, the thermodynamic limitations for the photoreactions are revealed. For example, to reduce the species in an electrolyte, the conduction band position of the semiconductor (or more precisely, the Fermi level) must be positioned above the relevant redox level. Likewise, to oxidize the species in the electrolyte, the valence band position (Fermi level) must be lower than the relevant redox level. The Fermi level is the chemical potential of the charge carrier in the semiconductor. In an intrinsic (undoped) semiconductor, the number of electrons equals the number of holes and the Fermi level is located halfway between the conduction band and valence band. As the semiconductor is doped with donors, for example interstitial Ti^{4+} ions or oxygen vacancies in the case of TiO_2, the Fermi level moves closer to the conduction band. There is a net excess of electrons over holes, and the material is called an n-type semiconductor. Figure 8 presents the energy vs. position diagram for n-type and p-type semiconductor electrodes (9). In the dark at equilibrium, the chemical potential of the electrons in solution must equal the chemical potential of electrons in the semiconductor, thus the Fermi level and redox level of the solution species are equal. If the Fermi level of the electron in the n-type material is initially above that of the electrons in solution, upon contact of the two phases electrons will flow from the semiconductor to reduce the species in solution. This depletion of conduction band electrons results in excess positive charge near the surface, which results in changes in the electric fields at the interface. The resulting "band bending" indicates the direction that free carriers will migrate in the field.

The region where this curvature exists in the electrode is often referred to as the space charge region. Thus, band bending provides a mechanism for inhibiting the back

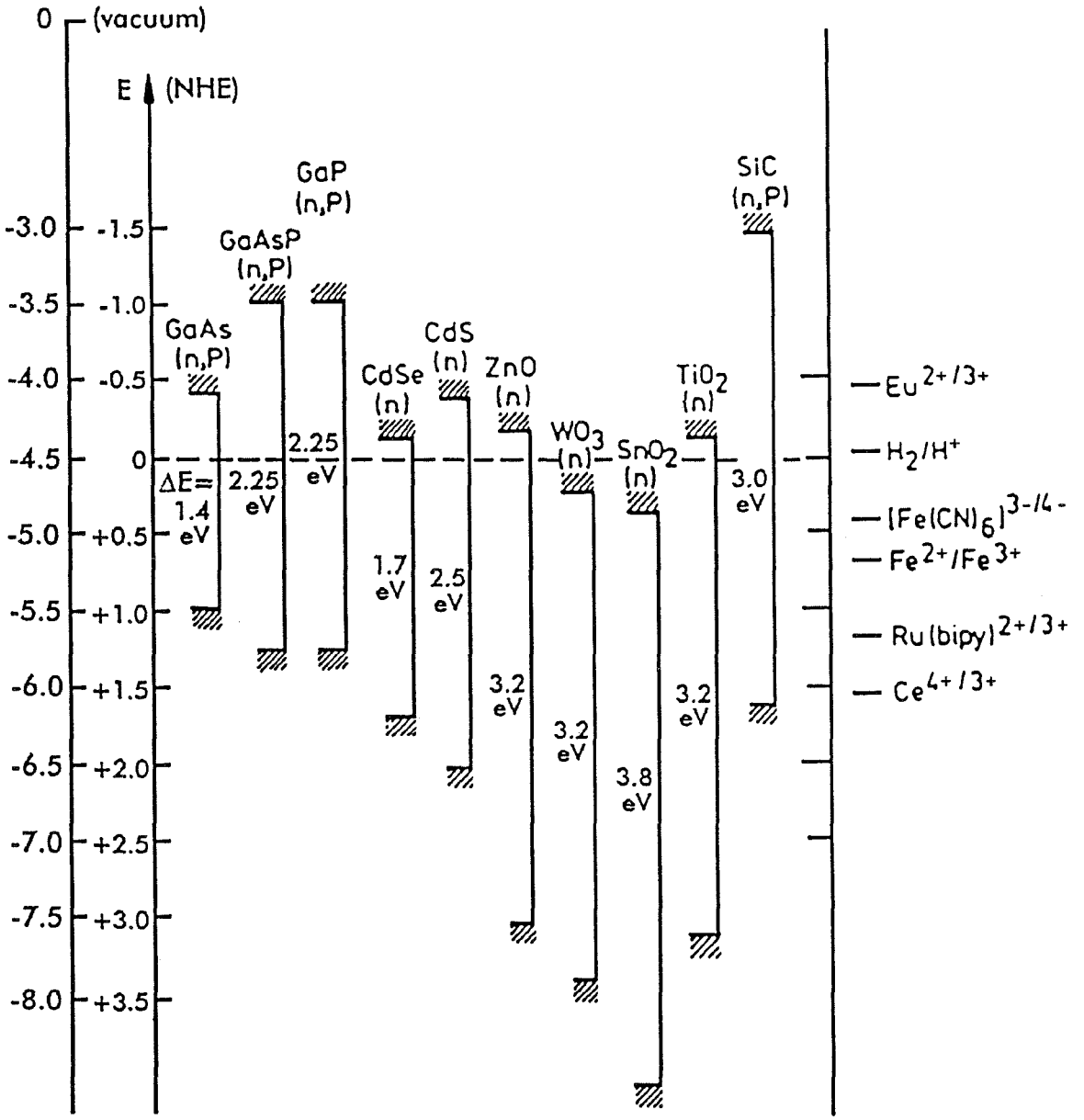

Figure 7: Band gap energies and band edge positions of semiconductors in contact with aqueous electrolyte at pH 1.

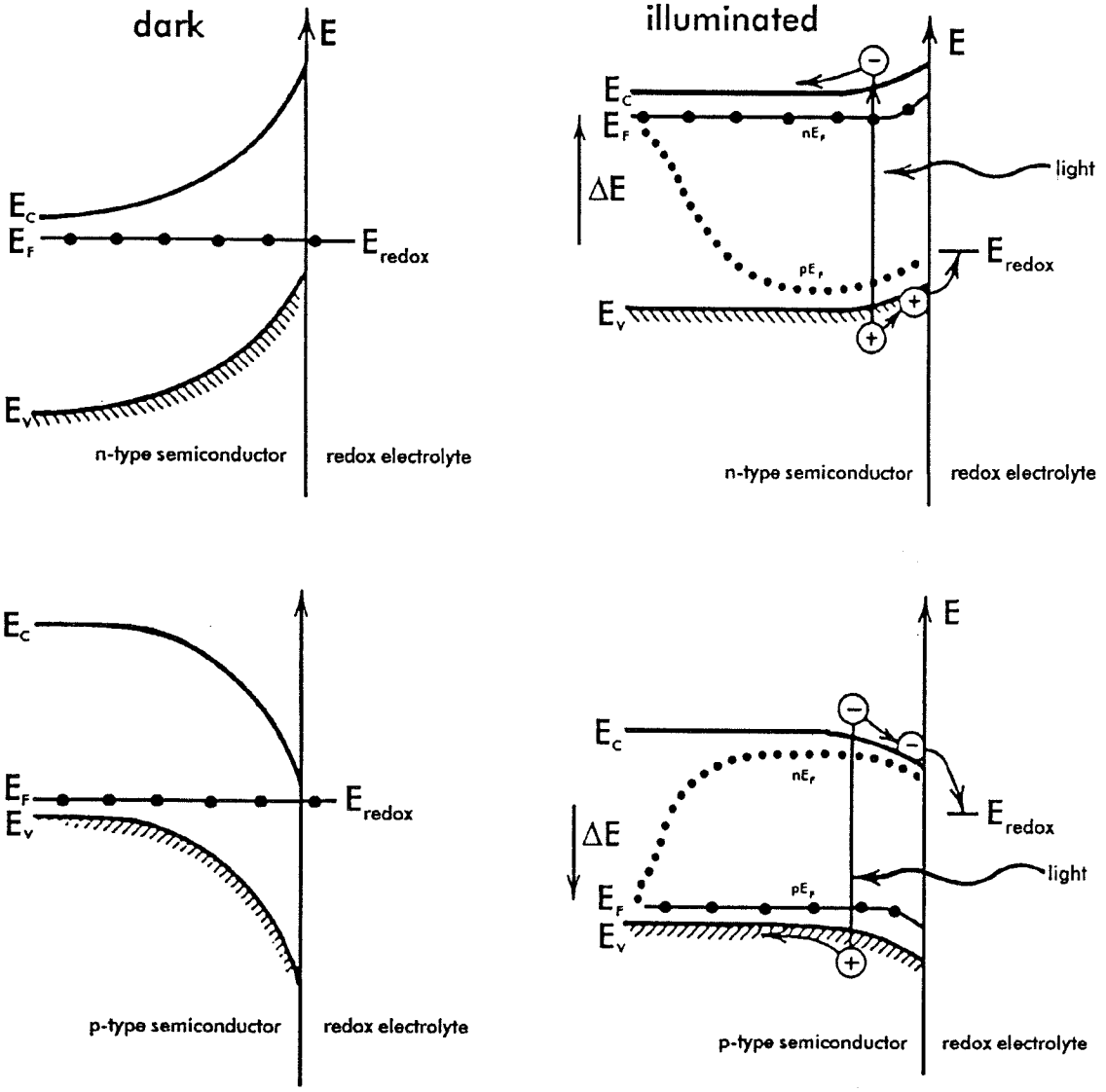

Figure 8: Energy levels and photovoltages at n-type and p-type semiconductor-electrolye interfaces under dark (right) and illuminated (left) conditions.

reaction of energetic redox products at a semiconductor/liquid electrolyte interface. For example, in the n-type semiconductor case discussed above, the majority charge carriers (the electrons) are driven away from the solution, while the minority carriers are driven in the opposite direction. The condition where there is no excess charge associated with the semiconductor and no associated electric field (no band bending) is referred to as the flat-band potential. Under illumination above the bandgap energy of the semiconductor, electrons are excited from the valence band to the conduction band. For an n-type semiconductor, the Fermi level increases and the band bending decreases as shown in Figure 8.

Special considerations for q-sized semiconductors

Due to their small particle dimensions, Q-sized semiconductors represent an unusual case regarding electron transfer at semiconductor-liquid junctions as compared to their bulk phase counterparts. The first distinction is the lack of compartmentalization of the anodic and cathodic processes in a semiconductor particle suspension as compared to a semiconductor electrode/metal electrode cell. Oxidation reactions by valence band holes and reduction reactions by conduction band electrons can occur concurrently in or near the small particle. This phenomenon manifests itself in the experimental observation that appreciable photodegradation of organic pollutants occurs only in the presence of either an efficient hole or electron scavenger, which is adsorbed to the semiconductor surface. The scavenger in these photodegradation reactions is usually oxygen. The role of oxygen is to trap the conduction band electrons as they are produced by illumination, which lowers the electron-hole recombination rate and prevents the buildup of charge as the pollutant is oxidized. Another major difference in Q-sized semiconductors versus bulk semiconductor electrodes is that the average transit time for a charge carrier from the interior of the particle to the surface is greatly reduced. For example, in colloidal TiO_2

with a radius of 6 nm, the average transit time is 3 psec (10). In addition, for particles exhibiting Q-size effects, the wave function of the charge carrier spreads over the whole semiconductor cluster, and it does not have to undergo diffusional displacement to accomplish reactions with species present at the surface.

Higher surface area-to-volume ratios (A/V) are another feature of q-sized semiconductors, which promote highly effective surface concentrations of adsorbed redox species. This effect, combined with low laser intensities and/or short excitation times, allows for the observation of fast electron transfer without diffusion limitations. Gratzel et al. attributed the fast oxidation of SCN^- on Q-sized TiO_2 (< 40 ps risetime) to surface adsorbed SCN^- (11). Another unusual facet of Q-sized semiconductors is the lack of appreciable band bending. The equation for the potential distribution in a spherical semiconductor particle has been derived by Albery and Bartlett using a linearized Poisson Boltzmann equation (12). The total potential drop within a Q-sized particle is given by the equation:

$$\Delta\phi_0 = kT/6e(r_0/L_D)^2 \qquad (6)$$

Using this equation with a 6 nm radius TiO_2 particle, Gratzel (13) calculated that an ionized donor impurity concentration of 5×10^{19} cm^{-3} was neccessary to obtain a 50 mV potential drop. Since undoped TiO_2 colloids have a much smaller carrier concentration (i.e., 1×10^{18} cm^{-3}) , the band bending within the particles is negligibly small. This implies for n-type TiO_2 that if the minority carriers are depleted rapidly from a Q-sized semiconductor in solution, the electrical potential difference caused by the transfer of charge from the semiconductor to the surface has to drop in the Helmholtz layer (neglecting diffuse layer contributions). As a result, the position of the conduction band edge of the semiconductor particles will shift negative. Bard et al. (14) have observed this

effect in small colloidal particles of FeS_2, CdS, WO_3, and TiO_2. When q-sized particles of transition metal sulfides are illuminated in the presence of hole scavengers, a blue shift of the absorption spectrum is observed. This so-called Burstein shift is caused by excess charge on the small particle and has been explained by a band filling model or alternatively by the polarization of subsequently formed excitons.

Dynamics of Charge Carrier Trapping and Recombination

The recombination rate plays a crucial role in photocatalytic reactions on semiconductor particles. Experiments using a frequency tripled Nd laser pulse of about 30 ps duration have been able to detect via optical absorption trapped electrons in colloidal 120 Å diameter TiO_2 particles (15). The spectrum of the trapped electron developed within the leading edge of the laser pulse, indicating that the trapping time of the electron was less than 30 ps. The electron absorption decayed due to recombination with valence band holes. The rate of recombination depends upon the illumination intensity. At low laser flux, i.e., low initial occupancy by electron/hole pairs, recombination follows a first order-rate law; however, at high laser flux the recombination follows an approximate second order-rate law. The electron/hole pair was observed to have a 30 ns lifetime in 120 Å diameter TiO_2, which gives a recombination rate coefficient of 3.2×10^{-11} cm^3 s^{-1}. At low laser flux, hole trapping at the surface can compete with the recombination. Under basic conditions, the rate constant for hole trapping by surface hydroxyl groups was measured at 4×10^5 s^{-1}. Chemically, a trapped electron near the particle surface can be described as Ti^{IV}.....e^- or a Ti^{3+} center. The trapped hole can be viewed as the radical Ti^{IV}-OH_s·. Illumination of ZnO particles in the presence of a hole scavenger such as isopropanol creates excess surface trapped electrons. In the presence of oxygen, those electrons are removed at a rate of 3.2×10^6 M^{-1} s^{-1} for 17 Å diameter particles, and a rate of 6.4×10^4 M^{-1} s^{-1} for 40 Å diameter particles (16). Both electrons and holes can

be injected into particles. For example, Kira et al. (17) have used transient grating techniques to detect an oxidized intermediate of isopropanol formed on single crystal TiO_2 at high anodic potential. The lifetime of the intermediate was only 100 ns, as the intermediate species quickly decayed by injecting electrons into the conduction band. In another study by Rajh et al. (18), strongly oxidizing radicals, which were formed by pulse radiolysis of aqueous TiO_2 colloids, injected holes into the colloid at a rate close to diffusion controlled. When OH radicals were formed by pulse radiolysis, a transient OH radical adduct was formed with the semiconductor, which completely disappeared when t-butyl alcohol was added as an OH radical scavenger.

Surface Chemistry of Semiconductors

To give an idea of the importance of the surface area in Q-sized semiconductor reactions, the geometrical surface area can be calculated based on the particle diameters from TEM and assuming a spherical shape for the particle. For a typical Q-sized TiO_2 particle of diameter 24 Å, using the density of anatase, 3.9 g/cm^3, the number of TiO_2 molecules per particle is 210. The surface area to volume ratio is 2.5×10^7 cm^{-1}. Approximately 67% of the TiO_2 molecules are on the surface of the Q-sized particle. In comparison, for a standard photocatalyst, P-25 TiO_2 manufactured by Degussa, of diameter 0.3 μm, the agglomeration number is 4.16×10^8, the surface area to volume ratio is 2×10^5 cm^{-1}, and approximately 0.1% of the TiO_2 molecules are on the surface. Clearly, the Q-sized particles represent an unusual case in terms of the enhanced surface area to volume ratios. Figure 9 shows a scanning tunneling microscope (STM) picture of the surface of a hematite (α-Fe_2O_3) sample. The two parallel bands are rows of oxygen

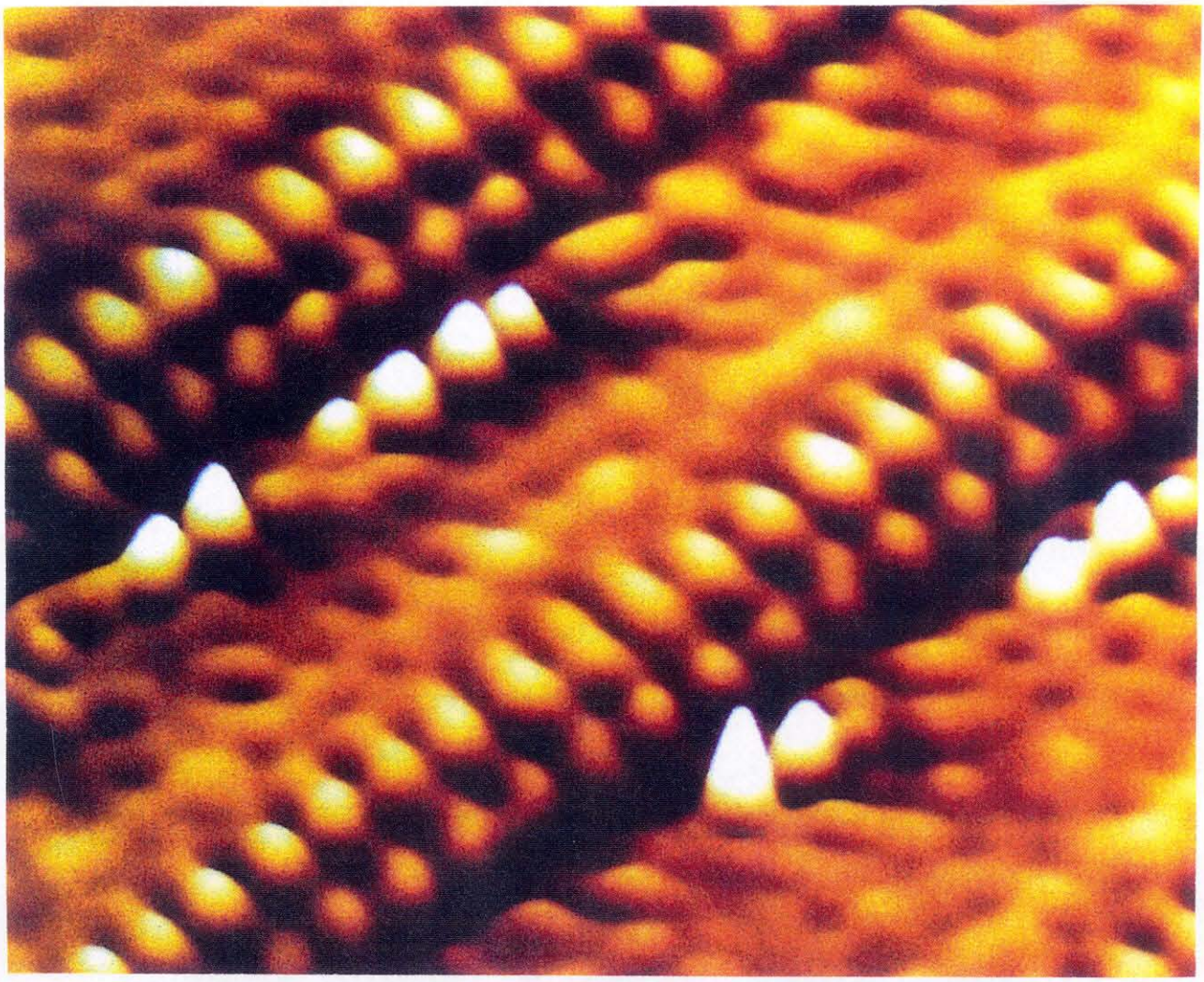

Figure 9: Scanning tunneling microscope (STM) picture of the surface of a hematite (α-Fe_2O_3) sample.

atoms at a step on the surface while the bright yellow features are sulfate-substituted surface sites.

A pictorial description of the surface of a metal oxide surface in contact with water is given in Figure 10 (19). Adsorption of water molecules at surficial metal sites is followed by hydrolysis to form metal-OH surface groups leading to a coverage of 4 to 10 groups/nm^2. The charge of a metal oxide in water results from proton transfers at this amphoteric surface (20):

$$>MeOH_2^+ \rightarrow >MeOH + H^+ \qquad K_{A1} = \{>MeOH\}\,[H^+] / \{>MeOH_2^+\} \qquad (7)$$

$$>MeOH \rightarrow >MeO^- + H^+ \qquad K_{A2} = \{>MeO^-\}\,[H^+] / \{>MeOH\} \qquad (8)$$

where [] and {} indicate concentrations of species in the aqueous phase (mol l^{-1}) and concentrations of surface species (mol kg^{-1}), respectively. Other species such as metal ions (Lewis acids) or ligands (Lewis bases) can also coordinate at a surface site. The specific binding of H^+ and cations increases the net charge of the particle surface, while the specific binding of anions decreases the net charge of the particle surface. The characteristic equilibrium constants of these processes can be used to quantify the extent of adsorption and the resultant net charge of the metal oxide particle surface as a function of pH and solute activity.

The surface charge may be measured experimentally by suspending a known amount of the metal oxide in a solution of an inert (nonspecifically adsorbable cations and anions) salt solution and titrating aliquots of the dispersion with standard base and with standard acid. The resultant titration curve may be compared with that obtained in the absence of the oxide, and the quantity of bound H^+ or OH^- may be calculated. Such an experiment for ZnO is shown in Figure 11. The pH of zero point of charge can be

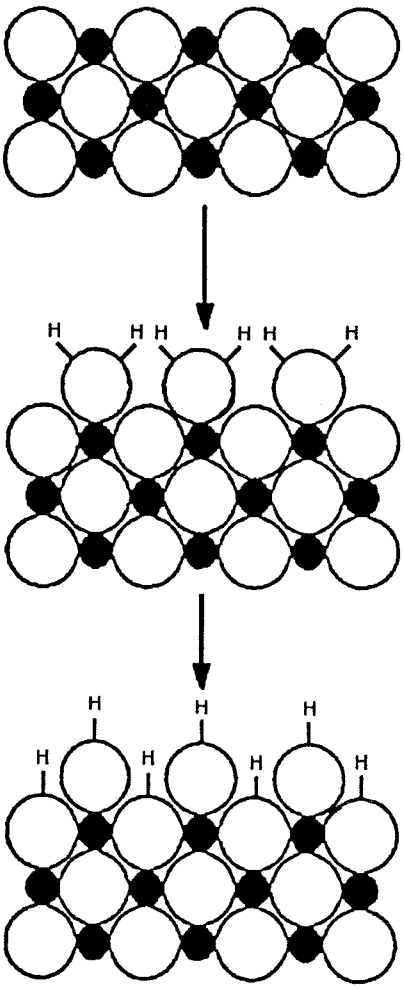

Figure 10: Cross-sectional representation of the processes occurring at the surface layer of a metal oxide in contact with water.

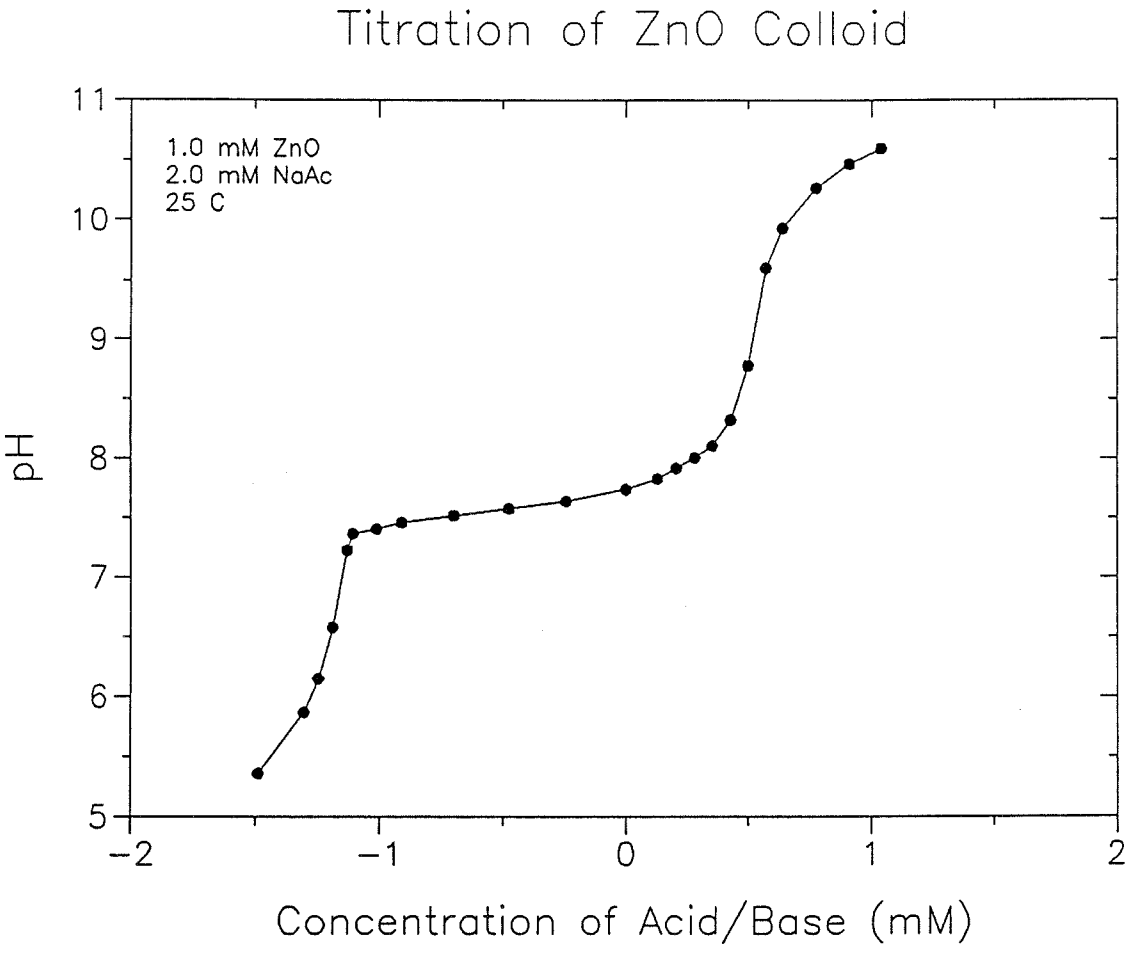

Figure 11: Titration curve of an aqueous Q-sized semiconductor colloid.

determined from the point of maximum slope in Figure 11 and has the value of 9.3 $\pm$ 0.2 which matches the literature value of 9.3 (21). In addition, at this pH the colloid's absorption spectrum evidenced increased light scattering, which indicates coagulation of the colloid is occuring. The value of the first pK_a can be determined from the point of minimum slope, i.e., maximum buffer capacity, in Figure 11. The experimentally determined value of 7.6 $\pm$ 0.1 reproduces the literature value of 7.6. In the absence of specifically adsorbable ions other than H^+ and OH^-, the pH of zero point of charge equals the average of pK_{a1} and pK_{a2} and is identical with the isoelectric point (iep). The isoelectric point is the pH where the particle is electrokinetically uncharged. Figure 12 shows the effect of specifically adsorbed ions on the pH_{zpc} (22). Specifically adsorbed cations increase the pH of the isoelectric point and lower the pH of the zero proton condition while the specifically adsorbed anions decrease the pH of the isoelectric point and raise the pH of the zero proton condition. Shown in Table 1 are the pK_a's of several common metal oxides (23).

The stability of a colloidal suspension is directly related to the charge at the surface. The development of a net charge at the particle surface affects the distribution of ions in the surrounding interfacial region, resulting in an increased concentration of counterions close to the surface. Thus, an electrical double layer is formed around the particle. The double layer (Figure 13) consists of an inner region that includes ions that are bound strongly to the surface by adsorption, and an outer or diffuse region in which ion distribution is determined by the balance of electrostatic forces and random thermal motion. The distribution of potential in the diffuse layer as a function of distance from the surface is given by Gouy-Chapman theory (24):

$$\phi = \phi_d \exp(-\kappa x) \qquad (9)$$

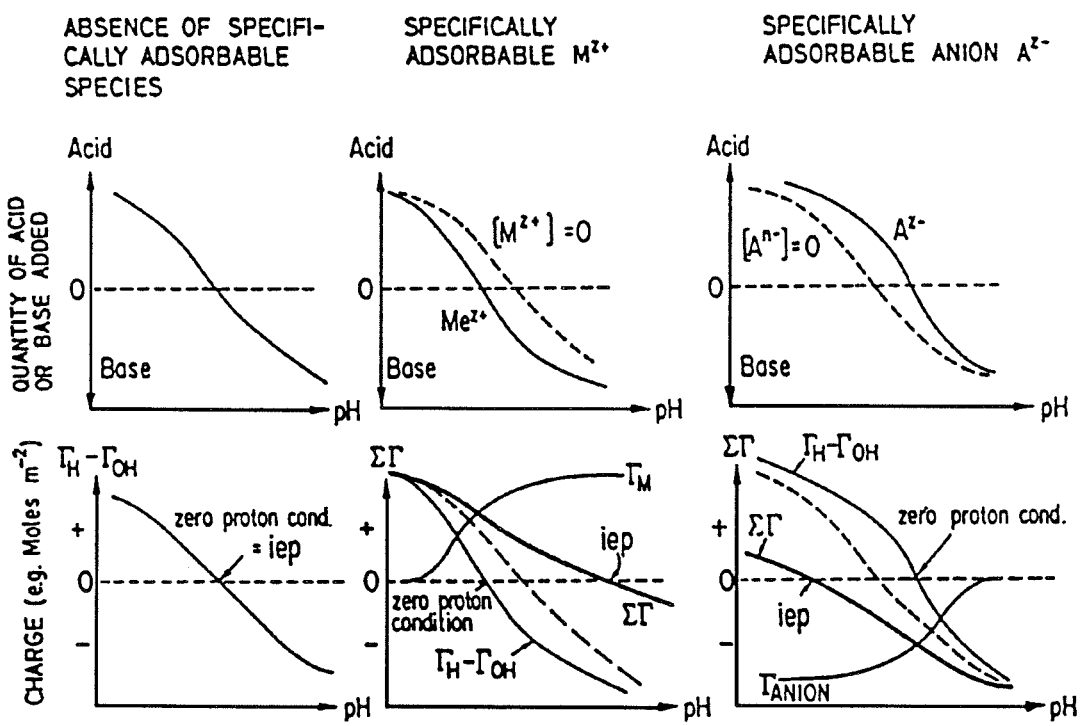

Figure 12: Effect of specifically adsorbable ions on the pH of the zero proton condition and on the pH of the isoelectric point.

Metal Oxide	pK_1	pK_2	pH_{zpc}
γ-Al_2O_3	7.4	10.0	8.7
α-FeOOH	6.4	9.25	7.8
am-SiO_2	7.5		
TiO_2 (anatase)	5.0	7.8	6.4
Q-sized ZnO	7.6	11.0	9.3

Table 1: Acidity constants of metal oxides.

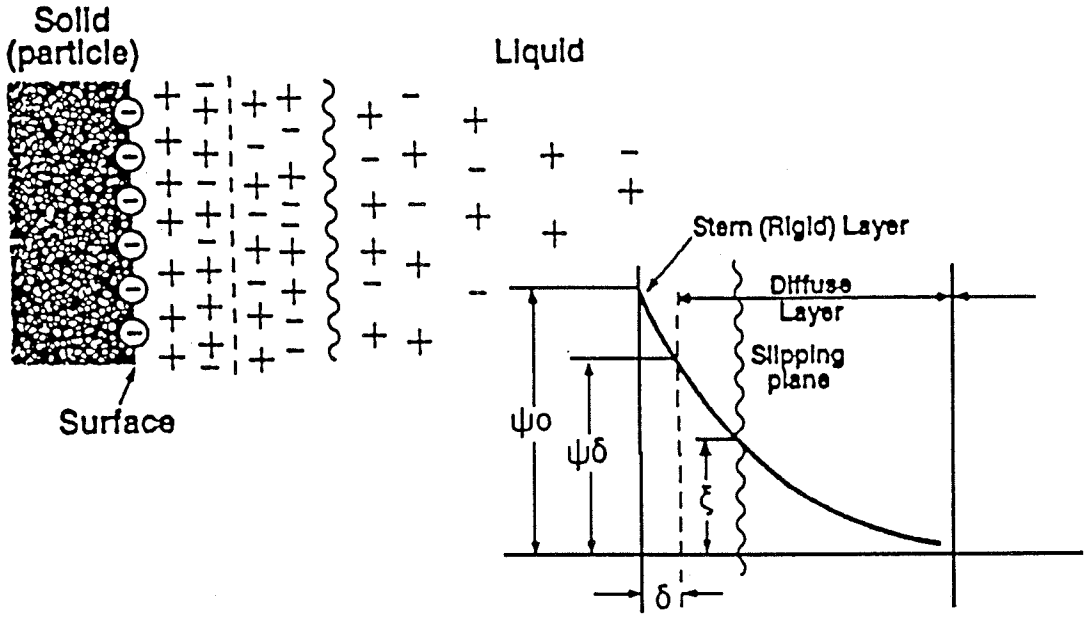

Figure 13: The electrical double layer and the potentials in the interfacial region near a charged surface.

where κ is the reciprocal Debye length of the double layer. The equation for κ is

$$\kappa = [e^2 \Sigma_i n_i z_i^2 / (\varepsilon \varepsilon_0 kT)]^{1/2}. \quad (10)$$

For a typical aqueous photocatalytic system of 1mM ZnO, an ionic strength of 2mM, and room temperature, the decay constant of the double layer is about 60 Å and the thickness of the double layer is 300 Å. In the absence of added polyelectrolytes, colloidal dispersions are stabilized by double layer repulsion. Thus the magnitude of κ and a related factor called the zeta potential ,Ψ_z, which is defined as the potential of the slipping plane in Figure 12, measures how rapidly a system of particles will flocculate. Conditions which tend to compress the electrical double layer, i.e., high ionic strength, solvents of low dielectric strength, and high temperature, lead to unstable colloids.

As a consequence of its amphoteric behaviour, a metal oxide surface is predominantly positively charged below the pH_{zpc} and negatively charged above the pH_{zpc}. The surface charge may have a significant influence on the photocatalytic activity. For example, Kormann et al. (25) determined that the oxidation of the anion trichloroacetate is only observed with reasonable yield below the pH_{zpc} of the catalyst TiO_2. Likewise, the cation chloroethylammonium is predominantly oxidized at high pH. This can be rationalized by an electrostatic adsorption model where cations are more readily accommodated at negative sites. The pH of the colloid also affects the energetic position of the band edges in the semiconductor. For metal oxides, H^+ and OH^- are potential determining ions. Changing their concentration changes the potential drop across the electrolytic double layer. In the case where the proton activity on the surface remains constant as the pH changes, the potential difference between semiconductor and solution is given by (26):

$$\phi_{oxide} - \phi_{sol} = \text{const} - 0.059\ \text{pH} \qquad (11)$$

Thus, the band edges shift in a Nernstian fashion by 59mV more negative for every increase in pH unit at room temperature. This results in a diminishing oxidation potential of h^+_{vb} at high pH, and to an increased reduction potential of e^-_{cb} at high pH.

Photocatalytic reactions in semiconductor colloids can be achieved with sizeable yield only if two scavengers (for electrons and holes) are present, and at least one of them is adsorbed at the colloidal particle. The adsorbed scavenger determines the yield of the reaction of the nonadsorbed one. Thus, adsorption-desorption phenomena play an essential role in reaction dynamics. Two limiting cases of adsorption can be considered: Physisorption, in which the solid is relatively inert and adsorption is due to physical attraction forces of the van der Waals type, and chemisorption, in which the surface contains coordinatively unsaturated atoms and molecules interact with free valencies and chemical reactions occur which create new bonds. The extent of adsorption (i.e., the coverage of the surface) is related to the concentration of the adsorbate at equilibrium by adsorption isotherms. The Langmuir isotherm is a common model and involves the three following assumptions: the surface is uniform, the adsorbed molecules form a monolayer, and the adsorption-desorption equilibrium is comparable to that of the dissociation of a ligand. The surface coverage, Θ, is given by the equation (27):

$$\Theta = KC/(1+KC) \qquad (12)$$

where C is the bulk equilibrium concentration of the solute species, and K is the Langmuir adsorption coefficient. The Freudlich-Temkin isotherms are derived from the Langmuir model by adding correcting assumptions regarding the heterogeneity of the surface (Freundlich) or regarding more than monolayer coverage (Temkin). Another important

consideration is that the extent of adsorption of species that carry a charge may be modified by the increase in the number of charge carriers caused by band-gap illumination.

Heterogeneous Reaction Kinetics

Heterogeneous catalysis involves five distinct steps: i) mass transport of reactant(s) to the catalyst surface from the bulk solution; ii) adsorption of reactant(s) on the surface; iii) chemical reaction at the surface; iv) desorption of product(s) from the surface; and v) mass transport of product(s) away from the surface into the bulk solution. The chemical reaction step at the surface includes light excitation of the semiconductor, charge transfer, and possibly rearrangement or bond breaking/formation. Any of these five steps could be rate-determining. Each will be considered in this section, together with their kinetic consequences.

Mass transport of uncharged reactant(s) to the catalyst surface from the bulk solution and vice versa can be calculated from the Smoluchowski equation for encounters through diffusion (28):

$$k = \frac{4\pi N}{1000}[D_A + D_b]r_{AB} \tag{13}$$

where D_A and D_B are the diffusion coefficients in solution, r_{AB} is the distance of separation upon collision, and N is Avogadro's number. The diffusion coefficient of a spherical molecule is given by the Stokes-Einstein equation (29):

$$D = \frac{RT}{6\pi\eta r N} \tag{14}$$

where r is the radius (cm), T is the temperature (K), η is the viscosity, and R is the Gas Constant. Using a viscosity of water at 25°C of 0.008904 poise, and a ZnO radius of 20 Å and a molecule radius of 2 Å gives values of the diffusion coefficients of 1.226 X 10^{-6} cm^2 s^{-1} and 1.226 X 10^{-5} cm^2 s^{-1} respectively. With a r_{AB} = 22 Å, the value of the bimolecular rate constant for collisions between A and B is 2.24X10^{10} M^{-1} s^{-1}. In the case of charged species A and B, the Debye-Smoluchowski equation for a bimolecular collision is (30):

$$k = \frac{N[D_A + D_B]Z_A Z_B[e^2]}{10\varepsilon_0 \varepsilon \kappa T\left[\exp(Z_A Z_B e^2 / 4\pi\varepsilon_0 \varepsilon \kappa T r_{AB}) - 1\right]} \tag{15}$$

where Z_A and Z_B are the charge numbers of the colloid and the molecule, e is the unit of charge, ε_0 is the permittivity in vacuum, ε is the dielectric constant of water, and κ is the Boltzmann constant. When r_{AB} = 22 Å and Z_A= 10 and Z_B = 1, the bimolecular rate constant for oppositely charged ions at 25°C is 7.5X10^{11} M^{-1} s^{-1}. Thus, in this case the coulombic effect increases the diffusion rate constant by approximately two orders of magnitude.

Once a species has diffused to the surface, adsorption can occur. The rate of adsorption, r_{ads}, and the rate of desorption, r_{des}, are given by the expressions:

$$r_{ads} = k_{ads} C_A C_s \tag{16}$$

$$r_{des} = k_{des} C_{AS} \tag{17}$$

where k_{ads} and k_{des} are the rate constants of adsorption and desorption respectively, C_A is the concentration of adorbate in solution, C_S is the concentration of free surface sites,

C_{AS} is the concentration of occupied states. If the activation energy for the adsorption reaction is low, i.e., $E_a << 20$ kJ/mol, the process is diffusion controlled and the rate constants are given by the Smoluchowski equation presented earlier. If the activation energy for the adsorption reaction is greater than 20kJ/mol, the process is chemically controlled, and the rate constant depends upon the activation energy of adsorption according to transition state theory by the Arrhenius equation (31):

$$k_{ads} = \frac{kT}{h} e^{-\frac{E_{ads}}{RT}} \tag{18}$$

where k is Boltzmann's constant, T is the temperature in Kelvin, h is Planck's constant, R is the gas constant, and E_{ads} is the activation free energy of adsorption. For an activation energy of 10 kcal/mol, the adsorption rate constant is $2.875X10^5$ s^{-1}, which corresponds to a characteristic reaction time of micoseconds. The desorption rate constant is given by an equation analgous to 16 using the activation energy of desorption, E_{des}. At equilibrium, the rate of adsorption equals the rate of desorption, and the coverage of the surface is given by the Langmuir adsorption equation discussed previously. In this expression the equilibrium constant, K, is the ratio of the rate constant of adsorption to the rate constant of desorption. In some cases, if more than one species can react at the surface, competitive adsorption can occur. Although the number of available surface sites is generally considered to be proportional to the overall surface area, the presence of different defects such as step edges, kinks, and pits may lead to sites of different activation energies for adsorption. The proportion of each type of defect may change depending upon the method of synthesis of the photocatalyst.

The rate of excitation of a semiconductor equals the rate of light absorbance, which was given earlier in equation 2. For a 1mM ZnO suspension of 36 Å diameter particles and an incident light intensity of $1X10^{-4}$ Molar photons min^{-1}, the concentration in terms of particles is $9.9X10^{-7}$ M and the number of photon hits per particle per second is 1.7. Under these conditions, on average a photon is absorbed by a particle every 0.6 sec. The rates of recombination and trapping at surface sites are given by the following expressions:

$$r_{RC} = k_{RC} [e^-] [h^+] \quad (19)$$

$$r_t = k_t [e^-] N_S \quad (20)$$

where k_{RC} and k_t are the rate constants of recombination and trapping, and N_S is the concentration of surface trap sites. At high light intensities corresponding to 67 photons/particle for 120 Å diameter colloidal TiO_2, the e^-/h^+ pairs recombine with a 30 ns exponential decay constant (32). At low light intensities, the recombination rate is much lower, with decay constants on the order of milliseconds to microseconds. The rate of hole trapping at the surface can compete with recombination at low light intensity. For example laser photolysis experiments with colloidal TiO_2 yielded a rate constant of 4 X 10^5 s^{-1} for hole trapping (33). The overall rate of initiation of the semiconductor is therefore a complex function of excitation intensity, recombination rates (both radiative and non-radiative), and surface trapping rates.

The rates of electron transfer will depend upon whether the reacting species is free or trapped, since trapping lowers the driving force for electron transfer. The rate constant of a bimolecular electron-transfer reaction is given by the expression (34):

$$k_{et} = A\exp(-\Delta G^*/kT) \quad (21)$$

The preexponential factor, A, in equation 21 represents a combination of electronic and frequency factors which are related to the overlap of the wavefunctions for A and B and the attempt frequency at which the transition state is reached. ΔG^* is the free energy of activation, which is related to the free energy of the interfacial reaction, $\Delta G^{0'}$, by the following expressions:

$$\Delta G^* = (\lambda + \Delta G^{0'})^2 / 4\lambda \quad (22)$$

where λ is the solvent reorganization energy. If either the surface or the electron acceptor are charged, then additional coulombic work terms are added to right hand side of equation 22. In the context of interfacial electron transfer at a semiconductor electrode, $\Delta G^{0'}$ is given by:

$$\Delta G^{0'} = E_{cb} - E^{0'}(A/A^-) \quad (23)$$

where E_{cb} is the conduction band energy at the electrode surface and $E^{0'}(A/A^-)$ is the formal potential energy for the solution redox couple. Using a reduction potential of oxygen of -0.33 V_{NHE} , a solvent reorganization of 1 eV, a conduction band edge position of -0.5 V_{NHE} for TiO_2 at pH 8.2, a frequency factor of 10^{12} s^{-1}, and an electronic factor of 1 (adiabatic process), the rate constant of electron transfer is approximately $1X10^9$ s^{-1}. If the electron transfer occurs via an electron trap of 0.3 eV depth, then the rate constant of electron transfer decreases to $4X10^6$ s^{-1}. After the electron transfer, other reactions such as rearrangement, fragmentation, or dimerization may also occur. The rate constants of such reactions are analgous to the rate constant of equation 18 with the proper E_{act}.

In order to examine the overall kinetics of a photocatalytic system, consider the scheme below in which the adsorbed organic substrate is oxidized by adsorbed valence band holes (Zn-OH·):

$$\text{Excitation:} \quad ZnO \rightarrow e^- + h^+ \tag{24}$$

$$\text{Adsorption:} \quad R + \text{Site} \rightarrow R_{ads} \tag{25}$$

$$\text{Recombination:} \quad e^- + h^+ \rightarrow \text{heat or light} \tag{26}$$

$$\text{Hole trapping:} \quad Zn(II)\text{-}H_2O + h^+ \rightarrow ZnOH\cdot \tag{27}$$

$$\text{H atom abstraction:} \quad ZnOH\cdot + R_{ads} \rightarrow Zn(II) + R\cdot_{ads} + H_2O \tag{28}$$

If the rate determining step is the oxidation of the adsorbed substrate with surface trapped holes, the rate of oxidation is given by:

$$R_{28} = k_{28}\,[ZnOH\cdot]\,[R_{ads}] \tag{29}$$

Using a steady state analysis on ZnOH· gives the expression:

$$[ZnOH\bullet] = \frac{k_{27}[Zn-H_2O][h^+]}{k_{-27} + k_{28}[R_{ads}]} \tag{30}$$

Likewise the steady state analysis on h^+ gives:

$$\frac{d[h^+]}{dt} = I_{abs} - k_{26}[e^-][h^+] - k_{27}[Zn-H_2O][h^+] + k_{-27}[Zn-OH\bullet] \approx 0 \tag{31}$$

Since the photogeneration rates of h^+ and e^- are equal and the intrinsic carrier density is comparitively low, $[h^+] = [e^-]$, and the equation becomes:

$$I_{abs} = k_{27}[h^+][Zn-H_2O] - k_{-27}[Zn-OH\bullet] + k_{26}[h^+]^2 \qquad (32)$$

Recent laser pulse photolysis studies have shown that the rate constants for free carrier recombination and electron trapping are much greater than those for hole trapping; therefore, at high hole concentrations, i.e., high light intensity, the third term in equation 32 is much larger than the other two terms and the equation simplifies to:

$$[h^+] = \sqrt{\frac{I_{abs}}{k_{26}}} \qquad \{\text{at high intensity}\} \qquad (33)$$

For very low light intensities, the third term in equation 32 is much less than the other two terms and the equation simplifies to:

$$[h^+] = \frac{I_{abs} + k_{-27}[Zn-OH\bullet]}{k_{27}[Zn-H_2O]} \qquad \{\text{at low intensity}\} \qquad (34)$$

When back reaction rate of equation 27 is slow compared to the rate of light absorption, then the equation for the concentration of holes simplies further to give:

$$[h^+] = \frac{I_{abs}}{k_{27}[Zn-H_2O]} \qquad (\text{at low intensity}) \qquad (35)$$

Substitution of equations 30 and 33 or 35 into equation 29 gives for the rate of oxidation of R:

$$R_{28} = \frac{k_{28}k_{27}[\mathrm{Zn-H_2O}]\mathrm{I}_{abs}^{1/2}k_{26}^{-1/2}[\mathrm{R_{ads}}]}{k_{-27}+k_{28}[\mathrm{R_{ads}}]} \qquad \text{(high intensity)} \qquad (36)$$

$$R_{28} = \frac{k_{28}\mathrm{I}_{abs}[\mathrm{R_{ads}}]}{k_{-27}+k_{28}[\mathrm{R_{ads}}]} \qquad \text{(low intensity)} \qquad (37)$$

Rearranging equations 36 and 37 and collecting constants gives the final result:

$$R_{28} = \frac{k_{obs}\mathrm{I}_{abs}^{1/2}\kappa[\mathrm{R_{ads}}]}{1+\kappa[\mathrm{R_{ads}}]} \qquad \text{(high intensity)} \qquad (38)$$

$$\text{with } k_{obs} = k_{27}k_{26}^{-1/2}[\mathrm{Zn-H_2O}] \text{ and } \kappa = \frac{k_{28}}{k_{-27}} \qquad (39)$$

$$R_{28} = \frac{\mathrm{I}_{abs}\kappa[\mathrm{R_{ads}}]}{1+\kappa[\mathrm{R_{ads}}]} \qquad \text{(low intensity)} \qquad (40)$$

$$\text{with } \kappa = \frac{k_{28}}{k_{-27}} \qquad (41)$$

These equations are similar to the Langmuir-Hinshelwood rate form. Turchi and Ollis (35) have demonstrated that similar kinetic schemes for reaction of the organic substrate and OH radical in solution, and adsorbed OH radical and R in solution all give the same

Langmuir-Hinshelwood rate form. Although the existence of both homogeneous and heterogeneous phase reactions is possible and may have a profound affect upon the observed rate; the form of the rate expression sheds little insight into which pathway predominates.

Conclusions

The fundamental ideas of semiconductor band edges, surface chemistry of metal oxides, dynamics of exicitation of semiconductors, light absorption, the Q-size effect, and heterogeneous reaction rates are essential to an understanding of the mechanisms of semiconductor photocatalyzed reactions. Throughout the next five chapters, this framework is used as a basis to interpret the results of experimental studies on the synthesis of Q-sized semiconductors, the polymerization of vinylic monomers, the photoproduction of hydrogen peroxide, the photodegradation of organic acids, and the formation of humic-like substances.

References

1. Rohatgi-Mukherjee, K. K. "Fundamentals of Photochemistry," Wiley Eastern Limited: New Delhi, **1978**, 3.

2. Hoffmann, R. *Angew. Chem. Int. Ed. Engl.*, **1987**, *26*, 846.

3. Boer, K. W. "Survey of Semiconductor Physics," Van Nostrand Reinhold: New York, **1990**, 249.

4. Serpone, N.; Pelizzetti, E. "Photocatalysis," Wiley and Sons: New York, **1989**, 42.

5. a) Brus, L. E. *J. Chem. Phys.*, **1984**, *80*, 4403. b) Brus, L. E. *J. Chem. Phys.*, **1983**, *79*, 5566.

6. Nedeljkovic, J. M.; Nenadovic, M. T.; Micic, O. I.; Nozik, A. J. *J. Phys. Chem.*, **1986**, *90*, 12.

7. Bahnemann, D. W.; Kormann, C.; Hoffmann, M. R. *J. Phys. Chem.*, **1987**, *91*, 3789.

8. Gratzel, M. "Heterogeneous Photochemical Electron Transfer," CRC Press: Boca Raton, **1989**, 101.

9. Wrighton, M. S. *J. Chem. Ed.* **1983**, *60(10)*, 877.

10. Memming, R. *Topics Curr. Chem.*, **1988**, *143*, 79.

11. Duonghong, D.; Ramsden, J.; Gratzel, M. *J. Am. Chem. Soc.*, **1982**, *104*, 2977.

12. Albery, W. J.; Bartlett, P. N. *J. Electrochem. Soc.*, **1984**, *131*, 315.

13. Gratzel, M. "Heterogeneous Photochemical Electron Transfer," CRC Press: Boca Raton, **1989**, 107.

14. a) Liu, C. -Y.; Bard, A. J. *J. Phys. Chem.*, **1989**, *93*, 3232. b) Liu, C. -Y.; Bard, A. J. *J. Phys. Chem.*, **1989**, *93*, 7047.

15. Rothenberger, G.; Moser, J.; Gratzel, M.; Serpone, N.; Sharma, D. K. *J. Am. Chem. Soc.*, **1985**, *107*, 8054.

16. Haase, M.; Weller, H.; Henglein, A. *J. Phys. Chem.*, **1988**, *92*, 482.

17. Nakabayashi, S.; Komuro, S.; Aoyagi, Y.; Kira, A. *J. Phys. Chem.*, **1987**, *91*, 1696.

18. Rajh, T.; Saponjic, Z. V.; Micic, O.I. *Langmuir*, **1992**, *8*, 1265.

19. Boehm, H. P. *Disc. Faraday Soc.*, **1971**, *52*, 264.

20. Stumm, W.; Morgan, J. J. "Aquatic Chemistry," Wiley and Sons: New York, **1981**, 625.

21. Bahnemann, D. W.; Kormann, C.; Hoffmann, M. R. *J. Phys. Chem.*, **1987**, *91*, 3789.

22. Stumm, W.; Morgan, J. J. "Aquatic Chemistry," Wiley and Sons: New York, **1981**, 633.

23. a) Matijevic, E., Ed. "Surface and Colloid Science, Vol. 12," Plenum Press: New York, **1982**, 119. b) Chatgilialoglu, C.; Asmus, K.-D., Eds. "Sulfur-centered Reactive Intermediates in Chemistry and Biology," NATO-ASI Series, Plenum Press: New York, **1990**, 103.

24. Hunter, R. J. "Zeta Potential in Colloid Science," Academic Press: New York, **1981**, 22.

25. Kormann, C. "Synthesis and Characterization of Q-Size Metal Oxide Colloidal Particles," doctoral thesis, California Institute of Technology, **1989**, 78.

26. Gerischer, H. *Electrochim. Acta*, **1989**, *34(8)*, 1005.

27. Adamson, A. W. "Physical Chemistry of Surfaces," Wiley and Sons: New York, **1982**, 533.

28. Stumm, W.; Morgan, J. J. "Aquatic Chemistry," Wiley and Sons: New York, **1981**, 96.

29. Tyrrell, H. J. V.; Harris, K. C. "Diffusion in Liquids," Butterworths: London, **1984**, 446.

30. Stumm, W.; Morgan, J. J. "Aquatic Chemistry," Wiley and Sons: New York, **1981**, 97.

31. Espenson, J. H. "Chemical Kinetics and Reaction Mechanisms," McGraw-Hill: New York, **1981**, 9.

32. Pellizzetti, E.; Serpone, N., Eds. "Homogeneous and Heterogeneous Photocatalysis," NATO-ASI Series, Reidel Publishing: Dordrecht, **1986**, 91.

33. Rothenberger, G.; Moser, J.; Gratzel, M.; Serpone, N.; Sharma, D. K. *J. Am. Chem. Soc.*, **1985**, *107*, 8054.

34. a) Marcus, R. A. *J. Chem. Phys.*, **1956**, *24*, 1966. b) Sutin, N. *Progr. Inorg. Chem.*, **1983**, *30*, 441. c) Gerischer, H. *J. Phys. Chem.*, **1991**, *95*, 1356.

35. Turchi, C. S.; Ollis, D. F. *J. Catal.*, **1990**, *122*, 178.

Chapter 3

Q-Sized CdS: Synthesis, Characterization, and Efficiency of Photoinitiation of Polymerization of Several Vinylic Monomers

[The text of this chapter appeared in A. J. Hoffman, G. Mills, H. Yee, and M. R. Hoffmann, *J. Phys. Chem.* **1992**, *96*, 5543.]

Abstract

Q-sized CdS semiconductors have been synthesized in several non-aqueous solvents without the use of added stabilizers. The effects of solvent viscosity and dielectric strength, concentration of excess cadmium ions, temperature, and stirring upon the colloids' absorption spectra have been examined. In addition, efficiency of photoinitiation of polymerization of several vinylic monomers has been examined using both bulk and quantum sized CdS, ZnO and TiO_2. The Q-sized semiconductors demonstrated significantly higher quantum yields for photopolymerization than their bulk-sized counterparts. A correlation between the reactivity of a monomer towards polymerization and its Alfrey and Price Q and e values was observed. Hole scavenging by the solvent was necessary for efficient polymerization to occur. A correlation between the semiconductor photoinitiation efficiency and the reduction potential of its conduction band electrons was also found. Based on these observations, a mechanism of an anionic initiation step followed by free radical chain propagation steps has been proposed.

Introduction

The photoelectrochemistry of ultrasmall semiconductor particles has been an area of active research interest in recent years. These ultrasmall particles with diameters ranging between 1 and 10 nm possess properties which fall into the region of transition between the molecular level and the bulk phase. Colloidal suspensions of such Q-sized colloids exhibit shifts of their band-gap absorption onsets from the UV for small agglomeration numbers to the visible or near-IR for the corresponding bulk-phase material. The apparent shifts in the band-gap energy have been explained in terms of quantum mechanical calculations which show that the energy of the first excited state of the exciton increases as the particle size decreases. This effect is seen as a blue shift in the absorption spectrum of the transparent colloids. The bandgap shift, ΔE_g, as a function of particle size is given by the following equation (1):

$$\Delta E_g = \left(\frac{h^2}{8R^2} * \frac{1}{\mu} \right) - \frac{1.8\, e^2}{\varepsilon R} \qquad (1)$$

where R is the radius of the particle, μ is the reduced mass of the exciton (i.e., $\mu^{-1} = m^*_e{}^{-1} + m^*_h{}^{-1}$), m^*_e is the effective mass of the electron, m^*_h is the effective mass of the hole and ε is the dielectric constant of the semiconductor. A wide variety of Q-sized semiconductors have been synthesized; they include ZnO, TiO_2, ZnS, CdS, As_2S_3, FeS_2, PbS, Zn_3P_2, Cd_3P_2, Cd_3As_2, CuCl, AgCl, AgBr, AgI, In_2S_3, CdSe, and ZnSe (2-14). Two generally employed synthetic approaches are controlled precipitation (2-4) or radiolysis (15,16). Henglein has provided an extensive review of the various synthetic procedures and general physiochemical properties of Q-sized colloids (17).

Although several different Q-sized semiconductors have been synthesized, the method of obtaining a stable colloid of the desired particle size remains a matter of trial and error. Many of the syntheses to date utilize an added stabilizer such as hexametaphosphate, polyacrylic acid, thiosulfate, polyvinylacetate, glycerine, or a styrene/maleic anhydride copolymer (5,18,19). Very little is known about the interaction between the colloidal particles and the foreign stabilizers. In addition the reactivity of such stabilizers in semiconductor photoinitiated reactions is generally unknown. Following the examples of Brus et al. (4) and Gratzel et al. (20), we chose to avoid such complications by synthesizing a variety of non-aqueous colloids without the addition of stabilizers other than the counter ions present from the synthesis. In order to develop further insight into the factors which control particle size and stability, we performed a systematic study of the effect of solvent, temperature, and nature and concentration of counter-ion upon the colloidal particle growth. CdS was selected for this study.

Illuminated semiconductor suspensions have been shown to be suitable initiators of the polymerization of methylmethacrylate, styrene, and 1-vinylpyrene (21-26). However, Q-sized semiconductor colloids have not been used previously as photoinitiators. The use of Q-sized semiconductors in heterogeneous photochemical studies has several advantages over suspended powders or solid electrodes. Since the Q-sized particles are extremely small (i.e., the particle diameters (5 nm) are much less than the excitation wavelengths (380 nm)), they exhibit negligible light scattering; thus the accurate determination of quantum yields in heterogeneous photochemistry is possible. Q-sized particles also have high surface area-to-volume ratios, thus enhancing their catalytic activity. These two factors are likely to combine to give high polymerization efficiencies. Another major advantage in the use of Q-sized particles is the increase in effective bandgap energy with decreasing particle size. This property potentially allows for the variation of the redox potential of the valence-band holes and the conduction-band

electrons via control of particle growth. A possible disadvantage of using Q-sized particles to initiate polymerization arises in the area of polymer separation and purification; however, in the case of CdS and ZnO, simply changing to a more acidic pH causes the Q-sized particles to dissolve and aids their removal from the polymer.

In this paper we describe our recent investigation of the synthesis of Q-sized CdS in several solvents without added stabilizers. We then examine the polymerization of vinylic monomers using Q-sized CdS as a photoinitiator. We investigate the effects of solvents, the efficiencies of different semiconductors, the photopolymerization rates of Q-sized versus bulk particles and determine the reactivity of different monomers towards semiconductor-initiated polymerization.

Experimental

Chemicals and solvents were reagent grade and were used without any further purification. The commercially-available monomers (e.g., methylmethacrylate, styrene, methyl acrylate, PETA, TRPGDA, Celrad 6696, Rohamere, acrylonitrile, and a-methyl styrene) contained inhibitors that were not removed before use. Quantum-sized CdS was synthesized according to the method of Rossetti et al. with modifications (4). 4 mL of a stock solution of 5 X 10^{-3} M cadmium acetate were diluted to 45 mL with solvent, then 2 mL of a stock solution of 5 X 10^{-3} M sodium sulfide in methanol were added rapidly. The sodium sulfide concentration was standardized by titration with Pb^{+2} ions against a sulfide-specific electrode (27). Solvents were isopropanol, ethanol, water, ethylene glycol, and glycerol. The total volume was diluted to 50 mL and then the solution was agitated vigorously for 15 seconds. Following initial synthesis the colloid was aged for one hour at room temperature (25°C). The Q-sized colloids were stored up to three months at 4°C

(i.e., in isopropanol) with only a small decrease in absorption intensity and a negligible shift in absorption band edge. In the polymerization experiments, Q-sized ZnO and TiO_2 were also used. Quantum sized ZnO and TiO_2 were synthesized according to the methods of Hoffmann and co-workers (2,3). ZnO was prepared as follows: 1 mmole of zinc acetate was dissolved with stirring at 50°C into 80-90 ml of isopropanol. After dissolution the resulting solution was diluted to 920 ml and the temperature lowered to 0° C. Then 80 ml of 2.0 X 10^{-2} M sodium hydroxide was added at 0°C with vigorous stirring. The transparent colloidal suspension was aged at 65°C for two hours before use. TiO_2 was prepared as follows: 1 mmole of titanium tetrachloride at -20°C was slowly added to 200 mL of solvent at 1°C with vigorous stirring. The transparent colloid was aged at 1°C for three hours. The average particle diameters obtained from these synthesis were 50 Å for ZnO and 24 Å for TiO_2.

The Q-sized colloids were characterized by absorption, fluorescence, and transmission electron microscopy. Either a Shimadzu MPS-2000 spectrometer or a Hewlett Packard 8451 A diode array spectrophotometer was used to measure UV/Vis absorption spectra. Fluorescence spectra were recorded using a Shimadzu RF 540 spectrophotometer. These techniques gave an approximate particle diameter according to the method of Brus (1). More exact particle sizes were obtained using a Philips EM 430 transmission electron microscope at 300 kV. Analysis by energy dispersion x-ray techniques were also performed using a EDAX 9900 analyzer and detector. Samples for TEM were prepared by placing 10 ml of colloidal suspension onto a substrate consisting of a copper mesh covered with a carbon film, followed by removal of the excess liquid with a piece of filter paper.

The irradiation apparatus consisted of a Osram XBO 450W xenon lamp in a Muller LX 1450-2 lamp housing or a Kratos 450W xenon lamp. Bandpass filters and a

water filter were employed to limit the heating of the sample and to select appropriate wavelengths. A fan was also employed to cool the sample during irradiation. Chemical actinometry was performed using (E)-2-(2,5 dimethyl-3-furyl-ethylidene) (isopropylidene) succinic anhydride (Aberchrome 540) in toluene according to the method of Heller and Langan (28). Typical light fluxes were 1.0×10^{-4} einsteins min^{-1} l^{-1}.

The Q-sized colloids (i.e., CdS, ZnO, and TiO_2) were used as synthesized with the exception of a series of experiments with ZnO in which the solvent effect was examined. In these latter experiments, samples of ZnO colloid in isopropanol were evaporated in a rotoevaporator to yield a thin film of ZnO which was immediately resuspended into the new solvent.

For the polymerization experiments the colloid, monomer, and solvent were measured volumetrically into a glass 3 dram vial, which was capped with a rubber stopper. In the ZnO case, a magnetic stirrer was also used. The samples were degassed for 25 minutes with argon prior to irradiation to reduce the induction period caused by oxygen inhibition. After irradiation, samples were filtered, washed with water, 4 N HCl (Aldrich), and additional solvent. The acid dissolves away the ZnO colloid from the polymer. In the case of methyl methacrylate monomer, the product was dissolved in chloroform and then washed several times with water and acid before rotoevaporation to remove the chloroform. This procedure provided a relatively pure product as shown by the FTIR spectrum. In most cases, solvents were chosen such that the monomer was soluble, but the polymer was not.

Molecular weights of the polymers were determined by gel permeation chromatography (GPC). Samples were dissolved in tetrahydrofuran and injected into the GPC system (a Waters 590 HPLC pump, a Waters 410 differential refractometer, and two

linear Ultrastyragel columns). The identity of the polymers was confirmed by FTIR using a Perkin Elmer Model 1600 FTIR and by differential scanning calorimetry using a Perkin Elmer Model 4 DSC.

Results and Discussion

Preparation and characterization of Q-sized CdS colloids

Since the solubility product of CdS is so low (i.e., 3.6 X 10^{-29} M^2 at 18°C in H_2O (29)), rapid mixing of sulfide into a cadmium acetate solution results in the immediate precipitation of many small crystallites. Once the crystallites have formed, they must be stabilized against further growth due to thermal aggregation and Ostwald ripening. The smaller crystallites have lower binding energies per atom and tend to dissolve and reprecipitate upon the larger, more stable particles leading to a net growth of particle size. The effect may be minimized by selecting low dielectric strength solvents, carrying out the synthesis at low temperature, and varying the ionic concentrations to increase the electrostatic repulsion of the electrical double-layer. With these factors in mind, different methods of synthesis of CdS were examined by varying temperature, nature and concentration of counter ions, solvent, stirring rate, and concentration of the metal ion.

Figure 1 shows the absorption spectra of CdS colloids prepared in different non-aqueous solvents. The spectra exhibit a relatively steep rise in absorption above the band gap and may be fit to the equation for a direct transition as follows (30):

$$\alpha(h\nu) = A\,(h\nu - E_g)^{1/2} \qquad (2)$$

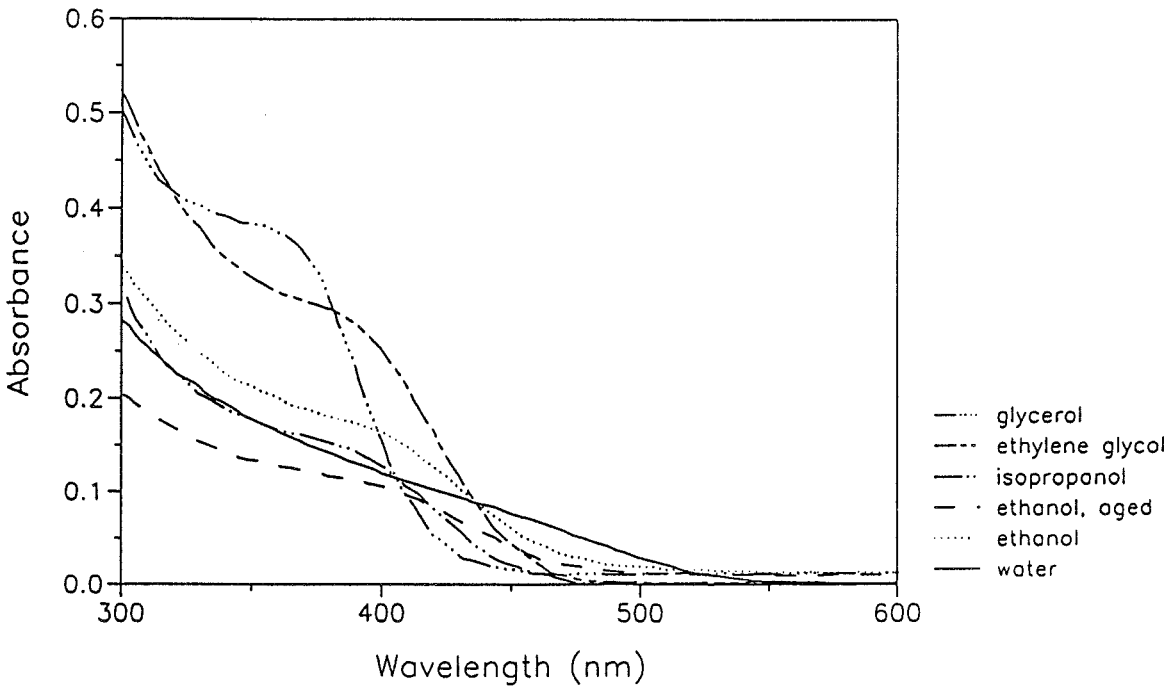

Figure 1: Absorption spectra of CdS colloids prepared in various solvents. [CdS] = 0.2mM, excess [$Cd(OAc)_2$] = 0.2mM.

where α is the absorption co efficient (cm^{-1}), A is a constant for the material, E_g is the bandgap energy (eV), and $h\nu$ is the photon energy (eV). α is calculated from the extinction coefficient, ε, by the equation $\alpha = \varepsilon\rho/M$ where ρ is the density of CdS (4.5 g/cm^3 for the cubic form) and M is the molecular weight. From the data in Figure 2, the bandgap energy of each colloid is calculated and compared to that of bulk CdS, 2.4 eV (31). The average particle diameter may be calculated from the shift in bandgap energy according to the method of Brus (1). The results are summarized in Table 1 along with the dielectric strength and viscosity of each solvent. As the dielectric strength decreases, the particle size decreases due to the decreased stability of the cadmium and sulfide ions, shifting the equilibrium to the left:

$$(CdS)_{crystalline} \Leftrightarrow Cd_{solv}^{+2} + S_{solv}^{-2} \qquad (3)$$

This effect has also been demonstrated by Brus using acetonitrile (5). A second effect is seen in more viscous solvents, where increasing solvent viscosity results in smaller diameter particles despite the high dielectric strength. The increased viscosity slows diffusion of the ions to the particles and retards particle growth. The particles prepared in high viscosity solvents have a more pronounced excitonic peak in their absorption spectrum, which is typically seen in samples with a narrow size distribution. As the crystallites age, the size distribution broadens. This provides further evidence for limited aging processes in the viscous solvents. The absorption spectra in Figure 1 show a tailing region around the bandgap energy. This tailing edge is due to absorption by surface defects and may be fit by the Uhrbach equation (Figure 3) (18):

$$\ln \alpha = \beta\, h\nu / kT \qquad (4)$$

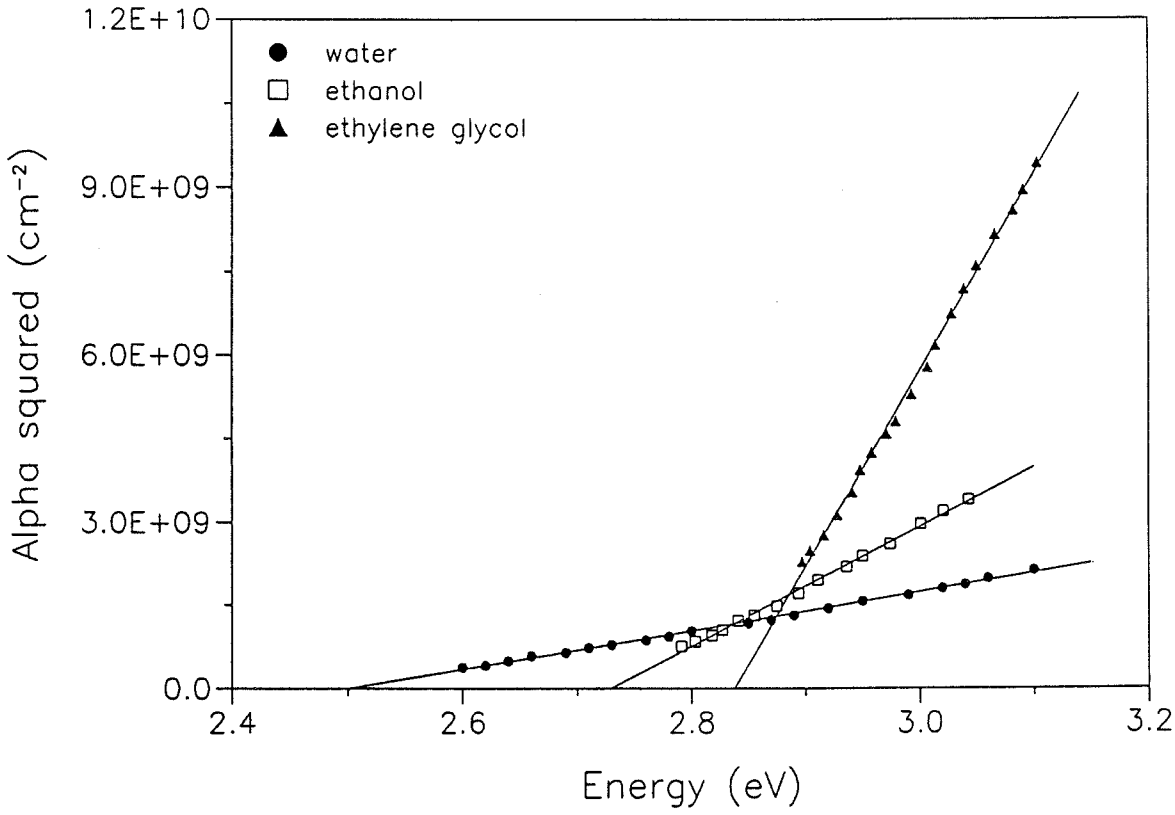

Figure 2: Fits of absorption spectra of CdS colloids to equation for a direct transition.

Solvent	ε (20°C)	Viscosity (cp)	Bandgap Energy (eV)	Radius (nm)
Water	80.4	1.0	2.50	6.9
Ethanol	24.3	1.2	2.73	4.4
Isopropanol	19.0	2.5	2.84	3.9
Ethylene Glycol	38.0	19.9	2.84	3.9
Glycerol	43.5	1490.0	3.07	3.2

Table 1: Average CdS particle diameter calculated from the shift in bandgap energy for various solvents.

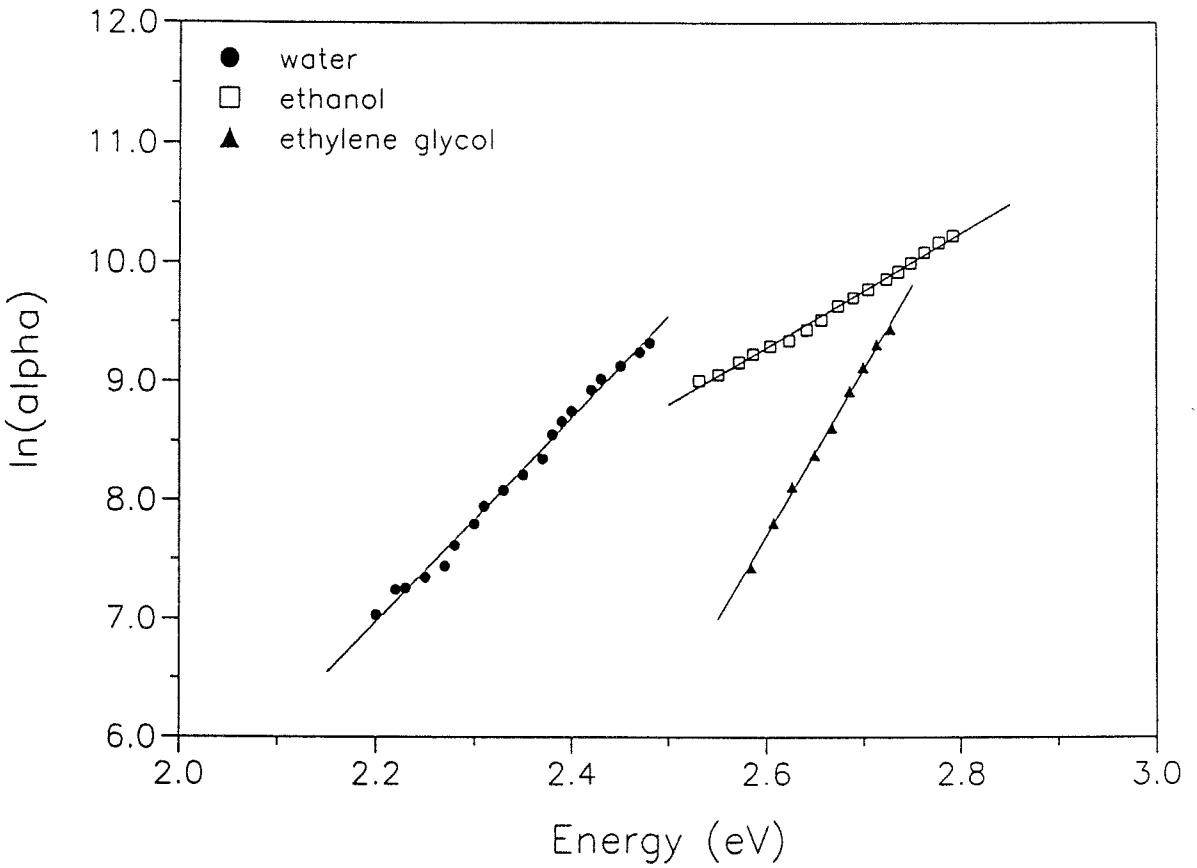

Figure 3: Fits of the tailing edge of the absorption spectra of CdS colloids to the Uhrbach equation.

The values of β for the colloids synthesized in water, ethanol, isopropanol, ethylene glycol and glycerol are 0.22, 0.12, 0.23, 0.36 and 0.13 respectively. These values are considerably lower than the β value (2.13) for bulk single crystal CdS. Ramsden and Gratzel (18) have obtained β value of 0.33 for aqueous CdS, and have attributed the low value to the minute size of the particles, which results in the exposure of many CdS molecules (40% for 50 Å diameter aggregates) to the solvent and to many crystal lattice imperfections. The particles, however, are not amorphous, as the TEM images will show. The aged CdS colloid in isopropanol followed Beer's law for absorption with an extinction coefficient at $\lambda = 350$ nm of $\varepsilon = 1086\ M^{-1}\ cm^{-1}$.

Increasing the concentration of excess metal ions in the case of CdS (Figure 4) resulted in higher energy absorption onsets and therefore smaller particles up to a limit where the effect was offset by an increase in ionic strength due to the metal ion and its counter ions. The excess metal ions chemisorb on the surface during synthesis and attract a cloud of oppositely charged counter ions which increase the double-layer repulsion, stabilizing the particles. As the ionic strength increases, the electrical double-layer is compressed and repulsions are decreased, leading to particle aggregation and precipitation. The effect is more pronounced for ethanol and isopropanol than for ethylene glycol and glycerol. Ethylene glycol and glycerol have larger dielectric strengths and therefore thicker double layers, in addition to their high viscosity which lowers the diffusional rates and slows growth.

Lowering the synthesis temperature gave smaller diameter particles; however, allowing the colloids to warm up to room temperature resulted in rapid precipitation. Absorbance spectra of the precipitated CdS colloids indicated little change in the absorption onset, but a large decrease in overall absorption intensity. Some of these coagulated CdS colloids appeared to redissolve upon stirring and/or sonication. These

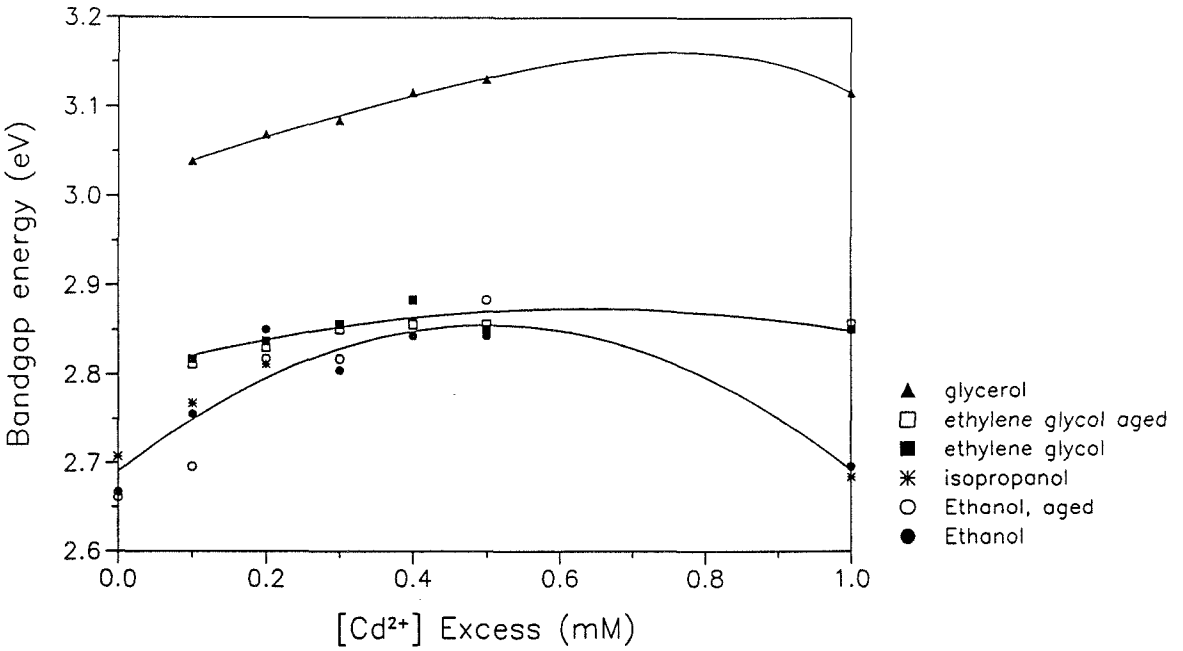

Figure 4: Effect of Excess [$Cd(OAc)_2$] during synthesis upon observed bandgap energy of CdS colloids. [CdS] = 0.2mM.

observations suggest that the precipitation is a coagulative phenomenon rather than a particle-size effect. The observation that a heating period during synthesis (1 hour at 25° C for CdS or 2 hours at 65°C for ZnO) increased both the particle size and the intensity of the visible absorption edge while stabilizing the colloid against precipitation suggests that an annealing of surface defects occurs. At low temperatures, the colloids retain defects which decrease their stability.

Stirring during aging promotes coagulation (i.e., perikinetic flocculation), suggesting that this process is diffusion controlled. Increasing the concentration of CdS created larger particle sizes and lowered stability. The chemical nature of the counter ion affects the size and stability of the colloid. Smaller diameter CdS colloids were obtained when the counter ions were perchlorate than when the counter ions were acetate. However, the colloids with perchlorate as a counter ion were also more susceptible to precipitation. A similar observation was made by Kormann et al. for ZnO (2). The differences in diameter are attributed to kinetically controlled effects on the initial formation of the crystallites.

The fluorescence spectra of the aged colloids consist of a weak green emission (λ_{max} = 520nm) and an intense red emission (λ_{max} = 700 nm). The weak green emission peaks around the bulk bandgap energy and is therefore assigned as the recombination of free electrons and holes (18). The red emission is due to trapped surface states, namely sulfide vacancies. Excess Cd^{+2} ions from the synthesis create sulfide vacancies which act as donors. The low bandgap fluorescence intensities despite high values of absorption indicate the occurrence of rapid radiationless electron/hole recombination and/or the presence of a high concentration of surface defects. The green emission peak shifts slightly to the blue as the solvent is changed from ethanol to isopropanol, as expected since the isopropanolic colloids have smaller diameters and thus a higher bandgap energy.

The intensity of the green emission is much lower in ethylene glycol than in ethanol or isopropanol, due to a higher concentration of surface defects. The green fluorescence intensity of the CdS colloids in ethylene glycol also decreased with time. We attribute this effect to slow coagulation of the colloid at room temperature.

The transmission electron micrographs of aged CdS colloids in ethanol and isopropanol are shown in Figure 5 and Figure 6. Electron diffraction patterns were obtained, which illustrated a moderately diffuse ring structure characteristic of crystalline CdS (Zn-blende cubic structure). Imaging the colloids at a resolution of 2.5 Å shows the majority of the crystallites to have an average dimension of 39 Å for the synthesis in isopropanol and 44 Å for the synthesis in ethanol. A fraction of the crystallites show lattice fringes. The occurrence of such fringes is explained as follows: If a crystallite happens to lie on the substrate such that one of its four <111> directions is in the plane of the substrate, then successive planes of cadmium atoms that are perpendicular to <111> direction lie parallel to the electron beam, and the TEM image directly resolves these planes (5). Direct measurement of the lattice spacing from the fringe patterns gives a lattice spacing of 3.18 Å, which agrees (within 6%) with that of the bulk-phase cubic CdS (3.36 Å). Even though the structure of the colloids is the same as bulk crystalline CdS, the colloids exhibit quantum size effects of a molecular nature. Brus et al. also observed this behavior for ZnS and CdSe (1). The particle sizes determined by TEM for aged CdS colloids in isopropanol and ethanol are slightly larger than the values calculated from the absorption spectra.

Polymerization reactions using Q-sized semiconductor colloids

In all polymerization experiments, blanks consisting of only the monomer and solvent were used to check for the degree of homogeneous polymerization. The

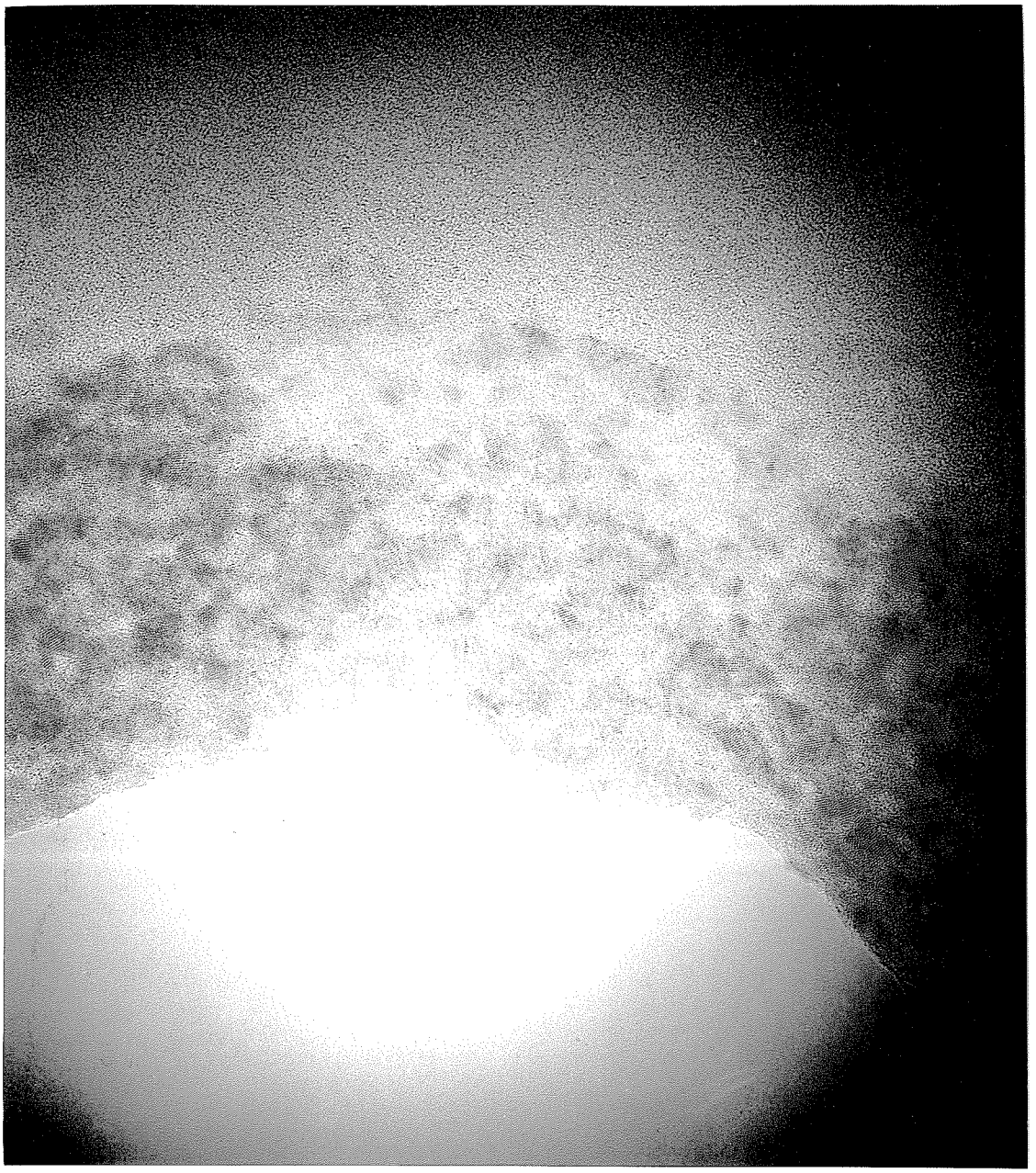

Figure 5: Transmission Electron Micrograph of aged CdS colloid in ethanol. Scale: 1cm = 90.9 Å.

Figure 6: Transmission Electron Micrograph of aged CdS colloid in isopropanol. Scale: 1cm = 90.9 Å.

appropriate excitation wavelengths and intensities were selected by using combinations of bandpass and neutral density filters in order to keep the self-polymerization to < 15% of the total yield. Preirradiation of the colloid followed by injection of monomer yielded no polymer. Thus we can conclude that the initiating radicals are short-lived. Long irradiation times of the colloids without monomer (and also in cases with monomer where no visible polymerization occurs) resulted in eventual precipitation of the semiconductor particles, probably due to photocorrosion. An induction period was observed and was found to depend upon the concentration of oxygen and inhibitors present and the incident light intensity. In the presence of oxygen, the induction period was > 1 hour for methylmethacrylate initiated by illuminated ZnO. Upon degassing with argon, the induction period decreased to < 10 minutes. In the case of CdS and methyl methacrylate, no polymerization was observed after two hours of irradiation in the presence of oxygen. However, after degassing with argon, the same sample had an induction period of < 3 min. It should be noted that the induction period is actually a combination of the time required to destroy inhibitors and the time required to produce sufficient quantities of precipitated polymer so that a white solid is visible. Increasing the light intensity shortened the induction period. This effect may be due to the more rapid destruction of the inhibitors. Vigorous stirring decreased the polymer yield due to enhanced termination rates. In all cases, the polymers were insoluble in the alcoholic solvents, and as the polymerization proceeded a visible white solid formed and the degree of light scattering increased. This increased turbidity resulted in a decrease in the efficiency of photoinitiation. After irradiation, dark periods of up to 24 hours increased the yield of polymer, suggesting the presence of long-lived polymer radicals. The presence of long-lived radicals has previously been observed by Koetsier et al. (32) for the occlusion polymerization of vinyl acetate. This effect has been exploited to make block copolymers. The effect can be explained as follows: in a poor solvent, the propagating radicals coil up and become inaccessible (which slows termination) while propagation continues relatively unhindered

and the reaction mixture may continue polymerizing for days after the discontinuation of illumination.

Monomer survey and polymer characterization

In order to further elucidate the mechanism and reactivity of the semiconductors, a survey of different vinylic monomers using ZnO and CdS was undertaken. The results are shown in Tables 2 and 3. Methyl acrylate, methyl methacrylate, acrylonitrile, and styrene successfully polymerized while isoprene, cinnamamide, dimethylfumarate, allyl alcohol, vinyl acetate, and a-methyl styrene gave no visible product. Acrolein and methylvinyl ketone polymerized, but the products decomposed during acidic washing. In the presence of allyl alcohol, CdS underwent cathodic corrosion to produce Cd(0). Several other commercial monomers were also successfully polymerized; they included TMPTA, TRPGDA, PETA, and Rohamere 6696. The reactivities of vinyl acetate is of special interest. Since vinyl acetate initiates polymerization only via a radical reaction, its lack of polymerization product suggests that the initiation mechanism may be anionic.

Literature values for the activation energies and rate constants of propagation and termination for free radical polymerization reactions allow the calculation of polymerization rates (33). According to simple kinetic theory for a given monomer concentration and initiation rate, the rate of polymerization is proportional to the ratio of the rate constant of propagation to the square root of the rate constant of termination (34). The calculated values of the rate of polymerization decrease in the following order: vinyl acetate > methyl acrylate > acrylonitrile > methyl methacrylate > styrene. However, this predicted order is not consistent with our results as seen in by comparing Tables 2 and 3 with Table 4. The reduction potentials of the monomers in isopropanol are not well known; however, the approximate values are -1.0V, -1.1V, and -1.3V vs. NHE for

CdS

Solvent	Monomer	Time (min)	Yield (g)	% Conversion
Ethanol	Methylmethacrylate	10	0.0173	0.4
Ethanol	Methylmethacrylate	60	0.1221	2.6
Ethanol	Methylmethacrylate	65	0.2021	4.3
Ethanol	Acrylonitrile	120	0.0266	0.7
Ethanol	Acrolein	120	0	▲
Ethanol	Methylvinylketone	60	0	▲
Ethanol	Methylacrylate	67	0	▲
Ethanol	Styrene	168	0.085	1.9
Ethanol	α-methyl styrene	75	0	0.0
Ethanol	Dimethylfumarate	194	0	0.0
Ethanol	Allyl alcohol	158	0	0.0
Ethanol	Isoprene	60	0	0.0
Ethanol	Cinnamamide	160	0	0.0
Ethylene Glycol	Methylmethacrylate	60	1.73	37.0
Isopropanol	Methylmethacrylate	74	0.2311	4.9
Glycerol	Methylmethacrylate	152	0	0.0

▲ = visible polymerization occurred; however, product not isolated.

Table 2: Monomer survey for Q-sized CdS photoinitiation of polymerization.

ZnO

Solvent	Monomer	Time (min)	Yield (g)	% Conversion
Isopropanol	Methylmethacrylate	140	0.4127	8.8
Isopropanol	Methylmethacrylate	90	0.2576	5.5
Isopropanol	TMPTA	60	0.1252	●
Isopropanol	TRPGDA	60	0.2333	●
Isopropanol	PETA	60	0	●
Isopropanol	Rohamere	88	0.0389	●
Ethylene Glycol	Methylmethacrylate	95	0	0.0
Acetonitrile	Methylmethacrylate	61	0	0.0
1-butanol	Methylmethacrylate	67	0.7136	15.2
t-butanol	Methylmethacrylate	72	0.0899	1.9
Ethanol	Methylmethacrylate	107	0.1297	2.8
Methanol	Methylmethacrylate	110	0.0564	1.2
Isopropanol	Methyl Acrylate	60	0	●
Isopropanol	Styrene	60	0	●
Isopropanol	Acrylonitrile	60	0	●
Isopropanol	Vinyl Acetate	60	0	●
Isopropanol	α-Methyl Styrene	60	0	0.0

● = visible polymerization occurred; however, product not isolated.

Table 3: Monomer survey for Q-sized ZnO photoinitiation of polymerization.

Monomer	k_p	k_t
Vinyl Acetate	2.24×10^4	5.36×10^5
Methyl Acrylate	6.22×10^2	1.92×10^6
Styrene	1.25×10^2	2.30×10^6
Methyl Methacrylate	2.05×10^1	9.02×10^5

Monomer	Q	e
α-methyl styrene	0.98	-1.27
Isoprene	3.33	-1.22
Sodium methacrylate	1.36	-1.18
Styrene	1.00	-0.80
Vinyl Acetate	0.03	-0.22
Methyl methacrylate	0.74	0.40
Methyl acrylate	0.42	0.60
Methyl vinyl ketone	0.69	0.68
Acrylonitrile	0.60	1.20

Table 4: Literature values for rates of propagation and termination and the Alfrey and Price Q and e values for selected monomers.

acrylonitrile, methylmethacrylate, and styrene respectively (35). Again, the reduction potentials fail to correlate directly to our results. Another method of analysis involves the Alfrey and Price equation (36).

$$Q_2 = (Q_1/r_1)\exp(-e_1-e_2))$$

which relates a monomer's reactivity to that of a reference species, styrene (Q=1). Q measures the reactivity, r is the ratio of rate constants for monomer-monomer versus monomer-styrene propagation, and e measures the polarity of the monomer. Although the Alfrey and Price equation is used to determine the relative reactivities of two monomers towards copolymerization, the general trend of resonance stabilization and degree of charge of the propagating radical of each individual monomer is reflected in its Q and e values respectively. The monomers that failed to polymerize all had either low Q values or negative e values (Table 4). Of the monomers that did polymerize (methyl acrylate, acrylonitrile, methylvinylketone, methyl methacrylate, acrolein and styrene), the Q values were higher. The yields from methyl acrylate, acrylonitrile, and methyl methacrylate increased in precisely the order of reactivity predicted by the Q values. Acrolein and methylvinylketone produced lower yields than predicted by reactivity due to decomposition of their polymers under washing with acid. A negative e value indicates that the double bond of the monomer possesses a partial negative charge due to electron donating groups and is likely to undergo initiation by a cationic initiator. The low reactivity of those monomers with negative e values also indicates an anionic initiation mechanism. Thus the Alfrey and Price Q and e values provides insight into the observed trends in reactivity.

Further insight into the reaction came via product analysis. The polymers of methylmethacrylate, acrylonitrile, and styrene were characterized by differential scanning calorimetry. The melting and glass transition temperatures agreed well with the literature

values in all three cases as may be seen in Table 5 (37). Analysis of the FTIR spectrum of an optically clear thin film of polymethylmethacrylate produced using ZnO showed no evidence of incorporation of solvent radicals into the polymer chain. The spectrum is also free of residual monomer as evidenced by the absence of the band at 1600 cm^{-1} . The FTIR spectra accurately reproduced the features of published spectra of predominantly syndiotactic polymethylmethacrylate (38). (Fig. 7). Anionic chain mechanisms produce predominantly isotactic PMMA, while free radical chain mechanisms produce syndiotactic PMMA.

GPC analysis of PMMA gave weight-average molecular weights ranging from 10K to 2000K. The molecular weight distributions of polymers isolated after 24-hour dark periods were bimodal. There are several different possible explanations for this apparent bimodality. Bard et al. (22) attributed the observed bimodality to partial homogeneous photopolymerization following light absorption by methylmethacrylate in addition to the heterogeneous semiconductor-initiated pathway; however, in our experiments bandpass filters were used to eliminate light absorption by methylmethacrylate. Odian (33) reported that with superdried styrene monomer, bimodal molecular weight distributions were observed due to the simultaneous occurrence of cationic and radical polymerization mechanisms. Although methylmethacrylate could polymerize via both anionic and radical mechanisms, sufficient water is present in the monomer and solvent to discourage anionic polymerization. In addition the FTIR only shows the presence of syndiotactic PMMA which is produced by a radical mechanism. Methylmethacrylate can undergo termination by both coupling and disproportionation at 25°C (33). Since the kinetic chain length for termination by coupling is twice that of termination by disproportionation, a bimodal weight distribution could be observed. However, this explanation fails to account for the dark-period dependence. The bimodality could be caused by reinitiation of terminated chains or by increasing competition of chain-transfer to solvent at long reaction times. We

Polymer	T_g (C) exptal.	T_m (C) exptal.	T_g (C) lit.	T_m (C) lit.
Methylmethacrylate	90	206		
isotactic			45	160
syndiotactic			115	200
Styrene	54	221		
atactic			-	150
isotactic			-	250
Acrylonitrile	-	244	-	245

Table 5: Glass transition and melting temperatures of polymethylmethacrylate, polystyrene and polyacrylonitrile.

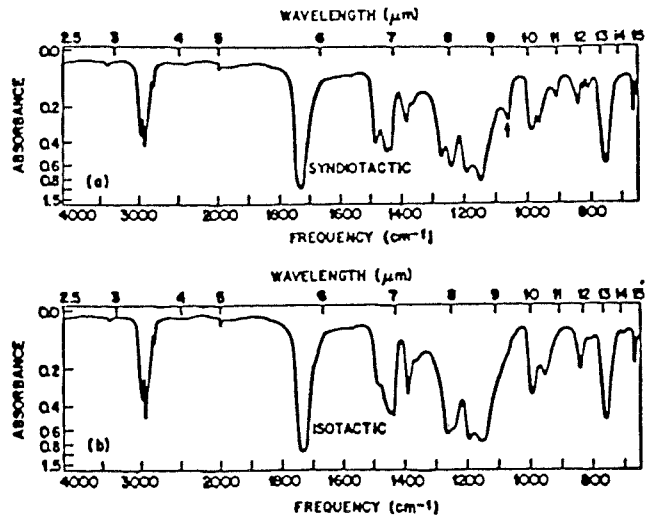

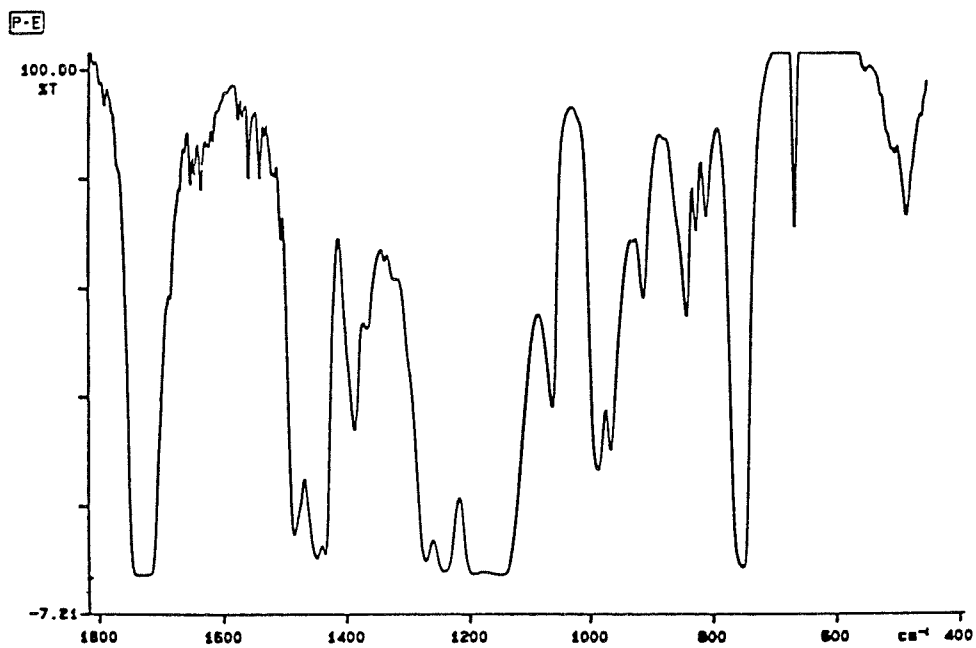

Figure 7: FT-IR spectra of polymethylmethacrylate film produced using q-sized CdS as a photoinitiator. [CdS]=0.05mM, [MMA]=2.34M, isopropanol.

believe the bimodality is most likely caused by the occurrence of both solution and occlusion type polymerization. A similar effect was observed by Brosse et al. for the polymerization of methylmethacrylate in ethanol using hydrogen peroxide as the photoinitiator, and was attributed to reactions occurring in different zones of local monomer concentration (39). The polydispersivity indexes were obtained via GPC from the ratio of the weight-average molecular weight to the number-average molecular weight. The PDI indexes ranged from 1.2 to 5.0. These values are consistent with the values observed in free radical polymerization mechanisms (33).

Solvent survey

The effect of solvent upon the quantum yield of polymerization is shown for ZnO and CdS in Table 6. The rate of polymerization for ZnO increases in the order acetonitrile < methanol < ethanol < isopropanol, which agrees with the redox potentials of the alcohol radicals (40). No polymerization was observed in acetonitrile as expected, since it is not an efficient hole scavenger. The separation of the electron and the hole pair formed upon illumination is necessary for polymerization to occur. The recombination rate is slowed by the solvent acting as an electron donor and trapping the hole. It should also be noted that acetonitrile (and oxygen) can scavenge electrons, which could interfere with anionic initiation. The order in solvent reactivity is not the order of increasing dielectric strength so solvation of the primary radicals is not the major factor controlling the rate of polymerization, and thus an anionic chain mechanism is disfavored. Since the order of reactivity matches the relative order of the redox potentials of the alcohol radicals, this may suggest that the propagating radical species is derived from the alcohol. The rate of polymerization initiated by CdS increases in the order glycerol < ethanol < isopropanol < ethylene glycol. The faster rate in ethylene glycol is most likely due to an

CdS

Solvent	Yield (g)	Time (min)	Intensity (μM hν / min)	Quantum Yield
Glycerol	0	120	200	0
Ethanol	0.1221	60	200	9.7
Isopropanol	0.2311	97	200	16.8
Ethylene Glycol	0.4803	90	200	33.5

ZnO

Solvent	Yield (g)	Time (min)	Intensity (μM hν / min)	Quantum Yield
Acetonitrile	0	61	51	0
Methanol	0.0564	110	53	6.3
Ethanol	0.1297	107	53	14.9
Isopropanol	0.1907	108	52	22.1

Table 6: Effect of solvent upon quantum yield of polymerization of methylmethacrylate using Q-sized CdS or ZnO as photoinitiators.

increase in the viscosity of the solvent (i.e., the higher viscosity decreases termination more than it slows propagation). The lack of polymerization in glycerol is probably due to its extreme viscosity which traps the primary radicals in a solvent cage and causes termination to occur faster than propagation. The reaction in ethylene glycol occurs with two liquid phases. Irradiation of the top methyl methacrylate layer alone produced no polymer; however, irradiation of the CdS/ethylene glycol layer resulted in polymer formation first at the interface and lower layer, and then spreading throughout the top layer. Some yellow color due to CdS was observed in the upper layer. The reaction proceeded more rapidly with stirring similar to emulsion polymerization. This latter effect is to our knowledge the first example of phase transfer photocatalysis in Q-sized semiconductors.

Semiconductor Survey

A comparison of the quantum yields for polymerization of methylmethacrylate in Table 7 for different Q-sized semiconductors in isopropanol with 2.34 M methylmethacrylate revealed that TiO_2 < ZnO < CdS. This observed order parallels the increased reduction potential of the conduction band electron (-0.1 V, -0.2 V, -0.4 V vs. SCE respectively) (41). The quantum yield, Φ, takes into account the light intensity, irradiation time, and the absorption of the semiconductor. We have defined Φ as the number of monomers polymerized divided by the number of photons absorbed (or the rate of polymerization divided by the rate of photon absorption). A comparison of the quantum yields of polymerization of methylmethacrylate for bulk vs. quantum-sized semiconductors is also shown in Table 7. The yields are substantially higher for polymerizations with Q-sized semiconductors. As predicted initially, the Q-sized colloids are more efficient photoinitiators than their large-particle counterparts due to their greater total reactive surface area.

Colloid	Yield (g)	Time (min)	Intensity (μM hν / min)	Quantum Yield
3.75mM TiO_2				
Q-sized	0.105	65	113	8.8
Bulk	0.019	65	113	1.5
0.75mM ZnO				
Q-sized	0.117	60	116	11.0
Bulk	0	60	116	0
0.15mM CdS				
Q-sized	0.231	97	200	16.8
Bulk	0	97	200	0

Table 7: Effect of type of semiconductor upon the quantum yields of polymerization of methylmethacrylate. Isopropanol solvent, [MMA]=2.34M.

Mechanistic Implications

With the results of the monomer survey, polymer characterization, solvent and semiconductor surveys in mind, we propose the following generalized mechanism for semiconductor photopolymerization:

$$CdS + h\nu \rightarrow h_{vb}^{+} + e_{cb}^{-} \quad (5)$$

$$ROH + h_{vb}^{+} \rightarrow ROH\cdot + H^{+} \quad (6)$$

$$e_{cb}^{-} + M \rightarrow M\cdot^{-} \quad (7)$$

$$M\cdot^{-} + H^{+} \rightarrow M\cdot \quad (8)$$

$$M\cdot + M \rightarrow MM\cdot \quad (9)$$

$$ROH\cdot + M \rightarrow M\cdot + RO \quad (10)$$

$$e_{cb}^{-} + O_2 \rightarrow O_2^{-} \quad (11)$$

$$2M\cdot \rightarrow MM \quad (12)$$

The proposed mechanism consists of an anionic initiation by conduction band electrons (either directly or via surface-traps), followed by free radical propagation. The solvent acts as a hole scavenger to prevent electron-hole recombination following UV excitation. The solvent radicals may also act as initiators for the monomer. Polymerization does not

occur in the presence of good electron scavengers (i.e., oxygen or acetonitrile) due to their interference with anionic initiation. Termination occurs by radical-radical recombination.

Conclusions

Stable Q-sized CdS colloids have been synthesized in a variety of solvents. The absorption spectra near the absorption onset fit equations for a direct bandgap transition and for a Uhrbach tailing edge. Average particle diameters are decreased in low dielectric strength or high viscosity solvents. Excess cadmium ions have the greatest effect in synthesis utilizing low viscosity solvents. During the ageing process, the size distribution of the crystallites increases and the degree of lattice imperfections decreases. Factors which limit particle growth by Ostwald ripening or combination (e.g., decreased temperature, no stirring, high viscosity solvents, low dielectric strength solvents, excess cadmium ions) result in smaller diameter aged colloids; however, these same factors decrease the rate of annealing of lattice defects and result in decreased stability of the colloids.

Q-sized semiconductor colloids are capable of photoinitiating polymerization of a wide variety of vinylic monomers via a radical pathway. Our experimental results suggest that the initiation step is anionic and the propagation steps involve free radicals. The scavenging of the valence band holes by the solvent is critical. Reactivity correlates with the reduction potential of the conduction band electron. The Alfrey and Price Q and e values may be used to predict the reactivity of different vinylic monomers. The quantum yields for polymer formation are much higher with Q-sized semiconductors than with bulk size semiconductor powders.

Further research is underway to examine the importance of the surface area and the effect of surface defects upon the quantum efficiency. A detailed investigation of the polymerization of methylmethacrylate using Q-sized ZnO appears in another paper (42).

Acknowledgements

We are grateful to the DuPont Company, Photosystems and Electronic Products Department, for financial support, and we appreciate the assistance of Drs. Detlef Bahnemann and Berhan Tecle in the early stages of this research.

References

1. Brus, L. *J. Phys. Chem.* **1986**, *90*, 2555.

2. Bahnemann, D. W.; Kormann, C.; Hoffmann, M. R. *J. Phys. Chem.* **1987**, *91*, 3789.

3. Kormann, C.; Bahnemann, D. W.; Hoffmann, M. R. *J. Phys. Chem.* **1988**, *92*, 5196.

4. Rossetti, R.; Hull, R.; Gibson, J. M.; Brus, L. E. *J. Chem. Phys.* **1985**, *82*, 552.

5. Rossetti, R.; Ellison, J. L.; Gibson, J. M.; Brus, L. E. *J. Chem. Phys.* **1984**, *80*, 4464.

6. Mills, G.; Zongguan, L.; Meisel, D. *J. Phys. Chem.* **1988**, *92*, 822.

7. Liu, C.; Bard, A. J. *J. Phys. Chem.* **1989**, *93*, 7047.

8. Weller, H.; Fojtink, A.; Henglein, A. *Chem. Phys. Lett.* **1985**, *120*, 552.

9. Itoh, T.; Kirihara, T. *J. Lumin.* **1984**, *31/32*, 120.

10. Ekimov, A. I.; Onushchenko, A. A. *JETP Lett.* **1981**, *34*, 346.

11. Rossetti, R.; Hull, R.; Gibson, J. M.; Brus, L. E. *J. Chem. Phys.* **1985**, *83*, 1406.

12. Kamat, P. V.; Dimitrijevic, N. M.; Fessenden, R. W. *J. Phys. Chem.* **1988**, *92*, 2324.

13. Chestnoy, N.; Hull, R.; Brus, L. E. *J. Chem. Phys.* **1986**, *85*, 2237.

14. Alivisatos, A. P.; Harris, T. D.; Brus, L. E.; Jayaraman, A. *J. Chem. Phys.* **1988**, *89*, 5979.

15. Mills, G.; Henglein, A. *Radiat. Phys. Chem.* **1985**, *26(4)*, 385.

16. Hayes, D.; Micic, O. I.; Nenadovic, M. T.; Swayambunathan, V.; Meisel, D. *J. Phys. Chem.* **1989**, *93*, 4603.

17. Henglein, A. *Chem. Rev.* **1989**, *89*, 1861.

18. Ramsden, J. J.; Gratzel, M. *J. Chem. Soc. Faraday Trans. I* **1984**, *80*, 919.

19. Nosaka, Y.; Ohta, N.; Miyama, H. *J. Phys. Chem.* **1990**, *94*, 3752.

20. Ramsden, J. J.; Webber, S. E.; Gratzel, M. *J. Phys. Chem.* **1985**, *89*, 2740.

21. Kuriacose, J. C.; Markham, M. C. *J. Phys. Chem.* **1961**, *65*, 2332.

22. Krautler, B.; Reiche, H.; Bard, A. J. *J. Polym. Sci., Polym. Lett. Ed.* **1979**, *17*, 535.

23. Eaton, D. F. *Pure Appl. Chem.* **1984**, *56*, 1191.

24. Funt, B. L.; Tan, S. J. *J. Polymer Sci., Polymer Chem. Ed.* **1984**, *22*, 605.

25. Kamat, P. V.; Basheer, R. A.; Fox, M. A. *Macromolecules* **1985**, *18*, 1366.

26. Kamat, P. V.; Todesco, R. V. *J. Polym. Sci.: Polym. Chem. Ed.* **1987**, *25*, 105.

27. Franson, M. A. Ed. "Standard Methods for the Examination of Water and Wastewater," 17th Ed., Port City Press: Baltimore, Maryland, **1989**; 4-192.

28. Heller, H. G.; Langan, J. R. *J Chem. Soc. Perkin Trans.* **1981**, *2*, 341.

29. Weast, R. C.; Astle, M. J. Eds. "CRC Handbook of Chemistry and Physics," 63rd Ed., CRC Press: Boca Raton, Florida, **1982**, B-222.

30. Pankove, J. I "Optical Processes in Semiconductors," Dover Publications: New York, **1971**, 36.

31. Strehlow, W. H.; Cook, E. L. *J. Phys. Chem. Ref. Data* **1973**, *2(1)*, 163.

32. Koetsier, D. W.; Tan, Y. Y.; Challa, G. *J. Polym. Sci., Polym. Chem. Ed.* **1980**, *18*, 1933.

33. Hiemenz, P. C. "Introduction to Polymer Chemistry," Marcel Dekker: New York, **1984**, 345.

34. Odian, G. C. "Principles of Polymerization, 2nd Ed.," Wiley and Sons: New York, **1981**; 179.

35. Funt, B. L.; Williams, F. D. *J. Polym. Sci. : Part A* **1964**, *2*, 865.

36. Brandup, J.; Immergut, E. H. Eds. "Polymer Handbook, 3rd Ed.," Wiley and Sons: New York, **1989**, II-267.

37. Elias, H.-G. "Macromolecules," Plenum Press: New York, Vol. 1, **1984**; 376.

38. Bovey, F. A. "Chain Structure and Conformation of Macromolecules," Academic Press, Inc.: New York, **1982**; 39.

39. Brosse, J-C.; Lenain, J-C.; Gauthier, J-M. *Makromol. Chem.* **1982**, *183*, 2685.

40. Breitenkamp, M.; Henglein, A.; Lilie, J. *Ber. Bunsen-ges. Phys. Chem.* ***1976****, 80,* 973.

41. Fox, M. A. "Topics in Current Chemistry, Vol. 142," Springer-Verlag: Berlin, **1987**; 71.

42. Hoffman, A. J.; Yee, H.; Mills, G.; Hoffmann, M. R.; *J. Phys. Chem.* **1992**, *96,* 5540.

Chapter 4

Photoinitiated Polymerization of Methyl Methacrylate Using Q-Sized ZnO Colloids

[The text of this chapter appeared in A. J. Hoffman, H. Yee, G. Mills, and M. R. Hoffmann, *J. Phys. Chem.* **1992**, *96*, 5540.]

Abstract

The polymerization of methylmethacrylate has been shown to occur readily using Q-sized ZnO semiconductors as photoinitiators. We have examined the effects of solvent, monomer concentration, initiator concentration, light intensity, and semiconductor particle size upon the reaction rates. The reaction pathway appears to be via anionic initiation, followed by free radical propagation steps. The holes formed upon illumination are scavenged by the solvent. Increasing the concentration of the photoinitiator increased the polymer yield until a saturation value was achieved. The rate of polymerization rapidly increased with increasing monomer concentration, due to the Trommsdorf effect. The rate of polymerization was found to depend upon the square root of the incident light intensity, as predicted from simple kinetic theory. Quantum yields of polymerization decreased as particle size decreased, due to either increased surface defects or enhanced rates of competing electron/hole recombination. Under the same experimental conditions, no polymerization occurred with bulk-size ZnO particles as photoinitiators; thus Q-sized ZnO particles were more efficient photoinitiators of polymerization.

Introduction

Previous research efforts in semiconductor photo-assisted polymerization have demonstrated that semiconductors can be used as initiators for radical polymerization reactions (1-4). For example Markham and Kuriacose (1) reported on the photopolymerization of methyl methacrylate in the presence of aqueous suspensions of ZnO, while Bard et al. (2) used a platinized TiO_2 powder to initiate the photopolymerization of methyl methacrylate. In more recent studies, Funt and Tan (3) have demonstrated the polymerization of methylmethacrylate and styrene on solid TiO_2 electrodes, and Kamat and Todesco (4,5) were able to polymerize 1-vinylpyrene on n-type GaAs electrodes and in suspensions of CdS, CdSe, or Fe_2O_3 powders. Although these studies clearly demonstrated the capability of semiconductors to photoinitiate polymerization, the photoefficiencies were limited by the use of solid electrodes or powders with a low surface area and a high degree of light scattering.

Some of these limitations may be overcome by the use of Q-sized semiconductor particles as photoinitiators. The synthesis and characterization of ultrasmall semiconductor particles has been a subject of much interest in recent years (6,7). These small particles, which typically have diameters between 1 and 10 nm, fall into the region of transition between molecular and bulk semiconductor properties. They exhibit shifts of the absorption onset (i.e., bandgap) from the UV for small agglomeration numbers to the visible or near-IR for the bulk material. These shifts are consistent with quantum mechanical calculations that suggest that the energy of the first excited state of the exciton increases as the particle size decreases, thus leading to a blue shift in the absorption spectrum (8). Because of the small particle diameters, colloidal dispersions of Q-sized semiconductors exhibit negligible light scattering. In addition, Q-sized colloids have relatively high surface-area-to-volume ratios and therefore act as better catalysts for

surface-controlled reactions. The increasing bandgap energy with decreasing particle size also provides the ability to influence reactivity by controlling the particle size distribution. Fox (9) has shown that the photoelectrochemical oxidation of the radical cation of diphenylethylene resulted in different reaction products than those obtained by electrochemical oxidation on a metal electrode.

With these studies in mind, we have investigated the polymerization of methyl methacrylate using Q-sized ZnO as a photoinitiator. In our study we have examined the effects of solvent, monomer concentration, light intensity, initiator concentration, and semiconductor particle size upon the rates and quantum yields of polymerization.

Experimental

Chemicals and solvents were reagent grade and were used without any further purification. This included the methylmethacrylate (Aldrich), which contained 10 ppm of hydroquinone monomethyl ether inhibitor that was not removed. Quantum sized ZnO was synthesized according to the methods of Bahnemann et al. (10). 1 mmole of zinc acetate was dissolved with stirring at 50°C into 80-90 ml of isopropanol. After the dissolution the resulting solution was diluted to 920 ml and the temperature lowered to 0°C. Then 80 ml of 0.02 M NaOH was added at 0°C with vigorous stirring. The ZnO colloids were stored up to three months at 4°C (i.e., in isopropanol) with only a small decrease in absorption intensity. The colloids were stabilized by pH-dependent electrostatic repulsion; no chemical stabilizers were added.

The ZnO colloids were characterized by absorption, fluorescence, and transmission electron microscopy. UV/Vis absorption spectra were measured with a Shimadzu MPS-

2000 spectrometer and/or a Hewlett Packard 8451A diode array spectrophotometer. Fluorescence spectra were obtained on a Shimadzu RF 540 spectrophotometer. The resulting absorption bands and edges gave an estimate of particle diameter according to the method of Brus (6). Exact particle size ranges were obtained using a Philips EM 430 transmission electron microscope at 300 kV. Analysis by energy dispersion x-ray techniques were also performed using a EDAX 9900 analyzer and detector. Samples for TEM were prepared by placing 10 microliters of the colloidal suspension onto a substrate consisting of a copper mesh covered with a carbon film. After 30 seconds, the excess liquid was drawn off with a piece of filter paper.

The photolysis apparatus consisted of an Osram XBO 450W xenon lamp in a Muller LX 1450-2 lamp housing or a Kratos 450W xenon lamp. Appropriate bandpass filters were employed to limit the heating of the sample and to select proper irradiation wavelengths. A fan was also employed to cool the sample during irradiation, and a water filter was used to absorb most of the infrared light. Actinometry was performed using Aberchrome 540 according to the method of Heller and Langan (11). Typical light intensities during photolysis were 1.0×10^{-4} einsteins l^{-1} min^{-1} .

The ZnO colloids were used as synthesized with the exception of a series of experiments in which the solvent effects were examined. In these latter experiments, samples of colloid in isopropanol were evaporated in a rotoevaporator to yield thin films of ZnO which were immediately resuspended into the alternate solvents.

The colloid, monomer and solvent were measured volumetrically into a 3 dram glass vial with a magnetic stir bar on the bottom. The vial was capped with a rubber stopper. Samples were degassed for 25 minutes with argon prior to irradiation to reduce the induction period caused by oxygen inhibition. After irradiation, samples were filtered

and then washed with water, 4N HCl, and extra solvent. The acid treatment dissolved the semiconductor colloid and effectively removed it from the polymer. The polymeric products were dissolved in chloroform and washed several times with water and HCl before rotoevaporation to remove the chloroform. This procedure provided the cleanest product as shown by FTIR spectra.

Molecular weights of the polymers were determined by gel permeation chromatography. Samples were dissolved in tetrahydrofuran and injected into the GPC system (i.e., a Waters 410 differential refractometer, and two linear Ultrastyragel columns). Identity of the polymers was confirmed by FTIR using a Perkin Elmer Model 1600 FTIR and by differential scanning calorimetry using a Perkin Elmer Model 4 DSC.

Results and Discussion

Preparation and Characterization of Q-sized Semiconductor Colloids

Absorption spectra of 1mM ZnO in isopropanol at different stages of growth are shown in Figure 1. Shown in Figure 2 is the fit of the absorption onset to the equation for a direct band gap semiconductor (12). As the colloid ages, the absorption onset shifts to longer wavelengths. This size-dependent shift is called the quantum-size effect. The total wavelength shift is about 50 nm. The bulk-phase ZnO bandgap energy is 3.3 eV (13). The average diameter of the aged colloids from our syntheses is 50 A as determined by TEM. Assuming spherical particles and a density of 5.610 g cm^{-3}, this diameter corresponds to an approximate agglomeration number of 2700 ZnO monomers per particle. Electron diffraction of the aged colloid reveals a moderately diffuse ring pattern

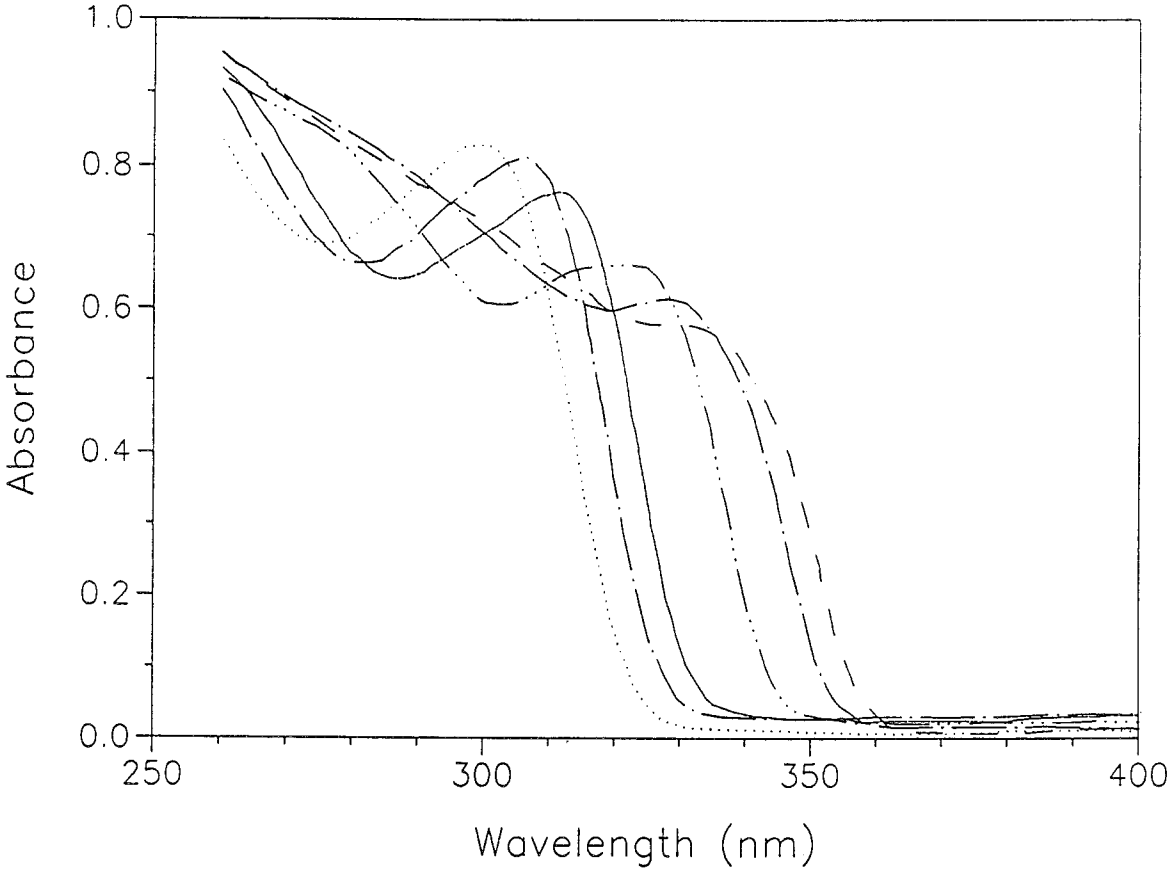

Figure 1: Absorption spectra of 1mM ZnO in isopropanol at different stages of particle growth. Dotted line (·····) is spectrum immediately after mixing $Zn(CH_3COO)_2$ and NaOH at 0 ^oC. Dashed line (----) is spectrum after aging for 2 hours at 65 ^oC.

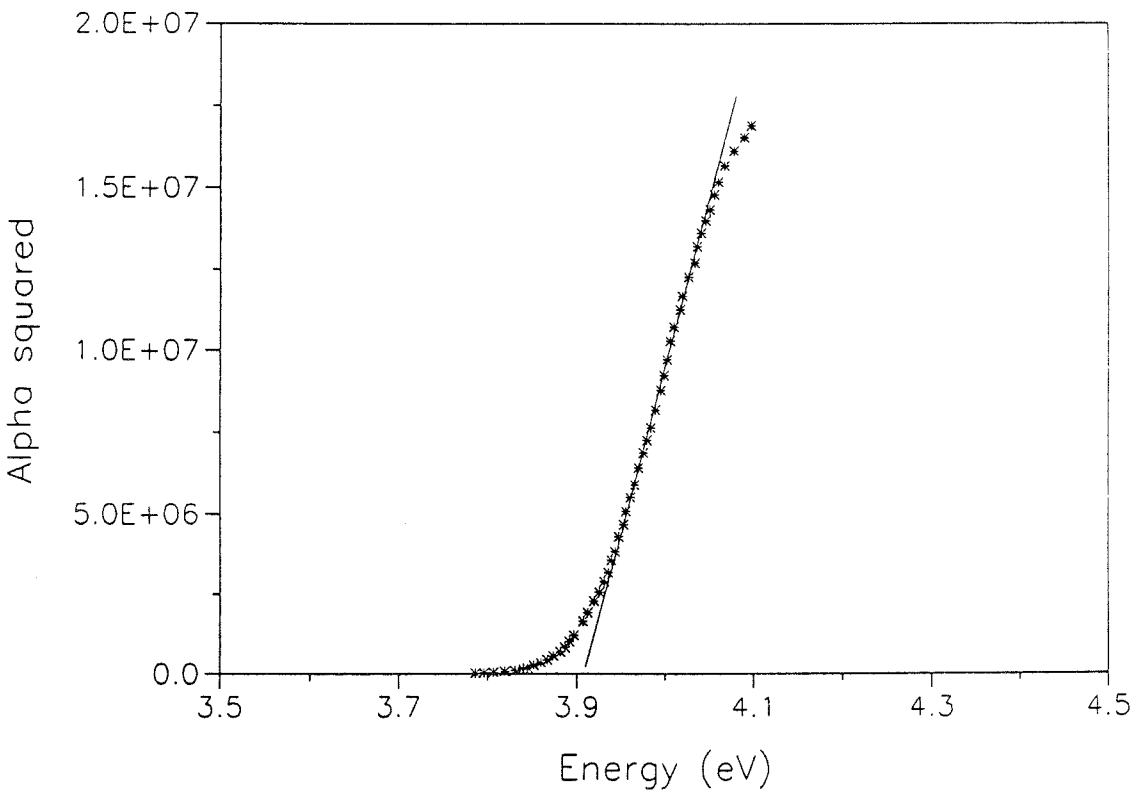

Figure 2: Fit of absorption edge of ZnO to equation for a direct transition.

characteristic of hexagonal wurtzite structure. Spanhel and Anderson (14) also recently observed ZnO crystallites of hexagonal character.

Polymerization reactions using Q-sized semiconductor colloids

In all polymerization experiments, blank samples consisting of only the monomer and solvent were used to check the extent of homogeneous polymerization. The appropriate excitation wavelengths and intensities were selected by using combinations of bandpass and neutral density filters in order to keep the self-polymerization less than 15% of the total yield. Irradiation of the colloid without monomer (and also in cases with monomer where no visible polymerization occurs) resulted in eventual precipitation of the semiconductor particles. Each of the solvents used was a non-solvent for the polymer, so as the polymerization occurred, a milky white color followed by visible precipitate was observed. The time required to produce precipitated polymer was named the apparent induction period. The length of the apparent induction period depended upon the amount of oxygen and inhibitors and the light intensity. In the presence of oxygen, the induction period was more than one hour for methylmethacrylate and ZnO. Upon degassing with argon, the induction period decreased to less than 10 minutes. After irradiation, dark periods of up to 24 hours increased the yield of polymer.

The polymethylmethacrylate product was characterized by differential scanning calorimetry, FT-IR, and GPC. The DSC analysis gave a glass transition temperature and a melting temperature of 90°C and 205°C respectively, which compares favorably with the literature values of 115°C and 200°C for predominantly syndiotactic PMMA (15). Isotactic PMMA exhibits a lower glass transition temperature and melting temperature of 45°C and 160°C, respectively. The FTIR spectra accurately reproduce the earlier published spectra of syndiotactic PMMA (16). Syndiotactic PMMA is observed in free

radical chain mechanisms while isotactic PMMA is produced by anionic chain mechanisms. The polymer was found to be free of residual monomer as indicated by the absence of an IR band at 1600 cm^{-1} . No evidence of incorporation of solvent radicals into the polymer was observed vide infra. The weight-averaged molecular weights varied from 50,000 to 2,000,000 depending upon experimental conditions (Table 1). The weight-average molecular weight (M_W) and the number-average molecular weight (M_n) are given by the following equations:

$$M_W = \frac{\sum N_i (M_i)^2}{\sum N_i M_i} = \frac{\sum A_i M_i}{\sum A_i} \quad \text{and} \quad M_n = \frac{\sum N_i M_i}{\sum N_i} = \frac{\sum A_i}{\sum A_i / M_i} \tag{1}$$

where M_i = molecular weight, N_i = number of molecules having molecular weight M_i, and A_i = the area of slice data corresponding to molecular weight M_i. Some of the polymers obtained exhibited bimodal GPC spectra and thus have two entries in Table 1. The polydispersivity indexes (i.e., the ratio of the weight-average molecular weight to the number-average molecular weight) ranged from 1.2 to 5, which is also typical of chain mechanisms. Note that the workup procedure for the polymer product includes a possible bias towards the high molecular weight species since they are more likely to precipitate from the fluid medium.

Apparent Induction Periods

Since the net induction period is reproducible for a given set of experimental conditions, it is probably not due to impurities in the solvent or to oxygen-degassing procedures. We propose the induction period is a combination of two factors: the time required to destroy the inhibitor and the time required to produce a concentration of

Table IA

Effect of Initiator Concentration Upon GPC Results
MMA = 2.34M, Isopropanol

Experimental Conditions	M_w(K)	M_n(K)	PDI
0.25mM ZnO	1,209	914	1.3
	137	62	2.2
0.4mM ZnO	1,320	1,093	1.2
	162	74	2.2
0.55mM ZnO	1,413	1,255	1.1
	191	76	2.5
0.75mM ZnO	1,080	868	1.2
	99	51	2.0

Table 1: GPC analysis of polymer products: A) Effect of initiator concentration.

Table IB

Effect of Monomer Concentration Upon GPC Results
ZnO = 0.25mM, Isopropanol

Experimental Conditions	M_w(K)	M_n(K)	PDI
1.40M MMA	298	77	3.8
1.87M MMA	361	96	3.8
2.34M MMA	1,209	914	1.3
	137	62	2.2
3.74M MMA	308	139	2.2
4.68M MMA	431	268	1.6

Table 1: GPC analysis of polymer products: B) Effect of monomer concentration.

Table IC

Effect of Irradiation Time Upon GPC Results
ZnO = 0.25mM, MMA = 2.34M, Isopropanol

Experimental Conditions	M_w(K)	M_n(K)	PDI
7 Min.	245	115	2.1
14 Min.	275	137	2.0
26 Min.	484	164	3.0
47 Min.	463	137	3.4
61 Min.	351	68	5.2
90 Min.	452	115	3.9
106 Min.	585	164	3.6

Table 1: GPC analysis of polymer products: C) Effect of irradiation time.

Table ID

Effect of Solvent Upon GPC Results

$ZnO = 0.25mM$, $MMA = 2.34M$

Experimental Conditions	$M_w(K)$	$M_n(K)$	PDI
Isopropanol	1,467	1,234	1.2
	228	109	2.1
Ethanol	1,654	1,060	1.6
	153	94	1.6
Methanol	2,084	1,249	1.7
	76	54	1.4

Table 1: GPC analysis of polymer products: D) Effect of solvent.

precipitated polymer sufficient to be visible to the naked eye. The effects of solvent, semiconductor concentration, monomer concentration, and light intensity upon the apparent induction period were examined.

The induction period increased as the solvent was changed from isopropanol to ethanol to methanol. This is an increase with increasing dielectric strength of solvent. Watanabe and Honda observed a similar effect with ZnO in alcoholic solvents (17): the quantum yield of reduction of methyl viologen decreased as the solvent was changed from ethanol to methanol to water. They suggest the different quantum yields reflect different rates of photocatalytic oxidation of the solvent. Henglein, Gutierrez and Fischer (18) detected the products of the oxidation of alcoholic solvents using Q-sized ZnS and found the same order of efficiency of hole scavenging. The mechanism of removal of the hydroquinone monomethyl ether inhibitor is unknown, since no reaction intermediates were isolated. We propose that the inhibitor is oxidized to produce a di- or tri-hydroxybenzene which is known to act as an inhibitor only in the presence of oxygen (19). The observed trend in induction periods is inconsistent with a competition for holes between the inhibitor and the solvent unless the solvent with the higher dielectric strength binds more strongly to the ZnO surface. Alternatively, the solvent could act as a "hole shuttle," effectively trapping the holes and preventing electron-hole recombination, followed by a slower reaction to remove the inhibitor.

Increasing the concentration of methyl methacrylate shortened the induction period up to a certain concentration, and then higher concentrations lengthened it again. Increasing the concentration of ZnO decreased the induction period. The effect can be explained as follows: with a constant monomer concentration, as the ZnO concentration was increased, the rate of inhibitor destruction increased because more photons are absorbed, and the rate of polymerization was faster because the rate of initiation increases

as the ZnO concentration increases. The net effect is that the induction period is shortened. With a constant ZnO concentration at very low concentrations of MMA (i.e., low inhibitor concentrations), the time required to destroy the inhibitor is less, but the rate of polymerization is also less because of the lower monomer concentration. Of these two opposing effects, the slower rate of polymerization predominates and the induction period is lengthened. Increasing the concentration of MMA increases the rate of polymerization more than the counter effect of increasing inhibitor and the induction period shortens. When the concentration of MMA is relatively high, the ratio of the concentration of inhibitor to ZnO is high, and then the rate of inhibitor destruction becomes a major factor that outweighs the increased rate of polymerization. For a given time period, if the inhibitor is not totally degraded, no polymer forms and the expected rate of polymerization is irrelevant. With degassed 0.25mM ZnO and 4.68mM MMA, no initiation is seen in one hour.

The induction period did not depend strongly upon light intensity. For example, as the light intensity was decreased from 1.9×10^{-4} einsteins min^{-1} l^{-1} to 5.0×10^{-4} einsteins min^{-1} l^{-1}, the induction period was increased slightly from 9 minutes to 14 minutes. Both the rate of destruction of inhibitor and the rate of polymerization are expected to be slower at lower light intensities.

Yield of Initiating Radicals

Ramsden and Gratzel (20) observed rapid reduction of MV^{+2} by semiconductor-initiated electrons in an isopropanolic TiO_2 system. The quantum yield of MV^{2+}/MV^{+} reduction was 100%. This result suggests a method to estimate the quantum yield of initiation in our system. A solution of methylviologen and Q-sized ZnO was degassed, then irradiated, and the absorption spectrum monitored. As MV^{2+} is reduced in the

absence of oxygen (E^0 = -440 mV vs. NHE), a concomitant blue color is observed with two peaks in the absorbance spectrum, λ_{max} = 398 nm with an ε = 41100 $M^{-1}cm^{-1}$ and λ_{max} = 602 nm with an ε = 13800 $M^{-1}cm^{-1}$ in ethanol (17). The presence of an effective electron donating solvent is necessary to scavenge the hole and to prevent recombination. The E^0 for the oxidation of isopropanol radicals to acetone is +1.8V; therefore, the solvent radicals can also reduce methylviologen directly. The absorbance spectra showed no evidence for the further reduction of MV^+ to MV^0 and the quantum yields calculated from the loss of MV^{2+} absorbance at 260 nm (ε = 18300 $M^{-1}cm^{-1}$) agreed within 10% to the quantum yields calculated from the rise of MV^+ absorbance at 602 nm. The plot of the concentration of MV^+ versus irradiation time was linear up to 100 seconds of illumination. The quantum yield of MV^+ formation is given by the equation:

$$\Phi = \frac{\Delta A}{\Delta t \varepsilon I_a} \qquad (2)$$

where $I_a = I_0(1-10^{-A})$ is the absorbed photon intensity. Assuming that the quantum yield for the solvent radicals reducing methylviologen is also 100%, then the quantum yield of initiation is 0.097 with the convention that the quantum yield of MV^+ formation is twice the quantum yield of initiation since two radicals are formed per photon absorbed. Analysis of a data recently published by Rabani (21) for a similar experiment gave a value of 0.167, which is higher due to the lower absorbed light intensity utilized. Nosaka et al. (22) demonstrated for Q-sized CdS as the photon density increased, the quantum yield of formation of MV^+ decreased due to faster rate of electron-recombination which competes with electron transfer. This value of the quantum yield of initiation is an upper limit.

Effect of Concentration of ZnO

Figure 3 shows the polymer yield as a function of concentration of ZnO. The yield increased as the concentration of ZnO increased until a saturation value was obtained. This saturation effect cannot be attributed to a saturation of surface sites by MMA/inhibitor because this would require a minimum of 6.3 X 10^6 methylmethacrylate sites per ZnO particle. The effect is also not due to saturation of the colloid absorption because even at the highest concentration not all of the incident photons are absorbed. Likewise an increase in surface-mediated recombination reactions similar to those in a homogenous solvent cage fails to explain the saturation phenomenon because the increased ZnO concentration results in fewer photon hits per particle. The most likely explanation is that at higher concentrations of ZnO, the primary radicals begin to compete with the monomer for the propagating radicals, and the apparent high molecular weight polymer yield levels off.

Both the weight-averaged molecular weights and the number-averaged molecular weights increased as the concentration of ZnO was increased up to 0.75 mM ZnO. The number-averaged molecular weight divided by the molecular weight of the monomer is proportional to the kinetic chain length, which also equals the ratio of the rate of propagation to the rate of initiation. According to the simple rate equations for initiation and propagation, the kinetic chain length should decrease as the concentration of ZnO increases and the absorbed photon flux increases. The opposite trend is actually observed in this case. For this to occur the rate of polymerization must increase faster than the rate of initiation as the ZnO is increased, and thus either the rate constant of polymerization is a function of ZnO or the initiator efficiency decreases as ZnO increases (i.e., the primary radicals are trapped more efficiently on the surface as the number of ZnO surface sites is increased).

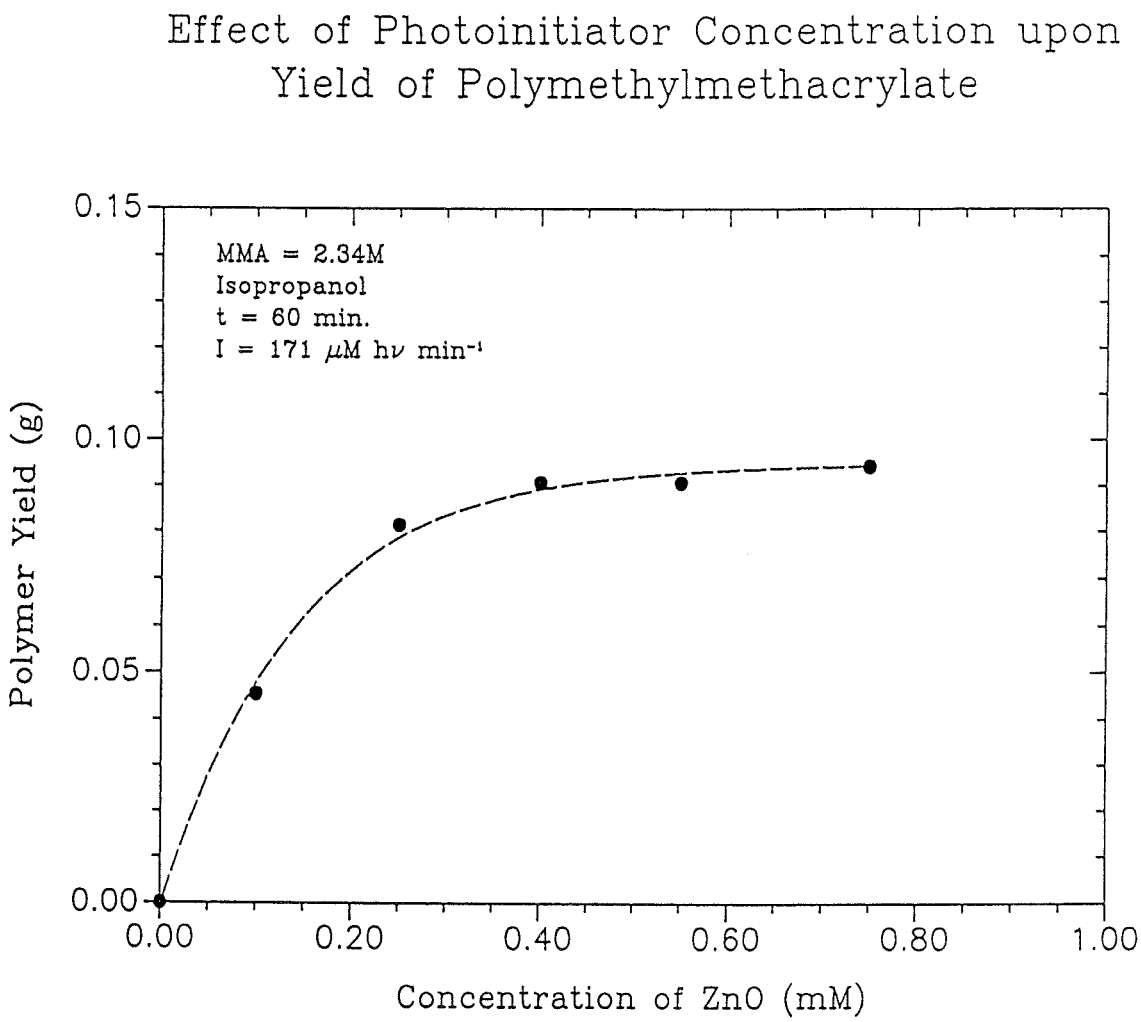

Figure 3: Effect of photoinitiator concentration upon yield of polymethylmethacrylate.

Effect of Monomer Concentration

Figure 4 illustrates the dependence of polymer yield on the concentration of methylmethacrylate. The observed trend is complex. The yield increases initially as [MMA] increases to 3.4M. It then reaches a maximum, followed by a decrease with increasing monomer concentration. In an ideal system, the rate of polymerization should increase as the monomer concentration increases. However, in the real system the monomer contains an inhibitor which serves to lower the yield at high concentrations. Since the amount of ZnO is constant, longer induction periods occur with increasing inhibitor concentrations. These opposing factors lead to an apparent maximum in the yield vs. [MMA] curve. Attempts to subtract the induction period and then to recalculate the yields based on an absolute polymerization time gave an almost exponential increase in yield with concentration of methylmethacrylate. A plot of the corrected rate of polymerization vs. the concentration of MMA (Figure 5) is linear for the first three points and then rapidly increases. The rapid increase is most likely due to the Trommsdorf effect (18). At high percent conversions the viscosity of the solution increases and termination reactions are slowed more than propagation with a net result of an acceleration of the rate of polymerization. This effect has been observed in highly concentrated (i.e., 25-100%) MMA solutions. MMA concentrations were as high as 50% in our experiments, and the acceleration was observed at low percent conversion (2%). Burnett and Loan (23) have observed in occlusion polymerization the acceleration occurs at much lower percent conversions than in the homogeneous case. In a poor solvent, the growing polymer tends to coil up and precipitate, making termination reactions more difficult to achieve. Propagation occurs inside the precipitated center, where the local concentration of monomer is high. Support for this theory comes from the observation that the yield and molecular weights of polymer increased during post-irradiation dark periods, indicating the presence of long-lived radicals.

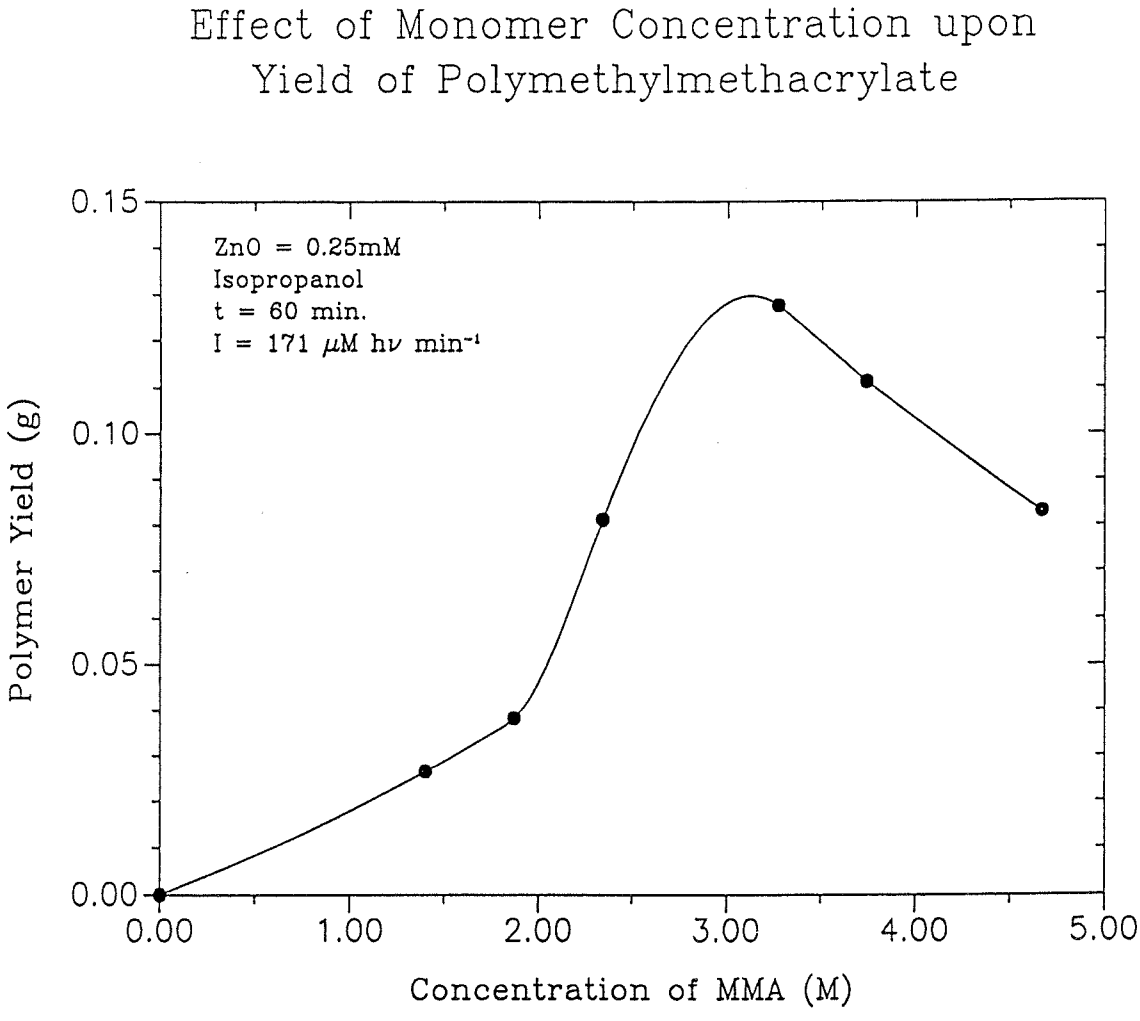

Figure 4: Effect of monomer concentration upon yield of polymethylmethacrylate.

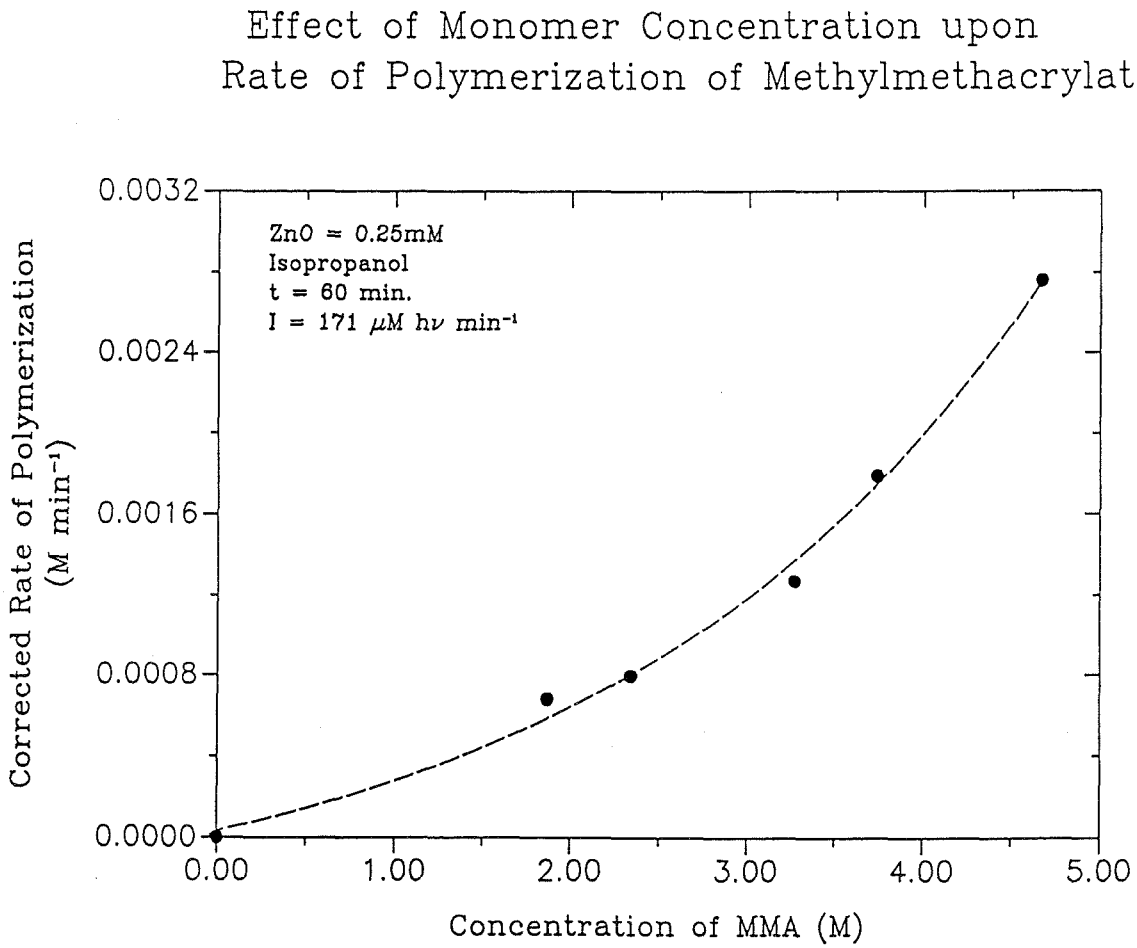

Figure 5: Effect of monomer concentration upon rate of polymerization of methylmethacrylate.

The kinetic chain length increases as the concentration of MMA increases, as expected since the rate of polymerization increases with increasing MMA and the rate of initiation decreases due to the increasing amount of inhibitor.

Effect of Light Intensity

The effect of light intensity upon the induction period has already been discussed. The plot of the rate of polymerization versus the square root of light intensity shown in Figure 6 is linear. The linear relationship of Figure 6 is predicted by simple theory assuming the mechanism of equations 3-10.

$$ZnO + h\nu \rightarrow h_{vb}^{+} + e_{cb}^{-} \quad (3)$$

$$ROH + h_{vb}^{+} \rightarrow ROH\cdot + H^{+} \quad (4)$$

$$e_{cb}^{-} + M \rightarrow M\cdot^{-} \quad (5)$$

$$M\cdot^{-} + H^{+} \rightarrow M\cdot \quad (6)$$

$$M\cdot + M \rightarrow MM\cdot \quad (7)$$

$$ROH\cdot + M \rightarrow M\cdot + RO \quad (8)$$

$$e_{cb}^{-} + O_2 \rightarrow O_2^{-} \quad (9)$$

$$2M\cdot \rightarrow MM \quad (10)$$

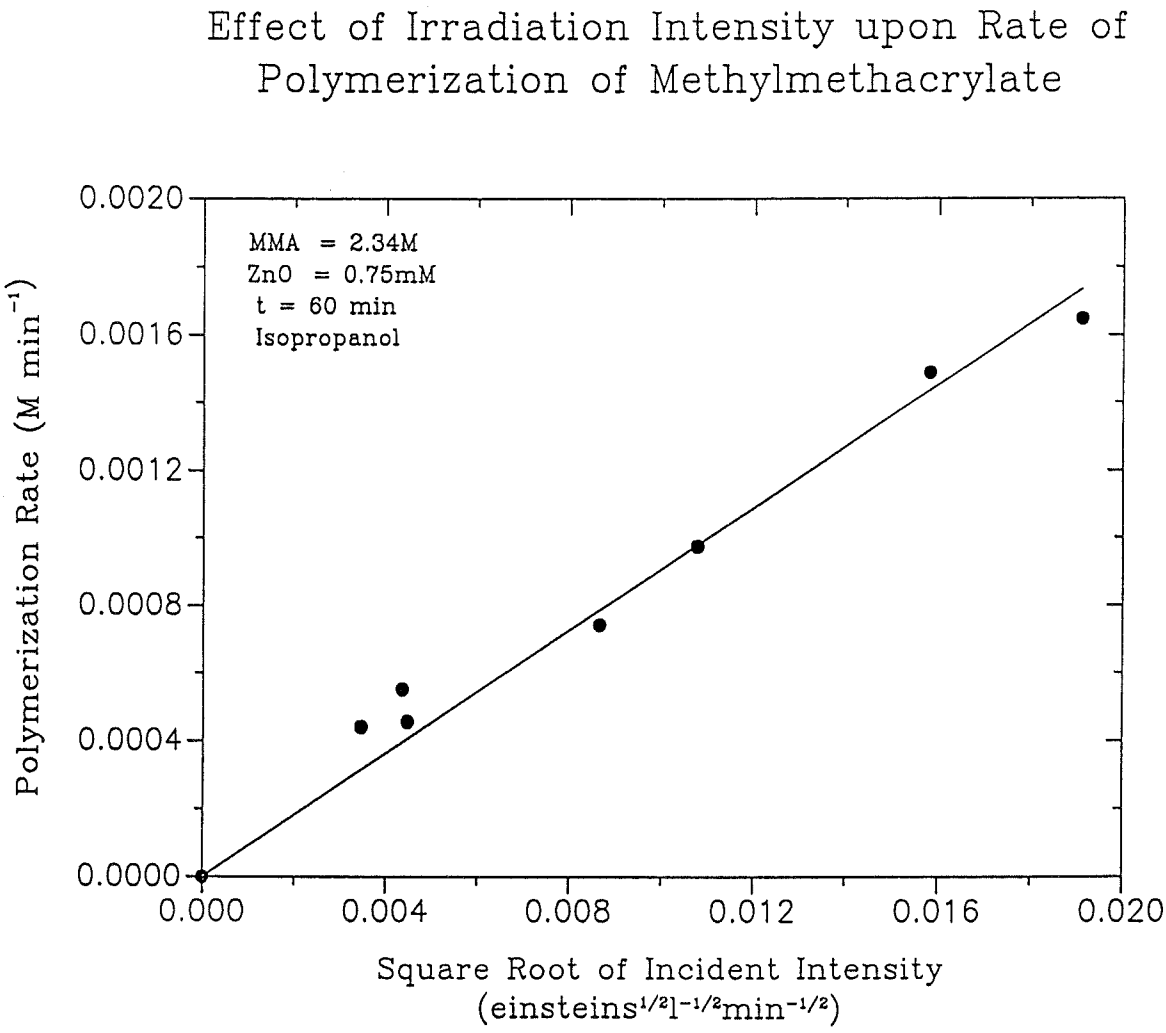

Figure 6: Effect of irradiation intensity upon rate of polymerization of methylmethacrylate.

It should be noted that the anionic initiation of the monomer may not occur directly via the conduction band electrons, since the reduction potential of methylmethacrylate is approximately -1.1V vs. NHE (24) and the E_{CB} of bulk ZnO is -0.3 V vs. NHE (pH 8) (25). Haase et al. (26) have shown that electrons are stored on the surface of ZnO upon UV illumination. They suggest that the stored electrons are either present in traps or in the form of Zn^{+} ions, which have a very negative redox potential (< -2.0 V). Thus, these stored electrons may initiate polymerization. For the purpose of our simple kinetic model, we have written the reaction as a direct. The kinetic expressions for the rate of initiation, propagation and termination of radical chain reactions are given in equations 11-13 (19). The rate of initiation is given by:

$$R_i = \Phi_i I_0 (1-10^{-A}) = \Phi_i I_a = \frac{dM\cdot}{dt} \qquad (11)$$

where Q_i is the quantum yield of initiation, I_0 and I_a are the incident and absorbed light intensity, M· is the initiated monomer, and A is the absorbance of the semiconductor; the rate of propagation is expressed as

$$R_p = k_p [M\cdot] [M] \qquad (12)$$

where k_p is the rate constant of propagation; and the rate of termination is written as

$$R_t = k_t [M\cdot]^2 \qquad (13)$$

where k_t is the rate constant of termination. Under the steady-state approximation the rate of initiation (eq. 11) equals the rate of termination (eq. 13). Equating these rates allows us to express the steady state concentration of M· as

$$[M\cdot] = k_t^{-1/2} (\Phi_i I_0 (1-10^{-A}))^{1/2} \quad (14)$$

Substituting eq. 14 into eq. 12 gives us an equation for the rate of polymerization as follows:

$$Rp = k_p k_t^{-1/2} [M] (\Phi_i I_0 (1-10^{-A}))^{1/2} \quad (15)$$

At low percent conversions, the monomer concentration remains essentially constant, so the ratio of the rate constant for propagation to the square root of the rate constant of termination may be calculated from the slope of Figure 6. This yields $k_p/k_t^{-1/2} = 1.23 \times 10^{-1}$ $M^{-1/2}$ $s^{-1/2}$.

Time- evolution of Yield

In another series of experiments, the polymer yield as a function of irradiation time was examined (Figure 7). A plot of the $\ln(MMA/MMA_0)$ versus time has two linear regions, indicating a first-order dependence of the rate of polymerization on the concentration of methylmethacrylate at low degrees of conversion. The ratio of the rate constant of propagation to the square root of the rate constant of termination may be calculated from the slope; thus $k_p/k_t^{-1/2} = 1.40 \times 10^{-1}$ $M^{-1/2}$ $s^{-1/2}$. At higher percent conversions the value is 2.34×10^{-1} $M^{-1/2}$ $s^{-1/2}$. The larger slope at later times is due to the decrease in the rate constant of termination in the occluded polymer. These values may be compared to the value calculated from literature for homogeneous polymerization of 2.5×10^{-2} $M^{-1/2}$ $s^{-1/2}$ (18).

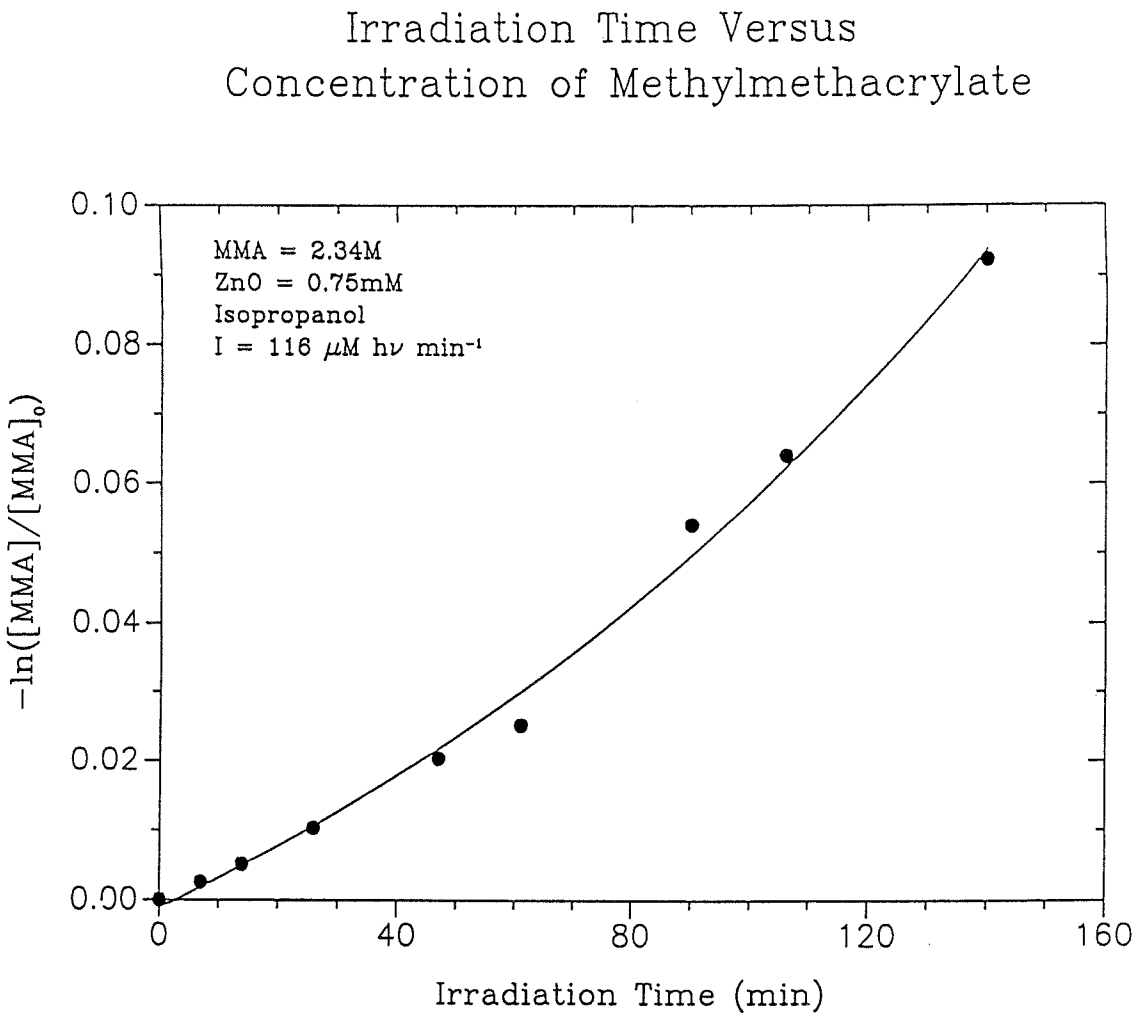

Figure 7: First order plot of irradiation time versus concentration of methylmethacrylate.

GPC analysis of the polymer molecular weights revealed that initially both the weight-averaged and number-averaged molecular weights increased, then after 60 minutes of irradiation time they decreased. The molecular weight distributions increased in width with increasing irradiation times. Bimodal molecular weight distributions were observed in polymers that were stored in the dark after illumination and prior to workup. In this case, the larger molecular weight peak was much higher than the molecular weight obtained from the polymers with no dark period, while the lower molecular weight peak was slightly lower. This suggests that the polymerization that continues in the dark is subject to very few termination reactions. The polydispersivity indexes for low percent conversions and no dark periods were 1.5, which is the theoretical value for termination by recombination. Since the scattering of light increases as polymer precipitates, the kinetic chain length should increase due to the slower rate of initiation. This could be offset by a decreasing rate of propagation due to less monomer and more chain transfer reactions.

Effect of Solvent

The effect of solvent upon the quantum yield of polymerization is shown for ZnO in Table 2. The rate of polymerization for ZnO increases in the order acetonitrile < methanol < ethanol < isopropanol, even when corrected for the differences in induction periods. Since the light intensities were constant, the solvent dependence reflects differences in the rate of polymerization. For ionic chain mechanisms, rates are relatively sensitive to the nature of the solvent (i.e., they are faster in more polar solvents). We observed a lower polymerization rate with an increasing polarity of the solvent. Free radical chain mechanisms are less sensitive to solvent polarity. The chain transfer ability of the solvent increases in the same order as the yields. The more the contribution of chain transfer to the reaction, the lower the molecular weights and yield of precipitated polymer.

Table II
Effect of Solvent Upon Polymerization

Solvent	Yield (g)	ZnO Time (min)	Intensity (μM hν/min)	Φ Corr
Acetonitrile	0.0	61	51	0
Methanol	0.0564	110	53	6.3
Ethanol	0.1297	107	53	14.9
Isopropanol	0.1907	108	52	22.1

Table 2: Effect of solvent upon polymerization of methylmethacrylate.

The solvent with the lowest chain transfer coefficient did produce the highest molecular weights (and the lowest yield), but this could also be due to the effect of shorter net polymerization times since the induction period was longer. The order of increasing yield also follows the trend in increasing hole-scavenging efficiency of the solvent (17,18). No polymerization was observed with acetonitrile as a solvent as expected, since it is not an efficient hole scavenger.

Copolymerization of Methylmethacrylate and Styrene

To provide insight into the mechanism of polymerization, methylmethacrylate and styrene were copolymerized in isopropanol using Q-sized ZnO as the photoinitiator. The monomer reactivity ratios, r_1 and r_2, have been evaluated at different temperatures and with different solvents (27,28). The ratio of the rate constants for the reaction of an M_1-type radical with M_1 and M_2 respectively, while r_2 is the ratio for the reaction of an M_2-type radical with M_2 and M_1 respectively. The different r_1 and r_2 values give rise to large differences in the composition of the copolymer depending on the mode of initiation. Methylmethacrylate shows increased reactivity in anionic copolymerization and decreased reactivity in cationic polymerization. The opposite effect is observed for styrene. If an equimolar mixture of methylmethacrylate and styrene is polymerized via a free radical mechanism, the copolymer is 50% methylmethacrylate and 50% styrene. For the same mixture under an anionic mechanism, the copolymer is almost pure methylmethacrylate. When a 50:50 mixture of methylmethacrylate and styrene were polymerized in isopropanol, the copolymer product had a percent carbon of 74.9%, which is indicative of the free radical mechanism.

Particle Size Effect upon Yield

MMA polymerizations were carried out with different size fractions of ZnO colloid. The results are shown in Figure 8. The quantum yields corrected for the absorbance of the colloid increased as the average size of the particle distribution increased. If the reaction were surface-mediated, increasing the total surface area by decreasing the particle size should increase the rate. This was the opposite of what was actually observed and contradicts the results of Nosaka et al. for Q-sized CdS and MV^{2+} (22). In our case, the small diameter particles were not annealed to remove the surface site defects, which act as low energy electron traps and decrease the efficiency of electron transfer. In addition, the small diameter particles may also have inherently faster rates of electron/hole recombination so that the rate of initiation is less and the yield is lower. This agrees with Warnock and Awschalom (29), who observed shorter exciton lifetimes for CdS as crystallite size decreased in colored glasses. With bulk-size ZnO particles (i.e., 0.1 to 1.0 mm) no initiation was observed and no polymer was formed. Thus above a critical size range the surface area appears to have a demonstrable effect.

Conclusions

Our results show the polymerization of methylmethacrylate occurs readily using Q-sized ZnO semiconductors as photoinitiators. The reaction pathway appears to involve hole scavenging by the solvent and anionic initiation by the electrons. The experimental results mimic many of the features of free radical homogeneous polymerization reactions; however, the rate constants are found to be higher. Increasing the concentration of the photoinitiator, ZnO, increases the polymer yield until a saturation value is achieved. The rapid increase in polymerization rate with increasing concentration of methylmethacrylate

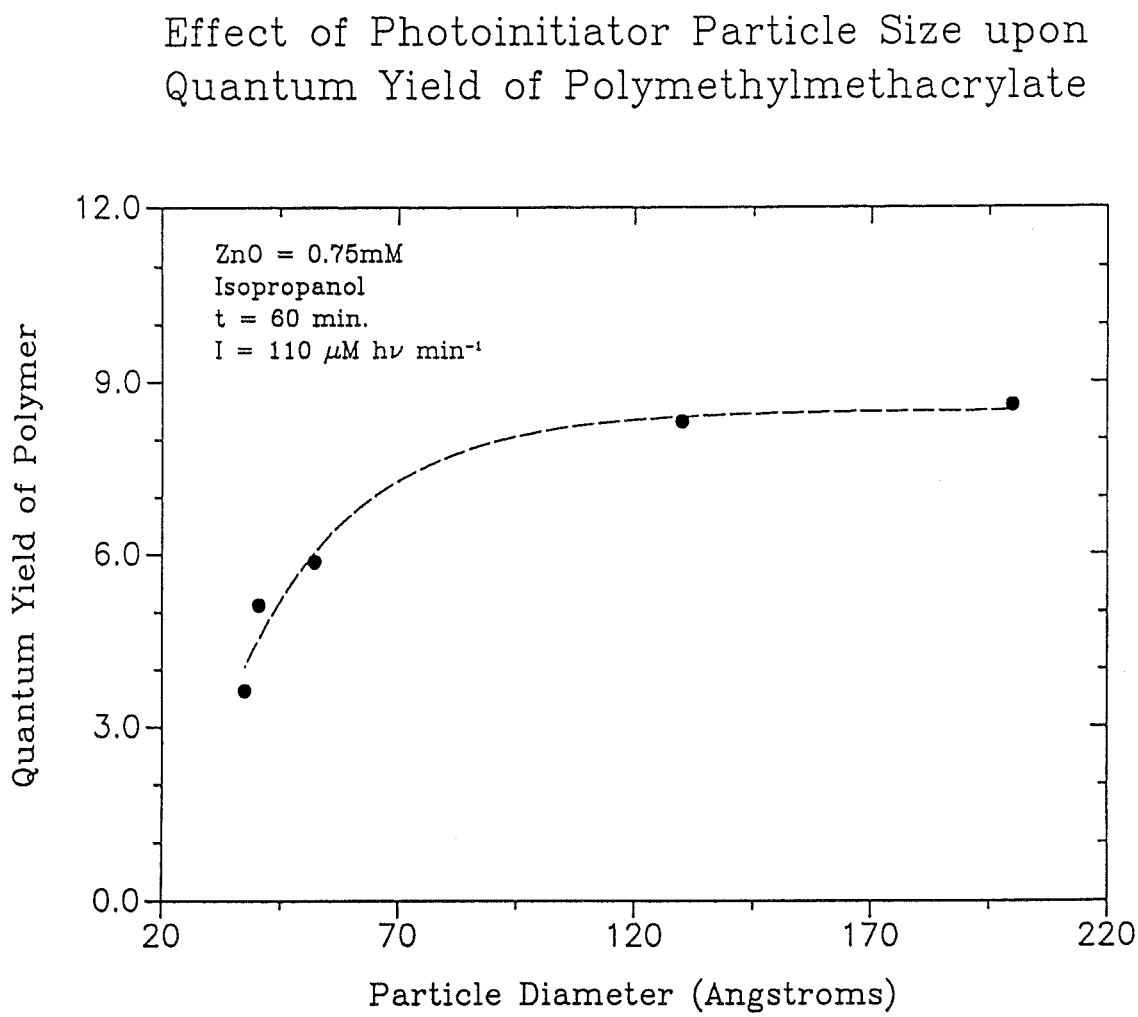

Figure 8: Effect of photoinitiator particle size upon quantum yield of polymethylmethacrylate.

is due to an early onset of the Trommsdorf effect. The primary radicals generated by illumination add to a monomer molecule dissolved in the alcohol phase. With the growth of the polymer chain by propagation, some critical chain size is reached at which the oligomers are no longer soluble, and precipitated polymer is observed. Polymerization can continue both inside the precipitated centers and in the bulk alcoholic solvent. Polymerization inside the precipitated centers is subject to a decreased rate of termination and a high local concentration of monomer, resulting in an acceleration of overall polymerization rates. The rate of polymerization depends upon the square root of incident light intensity, as predicted from simple kinetic theory. The quantum yields of polymerization decreased as the particle size decreased, due to either increased surface defects or enhanced rates of competing electron/hole transfer. Under the same experimental conditions, no polymerization occurred with bulk-size ZnO particles. Further experiments are needed to determine whether this inability of larger particles to initiate polymerization is an effect of decreased surface area or an effect of lower driving force due to decreased reduction potential of the conduction band electron.

Acknowledgements

We are grateful to the DuPont Company, Photosystems and Electronic Products Department, for financial support, and we appreciate the assistance of Drs. Detlef Bahnemann and Berhan Tecle in the early stages of this research.

References

1. Kuriacose, J. C.; Markham, M. C. *J. Phys. Chem.* **1961**, *65*, 2332.

2. Krauetler, B.; Reiche, H.; Bard, A. J. *J. Polym. Sci. Polym. Lett. Ed.* **1979**, *17*, 535.

3. Funt, B. L.; Tan, S. *J. Polym. Sci. Polym. Lett. Ed.* **1984**, *22*, 605.

4. Kamat, P. V.; Basheer, R. A.; Fox, M. A. *Macromolecules, 1985,* **18**, 1366.

5. Kamat, P. V.; Todesco, R. V. *J. Polym. Sci. Polym Chem. Ed.* **1987**, *25*, 1035.

6. Henglein, A. *Chem. Rev.* **1989**, *89*, 1861.

7. Gratzel, M. "Heterogeneous Photochemical Electron Transfer," CRC Press: Boca Raton, Florida, **1989**, 87.

8. Brus, L. *J. Phys. Chem.* **1986**, *90*, 2555.

9. Fox, M. A. "Topics in Current Chemistry, Vol. 142," Springer-Verlag: Berlin, **1987**, 71.

10. Bahnemann, D. W.; Kormann, C.; Hoffmann, M. R. *J. Phys. Chem. 1987, 91*, 3789.

11. Heller, H. G.; Langan, J. R. *J Chem. Soc. Perkin Trans.* **1981**, *2*, 341.

12. Pankove, J. I. "Optical Processes in Semiconductors," Dover Publications: New York, **1971**, 36.

13. Strehlow, W. H.; Cook, E. L. *J. Phys. Chem. Ref. Data* **1973**, *2(1)*, 163.

14. Spanhel, L.; Anderson, M. A. *J. Am. Chem. Soc.* **1991**, *113*, 2826.

15. Elias, H.-G. "Macromolecules, Vol. 1," Plenum Press: New York, **1984**, 376.

16. Bovey, F. A. "Chain Structure and Conformation of Macromolecules," Academic Press, Inc.: New York, **1982**, 39.

17. Watanabe, T.; Honda, K. *J. Phys. Chem.* **1982**, *86*, 2617.

18. Henglein, A.; Gutierrez, M.; Fischer, C.-H. *Ber. Bunsenges. Phys. Chem.* **1984**, *88*, 170.

19. Odian, G. G. "Principles of Polymerization," 2nd ed.; John Wiley and Sons: New York, **1981**, 179.

20. Ramsden, J. J.; Gratzel, M. *J. Chem. Soc. Faraday Trans. 1*, **1984**, *80*, 919.

21. Rabani, J. *J. Phys. Chem.* **1989**, *93*, 7707.

22. Nosaka, Y.; Ohta, N.; Miyama, H. *J. Phys. Chem.* **1990**, *94*, 3752.

23. Burtnett, G. M.; Duncan, G. L. *Makromol. Chem.* **1962**, *51*, 154.

24. Funt, B. L.; Williams, F. D. *J. Polym. Sci. : Part A* **1964**, *2*, 865.

25. Gerischer, H. *Topics in Applied Physics* **1979**, *31*, 115.

26. Haase, M.; Weller, H.; Henglein, A. *J. Phys. Chem.* **1988**, *92*, 482.

27. Lewis, F. M.; Walling, C.; Cummings, W.; Briggs, E. R.; Mayo, F. R. *J. Am. Chem. Soc.* **1948**, *70*, 1519.

28. Mayo, F. R.; Lewis, F. M. *J. Am. Chem. Soc.* **1944**, *66*, 1594.

29. Warnock, J.; Awschalom, D. D. *Appl. Phys. Lett. 1986, 48(6)*, 425.

Chapter 5

Photocatalytic Production of Hydrogen Peroxide and Organic Peroxides on Quantum-Sized Semiconductor Colloids

[The text of this chapter has been submitted to *Env. Sci. Technol.* **1993**.]

Abstract

Aqueous, oxygenated suspensions of quantum-sized ZnO particles with added hole scavengers are shown to produce steady-state hydrogen peroxide concentrations as high as 2 mM upon bandgap irradiation. Maximum hydrogen peroxide concentrations are observed only with added hole scavengers. The order of efficiency of hole scavengers is: formate > oxalate > acetate > water > citrate. Isotopic labeling experiments are consistent with the hypothesis that hydrogen peroxide is produced directly by the reduction of adsorbed oxygen by conduction band electrons. Quantum yields for H_2O_2 as high as 30% are observed at the lowest illumination intensities. The quantum yield is shown to follow an inverse square-root dependency on absorbed light intensity. The quantum yield also varies as a function of the light excitation wavelength. The initial rate of H_2O_2 production is 100 to 1000 times faster with Q-sized particles (D_p = 4-5 nm) than with bulk ZnO particles (D_p = 10-1000 μm). The quantum yield of H_2O_2 production increases as the Q-sized particle diameter decreases.

Introduction

Hydrogen peroxide plays a significant role as a primary oxidant in environmental systems, as indicated by a recent review of the atmospheric chemistry of peroxides (1). Below pH 5, the oxidation of sulfur dioxide by H_2O_2 appears to be the major pathway for the formation of sulfuric acid in humid atmospheres (2). Field concentrations up to 60 μM, 250 μM and 4.1 ppb have been measured in rainwater, cloudwater, and the gas phase respectively (3). H_2O_2 can be generated in the gas phase by the disproportionation of two hydroperoxyl radicals (4), at the air-water interface by photoinduced redox processes (5), and in the aqueous phase via photo-catalyzed reactions with humic/fulvic acid and green algae (6). In cloudwater droplets, scavenging of hydroperoxyl radicals from the gas phase leads to the *in situ* formation of H_2O_2. The combination of the *in situ* generation and scavenging of H_2O_2 from the gas phase is thought to be the main source of H_2O_2 in cloudwater droplets (7); however, photocatalytic reactions on naturally occurring metal oxides which are semiconductors may provide an additional source of H_2O_2. Some naturally occurring metal oxides, e.g., TiO_2 and ZnO, have been shown to act as photocatalysts for a large variety of reactions (8), including the production of ammonia from dinitrogen (9). Earlier research by Kormann et al. (10) demonstrated the formation of H_2O_2 in illuminated aqueous suspensions of desert sand.

H_2O_2 also plays an important role in the cleanup of the environment. Several researchers have reported enhanced UV degradation rates of organic pollutants in systems containing H_2O_2 (11). Semiconductor assisted photooxidation of organic pollutants has been demonstrated for PCB's, simple aromatics, halogenated alkanes and alkenes, surfactants, and pesticides (12). Complete mineralization has been obtained in some cases (13). In most experiments with semiconductor photocatalysts, oxygen was present to act as the electron acceptor. As a consequence of the two electron reduction of oxygen,

H_2O_2 was also formed. This reaction is of particular interest since Gerischer and Heller have suggested that electron transfer to oxygen may be the rate-limiting step in semiconductor photocatalysis (14). The detailed mechanisms of photooxidation on semiconductors are not fully understood; electron donors (i.e., pollutant) are either directly oxidized by valence band holes, or by adsorbed or freely-diffusing hydroxyl radicals. Hydroxyl radicals are formed by the reaction of holes with adsorbed H_2O, hydroxide, or surface zincanol groups (>ZnOH). H_2O_2 may also contribute to the degradation by acting as an electron donor or as a direct source of hydroxyl radicals due to either homolytic or heterolytic scission.

A detailed study of the mechanism of photocatalytic production of peroxides on various metal oxide surfaces may provide more insight into the potential environmental implications and applications of peroxides. The present work examines the mechanism of H_2O_2 and ROOH formation using Q-sized semiconductors as photocatalysts. Q-sized semiconductors are semiconductors that exhibit the quantum-size effect (i.e., a blue shift in absorption onset with decreasing particle size (15)). The advantage of using Q-sized semiconductors in this study is the efficacy of measuring quantum yields due to the negligible light scattering of the small diameter particles. In addition, the high surface area to volume ratios of Q-sized semiconductors enhances the rates of reactions that occur via surface states. We have examined the effect of the type and concentration of hole scavengers and semiconductor, pH, the concentration of oxygen, the semiconductor excitation wavelength, the semiconductor particle size, and the light intensity on the quantum yields of peroxide formation. Results of ^{18}O isotopic labeling experiments are presented as evidence for hydrogen peroxide formation via oxygen reduction in the ZnO/formate system. In a companion paper, the oxidative pathways are examined in more detail through product analyses using acetate or formate as hole scavengers.

Experimental

Colloidal suspensions of ZnO with a mean diameter of 5 nm were synthesized via the controlled hydrolysis of $Zn(CH_3COO)_2$ in isopropanol (16). Chemicals and solvents were reagent grade and were used without any further purification. For the hole scavenger experiments, acetate ions were removed by dialysis using Spectrapor membranes (MWCO 12,000-14,000) in isopropanol. Before illumination, isopropanol was removed by rotary evaporation. The solid ZnO was then immediately resuspended in water. Water was purified by a Milli-Q/RO system resulting in a resistivity > 18 MΩ cm. In a typical experiment, 25ml of aqueous ZnO colloid in a quartz cell was saturated with oxygen (P_{O_2}= 1 Atm) for 30 minutes prior to illumination with either a Kratos 450W Xe arc lamp or a Spindler and Hoyer 1000W Xe arc lamp. Continuous oxygen bubbling during the illumination provided a constant dissolved oxygen concentration and enhanced mixing. A combination of a $CuSO_4$ water filter, a glass IR filter, and a Corning GS7601 filter (bandpass 330-370 nm) was employed to limit heating of the sample and to prevent direct photolysis of hydrogen peroxide. Actinometry was performed using (E)-2-[1-(2,5-dimethyl-2-furyl)-ethylidene]-3-isopropylidenesuccinic anhydride in toluene (Aberchrome 540) according to the method of Heller and Langan (17). Light intensities were varied using neutral density filters. For Q-sized suspensions the amount of photons absorbed could be calculated from the absorption spectrum of the colloid and the incident light intensity as measured by actinometry according to the equation: $I_{abs} = I_{inc} - I_{trans} = I_{inc}(1-10^{-\varepsilon_V C l})$. Reaction temperatures were 24 °C ± 1 °C. Fluorescence spectra were measured on a Shimadzu RF-540, while absorption spectra were measured on a Hewlett-Packard 8451A Diode Array spectrophotometer.

Hydrogen peroxide concentrations were determined by two different methods. The first method, sensitive to 1μM H_2O_2, involved the oxidation of iodide to the triiodide

anion (ε_{352nm} = 26,400 M^{-1} cm^{-1}) by peroxides catalyzed by ammonium molybdate (18). This method allows one to distinguish between H_2O_2 and organic peroxides (ROOH) since the latter react more slowly with the molybdenum-iodide system. Aliquots were diluted with water, then 0.1M potassium biphthalate was added to dissolve the ZnO colloid. At t = 0 min., the iodide reagent (0.4 M potassium iodide, 0.06 M NaOH, 0.1 mM ammonium molybdate) was added and the absorbance vs. time profile was recorded. The amount of H_2O_2 formed is calculated from the absorbance at 2 minutes, while the total peroxide is calculated from the absorbance at 60 minutes. The second method, sensitive to 10 nM H_2O_2, involved the dimerization of p-hydroxyphenylacetic acid (POPHA) in the presence of H_2O_2 and horseradish peroxidase to yield a fluorescent product (λ_{ex}= 315 nm, λ_{em}=406 nm) (19). A stock solution of H_2O_2 was calibrated by titration with permanganate. Calibration curves from standards were used to calculate the response factors for each method.

For the isotopic labeling experiments, ^{18}O enriched water and oxygen were purchased from Isotec. All reactions were run in a closed cell using 100 ml of solution and 10 cc of gas headspace. 2mM formate was added as the hole scavenger. Constant stirring was employed to insure good liquid-gas mass transfer. The colloidal suspensions were degassed by three freeze-pump-thaw cycles using a vacuum line system prior to addition of the isotopically labeled oxygen or water. Oxygen pressures were 1 atm. The irradiation apparatus consisted of a 1000W Spindler and Hoyer Xe arc lamp equipped with a 320 nm bandpass filter. Each colloidal suspension was irradiated to produce a 0.2mM concentration of hydrogen peroxide, then acidified with formic acid to pH 3 to dissolve the ZnO colloid, and subsequently concentrated by two vacuum distillations. Blanks containing 2mM formate and either labeled oxygen or water were stirred in the dark for the same time period as the ZnO/formate irradiated runs, and were concentrated by a similar vacuum distillation procedure. The resulting solutions (typically 0.5 ml of 2-20

mM peroxide) were bubbled with argon and stored in septum sealed vials at 4 °C prior to analysis by GC-MS. Samples of the colloidal suspension and headspace at the beginning and end of each irradiation were also saved for analysis.

Peroxide isotopic analyses were performed on a Hewlett Packard Model 5890/5989A GC-MS operating in the single-ion mode. The separation of hydrogen peroxide from water, acetic acid, and formic acid was achieved using a 25 meter Hewlett Packard HP-1 capillary column. The GC-MS was operated under relatively low temperatures in order minimize thermal degradation of hydrogen peroxide. The temperatures were 120 °C, 100 °C, 100 °C, and 80 °C for the GC inlet, GC-MS interface, MS source and quadropole chamber, respectively. The column temperature was held constant at 30 °C for the hydrogen peroxide standards, and was ramped from 30 °C to 150 °C over a period of 10 minutes for the samples containing formic and acetic acid. The ionization mode was by electron impact, with an electron energy of 70 eV. Ion mass-to-charge ratios of 18, 19, 20, 32, 33, 34, 35, 36, 37, 38, 45 and 60 were monitored with a mass resolution of $\pm$ 0.3 amu. A series of hydrogen peroxide standards ranging in concentration from 50 μM to 100 mM were used to generate calibration curves. Typical injection volumes were 0.8 μL for liquid samples and 5 to 100 μL for gaseous samples. The retention times were 4.41 min., 5.18 min., and 5.85 min. for formic acid, hydrogen peroxide, and acetic acid respectively.

Hydrogen peroxide was also separated from water using a Hewlett-Packard Model 1090 (Series II) HPLC equipped with a Hewlett Packard Hypersil ODS column (5 μm beads, 100 mm X 2.1 mm). The HPLC was connected to the mass spectrometer via a Hewlett Packard Model 59980B particle beam interface. The eluant was a mixture of 70% H_2O and 30% MeOH, which also contained 1 mM acetic acid. The temperatures of the particle beam desolvation chamber LC oven temperature were 50 °C and 45 °C,

respectively. The injection volumes ranged from 6 to16 μL, depending upon the concentration of H_2O_2 in the sample. The mass spectrophotometer conditions were identical to those conditions used in the GC-MS analysis.

Results and Discussion

In general, semiconductors can act as sensitizers for light-induced redox processes due to their electronic structure consisting of a filled valence band and empty conduction band (20). Absorption of a photon of energy greater than the bandgap energy leads to the formation of an electron/hole pair. In the absence of suitable scavengers, the stored energy is dissipated within a few nanoseconds by recombination. If a suitable scavenger or surface defect state is available to trap the electron or hole, recombination is prevented and subsequent redox reactions may occur. The valence band holes are powerful oxidants (+1.0 to +3.5 V Vs NHE depending on semiconductor and pH), while the conduction band electrons are good reductants (+0.5 to -1.5V Vs NHE) (21). Most organic photodegradation reactions utilize the oxidizing power of the holes; however, to prevent a buildup of charge one must also provide a reducible species to react with the electrons. Unlike bulk semiconductor electrodes, where due to band bending, only one species (e.g., the hole for n-type semiconductors) is available at the surface for reaction (22), in very small semiconductor particle suspensions both species are present on the surface. Therefore, careful consideration of both the oxidative and reductive paths is required. Due to the redox potentials of the electron/hole pair, H_2O_2 can theoretically be formed via two different pathways in an aerated aqueous solution: the reduction of oxygen and the oxidation of water:

$$O_2 + 2e_{cb}^- + 2H_{aq}^+ \rightarrow H_2O_2 \quad (1)$$

$$2\,H_2O + 2h_{vb}^+ \rightarrow H_2O_2 + 2H_{aq}^+ \quad (2)$$

We will present evidence that in our system only the reductive pathway occurs to yield appreciable amounts of H_2O_2.

Figure 1 shows the formation of peroxides in an aqueous ZnO colloid containing 2mM acetate (pH = 7.8, buffered by the amphoteric mineral surface) using a 450W Xe arc lamp. Detection was by the iodometric method. Both the H_2O_2 (top line) and ROOH (lower line) increase linearly with irradiation time. At long irradiation times (>200 minutes) the rate of peroxide production begins to slow down. The open and closed symbols represent two different batches of colloid, which gave similar results. The initial rate of peroxide production calculated from the slope of Figure 1 is 1.23×10^{-8} M s^{-1} for H_2O_2 and 1.72×10^{-9} M s^{-1} for ROOH. The initial quantum yield (Φ_i) equals the ratio of the initial rate of peroxide production to the rate of photon absorption. The initial quantum yields are 30.7% and 4.3% for H_2O_2 and ROOH respectively. No peroxides are produced in the absence of light absorption by ZnO. It should be noted that in long illuminations, the ZnO colloid is unstable and begins to coagulate due to the intense mixing induced by oxygen bubbling.

Figure 2 shows an analogous profile for the formation of peroxides in an aqueous ZnO colloid containing 2mM acetate using an 1000W Xe arc lamp. In this case the H_2O_2 reaches a limiting concentration of 1.18 mM in 500 minutes. The ROOH is produced in much lower quantity relative to H_2O_2 than in the lower intensity case. The initial quantum yields are 3.4% and 0.08% for H_2O_2 and ROOH respectively. The solid line is a fit of the data to the equations suggested originally by Kormann et al. (23) :

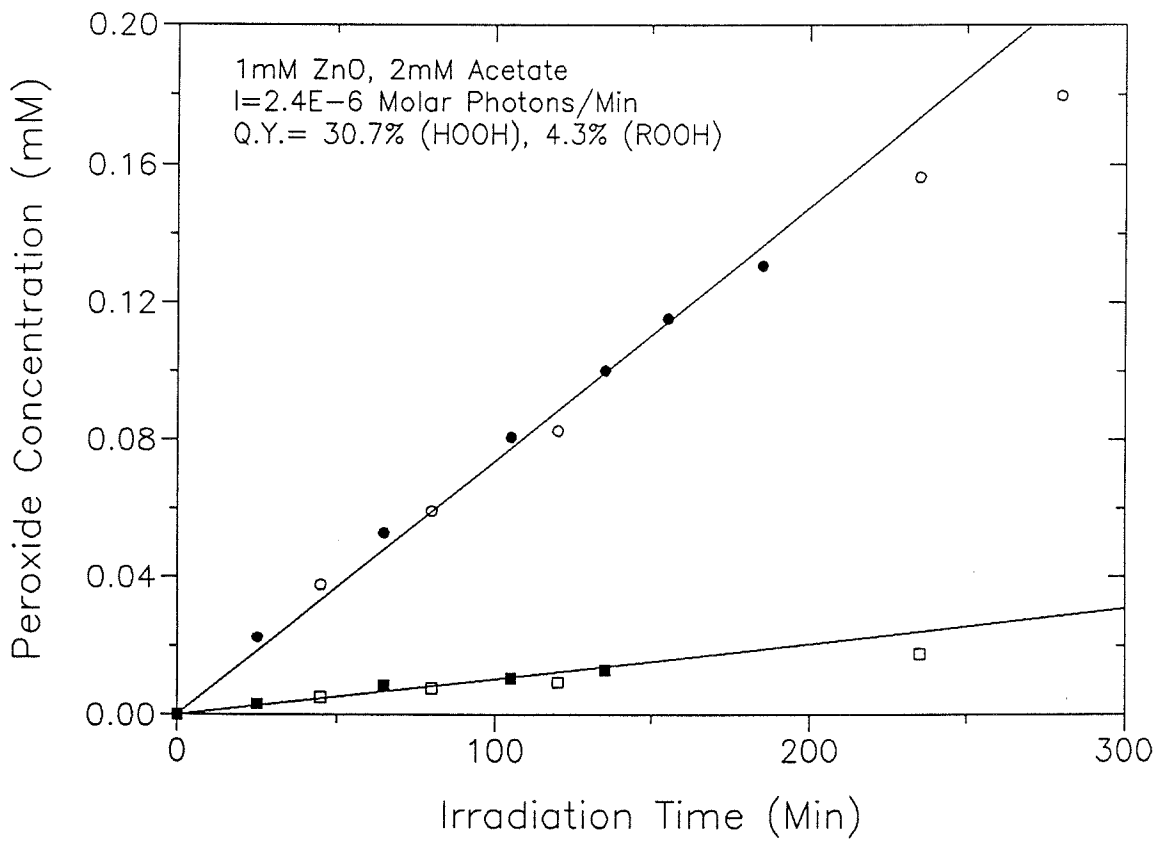

Figure 1: Peroxide production in an aqueous 1mM Q-sized ZnO colloid at low light intensity. Detection via the iodometric method. Upper curve equals H_2O_2, lower curve equals ROOH. The open and closed circles represent two different batches of colloid.

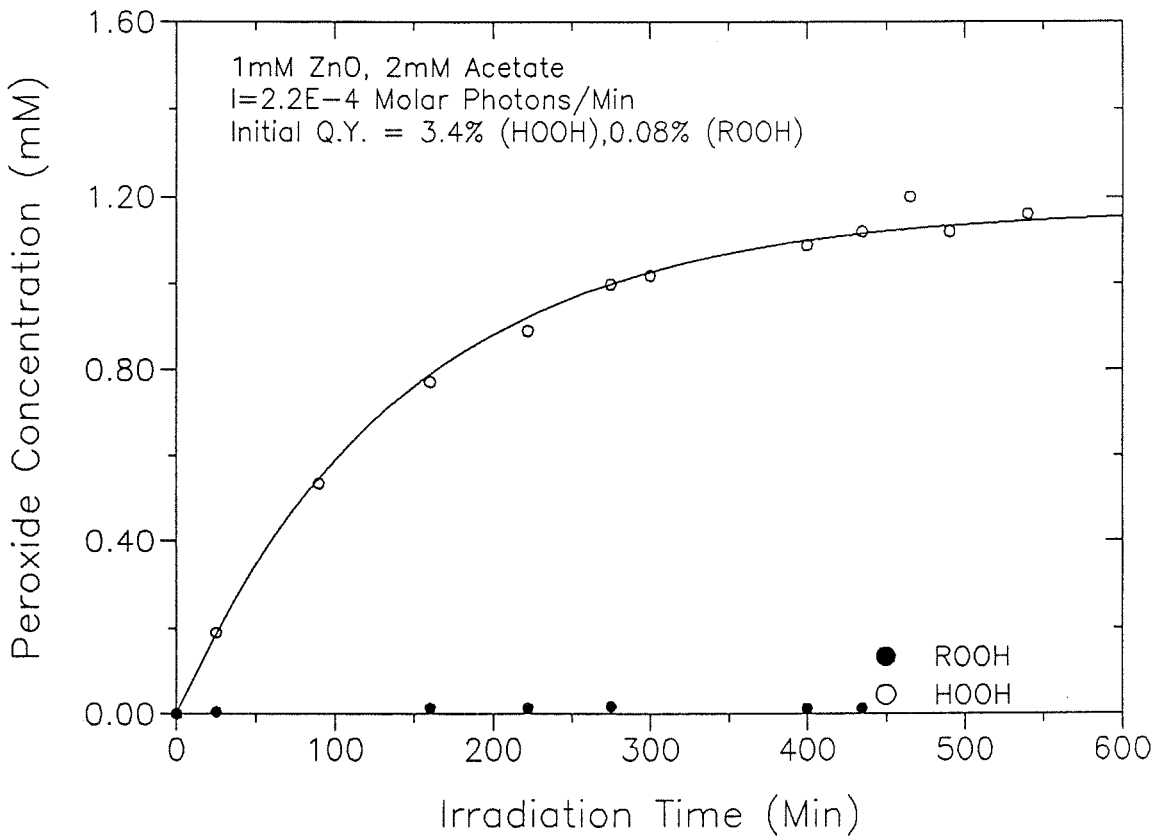

Figure 2: Peroxide production in an aqueous 1mM Q-sized ZnO colloid at high light intensity. Upper curve equals H_2O_2, lower curve equals ROOH. Solid line is fit of the data to equations of Kormann et al.

$$\text{Semiconductor} \xrightarrow{h\nu} e_{cb}^- + h_{vb}^+ \quad (3)$$

$$O_2 + 2\,e_{cb}^- + 2\,H_{aq}^+ \rightarrow H_2O_2 \quad (4)$$

$$2\,H_2O + 2\,h_{vb}^+ \rightarrow H_2O_2 + 2\,H_{aq}^+ \quad (5)$$

$$h_{vb}^+ + CH_3COO^- \rightarrow \text{products} \quad (6)$$

$$\frac{d[HOOH]}{dt} = f(CH_3COO^-, O_2) = \Phi_0 \frac{d[h\nu]_{abs}}{dt} \quad (7)$$

$$H_2O_2 + 2\,e_{cb}^- \xrightarrow{H^+} 2\,H_2O \quad (8)$$

$$H_2O_2 + 2\,h_{vb}^+ \rightarrow O_2 + 2\,H_{aq}^+ \quad (9)$$

$$\frac{-d[HOOH]}{dt} = f(CH_3COO^-, O_2, HOOH) = \Phi_1\,[HOOH]\frac{d[h\nu]_{abs}}{dt} \quad (10)$$

$$\frac{d[HOOH]}{dt} = (\Phi_0 - \Phi_1\,[HOOH])\frac{d[h\nu]_{abs}}{dt} \quad (11)$$

$$[HOOH]_{ss} = \Phi_0 / \Phi_1 \quad (12)$$

From the steady state concentration of hydrogen peroxide and the quantum yield of peroxide formation, the quantum yield of peroxide degradation (Φ_1) is calculated to be 28.8 M^{-1}. The contribution of peroxide degradation via direct photolysis can be calculated from literature values of the hydrogen peroxide extinction coefficient and quantum efficiency as a function of wavelength (24). Using the values of $\varepsilon_{340} = 0.047$ $M^{-1}\,cm^{-1}$ and $\Phi_{340} = 0.96$ gives a rate of degradation of 8.13×10^{-8} M min^{-1} for a 1.18

mM HOOH solution. This represents only 1.2% of the actual degradation rate of 6.47 X 10^{-6} M min^{-1}.

The effect of the concentration of hole scavenger was examined. As the acetate concentration increased from 0.2 mM to 2.0 mM at constant light intensity, the quantum yields increased from 2.8% to 3.1%. We were unable to increase the acetate concentrations to higher values due to the increased ionic strength causing coagulation of ZnO colloid. In a previous study, using bulk size TiO_2, increasing the acetate concentration from 1mM to 50 mM increased the peroxide concentration by a factor of 8 for similar light intensities and irradiation times (25) . Irradiation of a dialyzed sample of ZnO colloid also produced low concentrations of H_2O_2 probably due to the presence of 0.2mM acetate which could not be removed by dialysis. A sample of bulk ZnO with no added hole scavengers gave an initial H_2O_2 production rate of 1.26 X 10^{-8} M s^{-1}; however, the H_2O_2 concentration reached a maximum of only 10 μM versus the maximum H_2O_2 concentration of 1 mM in the case of bulk ZnO with 2 mM acetate. This evidence suggests that the acetate is necessary for efficient H_2O_2 production, either by acting as a hole scavenger and preventing recombination or by its degradation to yield peroxide products.

In order to further assess the importance of hole scavenging upon the rate of peroxide production, we examined the quantum yields of peroxide production with different electron donors. These donors include citrate, acetate, oxalate, and formate. The results are shown in Table 1 along with the corresponding metal complexation constants for the 1:1 complexes (26) and the hydroxyl radical reaction rates (27). All samples were dialyzed to remove 2 mM acetate which remained from the synthesis of the ZnO colloids. At the pH of the experiments (7.5 - 8.0), the surface is positively charged (pH_{zpc}= 9.2) and the donors are all anionic. The quantum yields of H_2O_2 production

Hole Scavenger	HOOH (%)	ROOH (%)	log $K_{Zn^{2+}}$	log $K_{OH\cdot}$
None	2.8	0.3	-----	------
Acetate	3.1	0.6	1.1	7.9
Oxalate	4.2	0.0	3.9	6.9
Formate	5.4	0.1	0.7	9.4

Table 1: Quantum yields of peroxide production for various electron donors. 1mM dialyzed ZnO colloids, pH 7.5-8.0, 1mM electron donor, I_{abs}=6.85 X 10^{-4} M photons min^{-1}.

increased in the order citrate < no hole scavenger < acetate < oxalate < formate. The observed order fails to match either the trends in the complexation constants or the hydroxyl radical reaction rates, probably indicating that both factors are significant in this system. Formate is unique in that it is known to exhibit a current doubling effect (28). Once oxidized, the $CO_2 \cdot^-$ radical can inject an electron into the conduction band of ZnO. This may explain the high quantum yield for formate. The rate of peroxide production was extremely slow when citrate was used as the electron donor; however, prolonged illumination produced an intermediate (detected spectroscopically) and thereafter the rate of peroxide production increased rapidly. The identity of this intermediate is not known. The quantum yields of organic peroxide (ROOH) were essentially zero for citrate, oxalate, and formate. This result is expected, since oxidation of these anions leads primarily to the formation of $CO_2 \cdot^-$ radicals which are further oxidized to CO_2. In the case of acetate, the quantum yield of organic peroxides is 0.6%. Significant organic peroxides were also produced in the absence of added hole scavenger due to the 0.2 mM acetate remaining from the dialysis. The oxidative pathway with acetate was examined in more detail in a following paper.

Figure 3 illustrates the pH dependence of the quantum yield of hydrogen peroxide production using 2.0 mM acetate as the hole scavenger. The pH range of these experiments was limited by the stability of the colloid: below pH 6 the colloid dissolves, and above pH 9, the colloid rapidly coagulates. The behavior in Figure 3 cannot readily be explained in terms of surface charge since the pH_{zpc} for Q-sized ZnO is 9.2, as determined from the titration curve inset in Figure 3. If adsorption of the hole scavenger, acetate, to the surface was a controlling factor, an increase in the pH from 6 to 11 would decrease the positive surface charge, and should lower the quantum yield. Instead, the opposite result was observed. As the pH increased, the quantum yield of hydrogen peroxide formation increased. This behavior can be explained in terms of changing redox

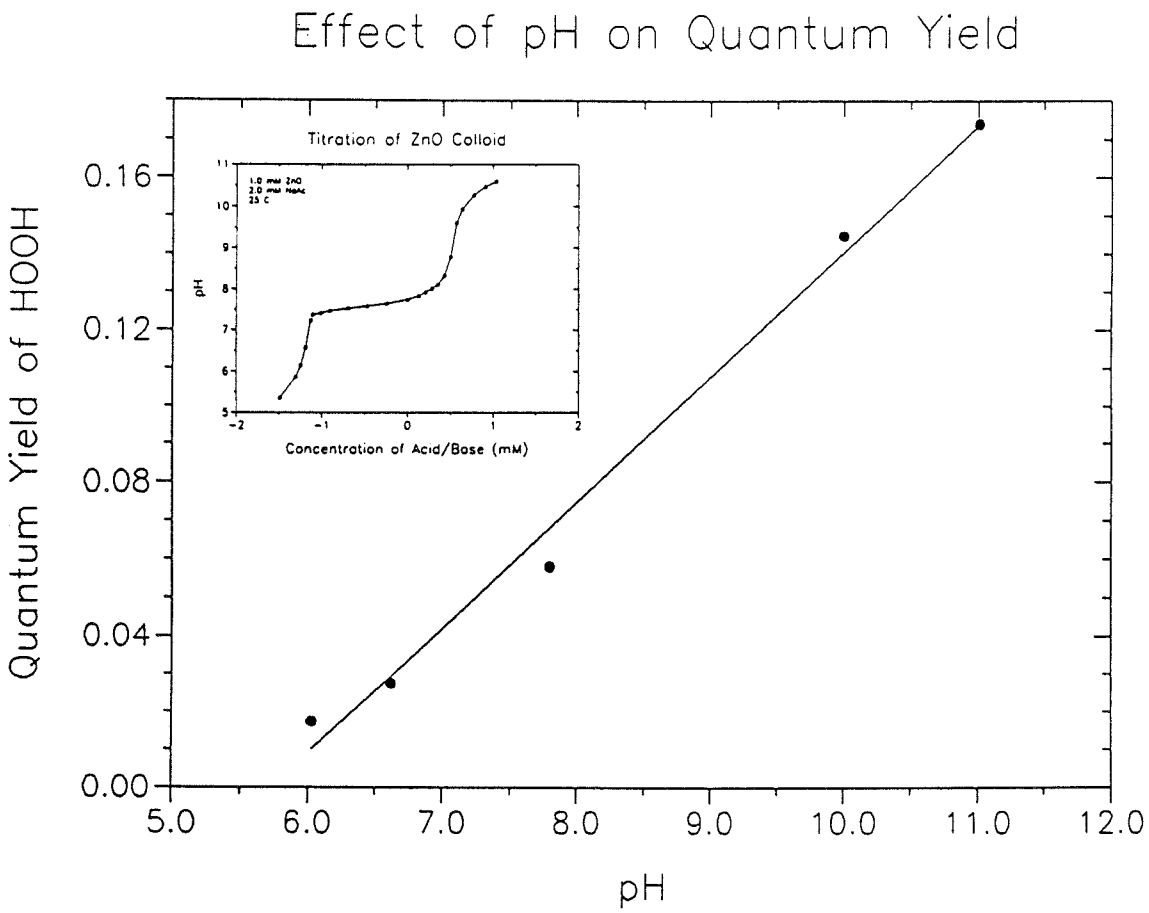

Figure 3: The pH dependence of quantum yields. 1mM Q-sized ZnO colloid, 2mM acetate.

potential of the conduction band electron with pH. The redox potential shifts negative by 59mV per each unit increase in pH. Thus at high pH, the driving force for oxygen reduction to form hydrogen peroxide should increase, and the quantum yields would be expected to be higher, as is experimentally observed. The pH effect is actually more complex, due to the fact that the OH^- added to increase the pH is also a good hole scavenger and could form additional H_2O_2 by $OH\cdot$ reactions. In the case of bulk ZnO, we observed that the initial rate of peroxide production in the presence of 0.2 mM hydroxide ions was 4.7×10^{-6} M min^{-1} versus 6.09×10^{-6} M min^{-1} in the presence of 2.0 mM acetate ions.

The effect of isopropanol on peroxide production is presented in Figure 4. As the concentration of isopropanol increased from 0.1 to 10.0 M, the initial rate of peroxide production increased from 1.1×10^{-8} M s^{-1} to 2.49×10^{-8} M s^{-1}. Thus, we utilized an additional vacuum step to remove any traces of isopropanol prior to resuspension. This result is significant because if the oxidative pathway was responsible for the production of H_2O_2, increasing the concentration of isopropanol should decrease the rate of peroxide production since isopropanol is a very efficient hole scavenger. We observe the opposite trend, thus the reduction of oxygen is the primary pathway for the formation of peroxide in our system. It should be noted, however, that increasing the isopropanol concentration did lead to higher concentrations of organic peroxides relative to the inorganic peroxide. At high isopropanol concentrations, hydrogen peroxide may also be formed efficiently by secondary reactions of the initially-formed ketyl radicals with dioxygen to form hydroperoxyl radicals.

Figure 5 demonstrates the oxygen dependence of peroxide production. As the partial pressure of oxygen increased in the bubbling gas, the quantum yield of H_2O_2 reached a limiting value of 2.8%. The solid line is a fit of the data to a Langmuirian

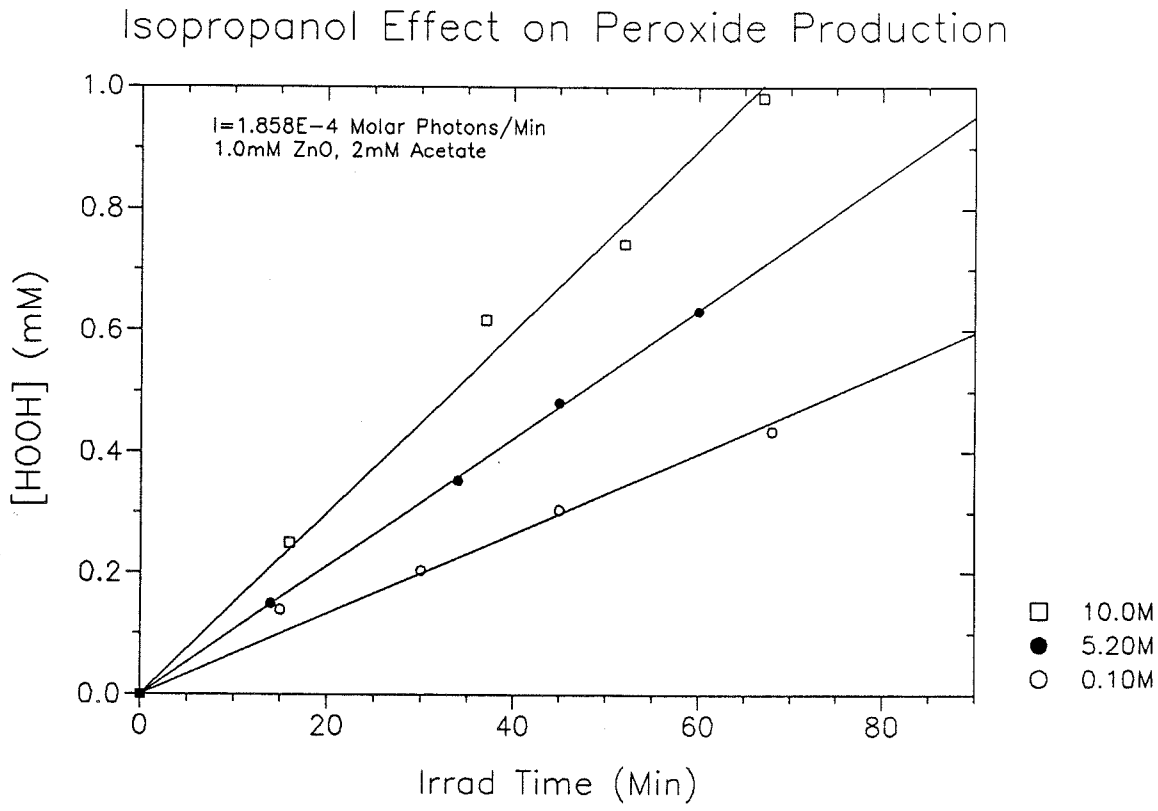

Figure 4: Effect of isopropanol concentration on hydrogen peroxide production rate. 1mM Q-sized ZnO, 2mM acetate.

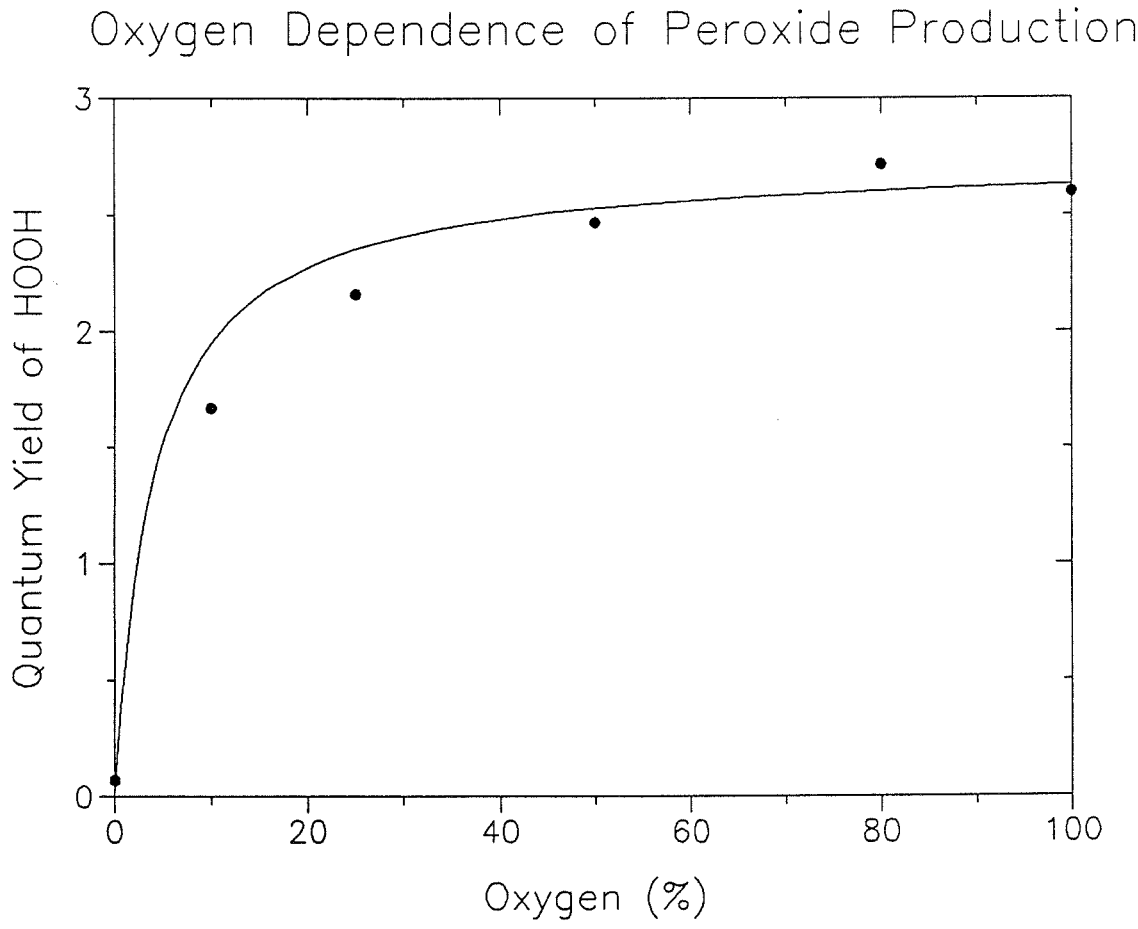

Figure 5: Effect of oxygen on hydrogen peroxide production. Solid line is fit of data to Langmuirian model. 1mM Q-sized ZnO, 2mM acetate

adsorption model. The quantum yield is not zero at 0% oxygen due to the presence of a small amount of oxygen that could not be removed by sparging. The data suggest that the oxygen which is reduced by conduction band electrons to produce H_2O_2 is adsorbed on the surface of the Q-sized semiconductor. At 20% O_2 where the quantum yield of hydrogen peroxide formation begins to saturate, the ratio of dissolved oxygen molecules to ZnO particle is calculated to be 300. The Langmuirian dependence on oxygen concentration has also been observed by Okamoto et al. (29) and by Turchi and Ollis (30) for the photodegradation of organic pollutants using TiO_2 powder as the photocatalyst.

In order to elucidate the mechanism of peroxide production, isotopic labeling experiments were performed. 2mM formate was chosen as the hole scavenger because ZnO/formate systems demonstrated the fastest rate of peroxide production and produced no organic peroxides. In 1953, isotope studies on bulk ZnO suspensions were performed by Calvert et al. (31). Although these experiments clearly demonstrated that all the oxygen atoms in the peroxide product arose from dioxygen, the experimental procedure was quite difficult: involving thorough degassing of the solution and oxidation of the hydrogen peroxide by ceric sulphate to form oxygen, which was then analyzed at mass 34 and 32. In addition, the isotopic enrichments were very low, so the sensitivity was low. The analysis were based upon the premise that the oxidation of H_2O_2 by ceric sulfate did not scramble the isotopic label; however, prior research by Cahill and Taube suggested that a small amount of fractionation did occur (32). By increasing the isotopic enrichment, and developing a method for hydrogen peroxide analysis via GC-MS, we were able to analyze all the expected product mass-to-charge ratios without converting the hydrogen peroxide to oxygen. Although this method requires an increased investment in isotopes, it has the advantage of simplicity of sample preparation and ease of analysis.

The hydrogen peroxide calibration curves for two different length HP-1 columns are shown in Figures 6 and 7. The longer column length exhibited better sensitivity due to increased separation of peroxide from the solvent peak and the fact that it was a fresh column. Long-term exposure to hydrogen peroxide irreversibly decreases column sensitivity by 70% or more. Under optimal concentrations, we were able to detect hydrogen peroxide concentrations as low as 50 μM. We believe this to be the lowest hydrogen peroxide concentration detected by mass spectrometry to date. Most peroxide research utilizing the MS technique reports using concentrations of 1-99% H_2O_2 which corresponds to 0.3 to 33 M (33). This detection limit is not as low as that reported for GC and IC systems (10^{-9} M H_2O_2) which utilize either a redox chemiluminescence detector or post column derivatization techniques to detect the hydrogen peroxide (34). Fragmentation of the hydrogen peroxide in the mass spectrometer ionization chamber is responsible for the higher detection limits in our case. We were also able to detect hydrogen peroxide in a LC/MS thermospray system using a water/methanol mixture as the solvent; however, the sensitivity and signal to noise ratios were lower probably due to lack of good mass separation in the desolvation chamber. In addition the LC/MS technique had the disadvantage of requiring larger sample sizes.

The results of the labeling experiments are presented in Table 2. At the short irradiation times employed in these experiments, the rate of peroxide production in the closed system was equal to the initial rates obtained in the open, continuously oxygen bubbled system. Within an experimental error of $\pm$ 6%, the mass ratios of the oxygen analysis were identical at the beginning and end of each run. Futhermore, the observed mass ratios were equal to the calculated ratios for isotopically enriched oxygen gas containing 21% ^{16}O, 65% ^{17}O, and 14% ^{18}O. The similarity of oxygen mass ratios between the runs containing ZnO and those without ZnO suggests that the rate of oxygen isotopic exchange between oxygen and water is slow compared to the time scale of the

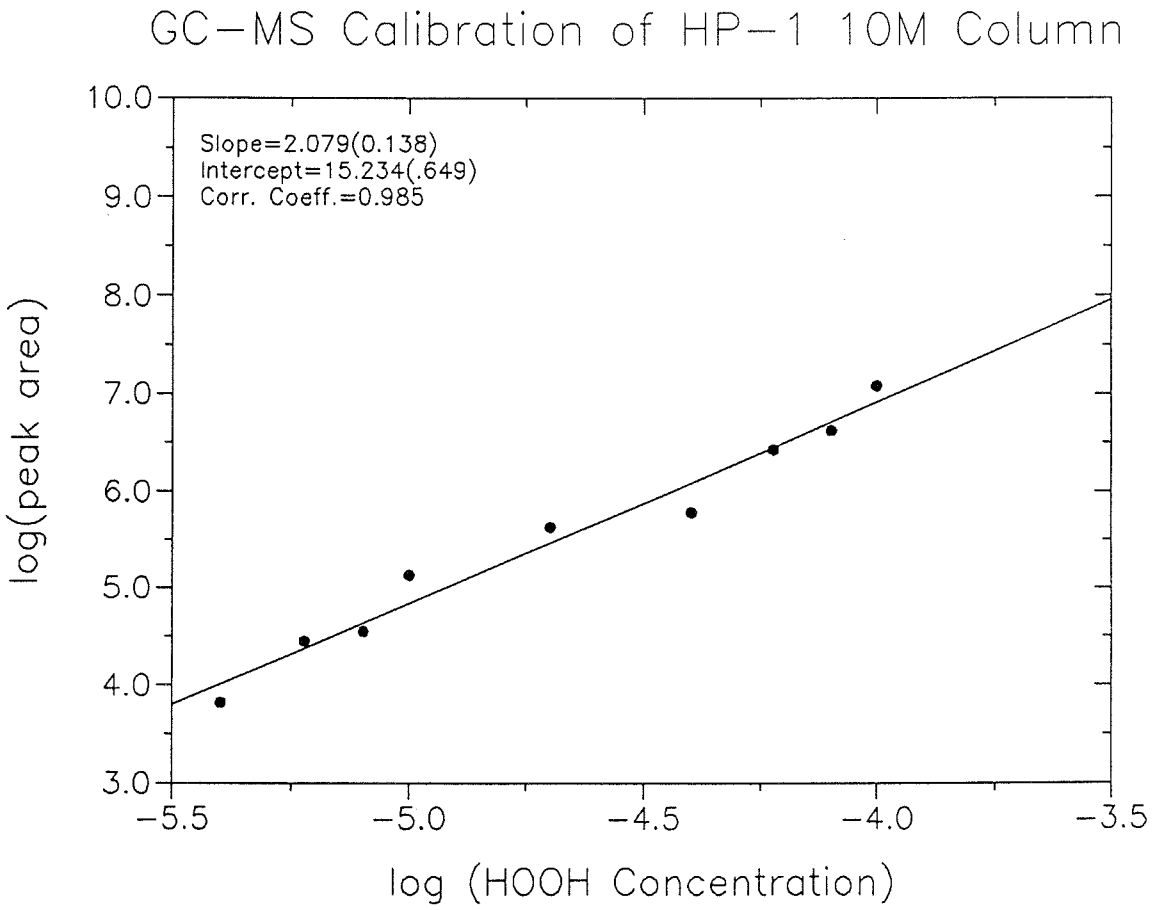

Figure 6: GC-MS hydrogen peroxide calibration curve using 10 meter HP-1 Column.

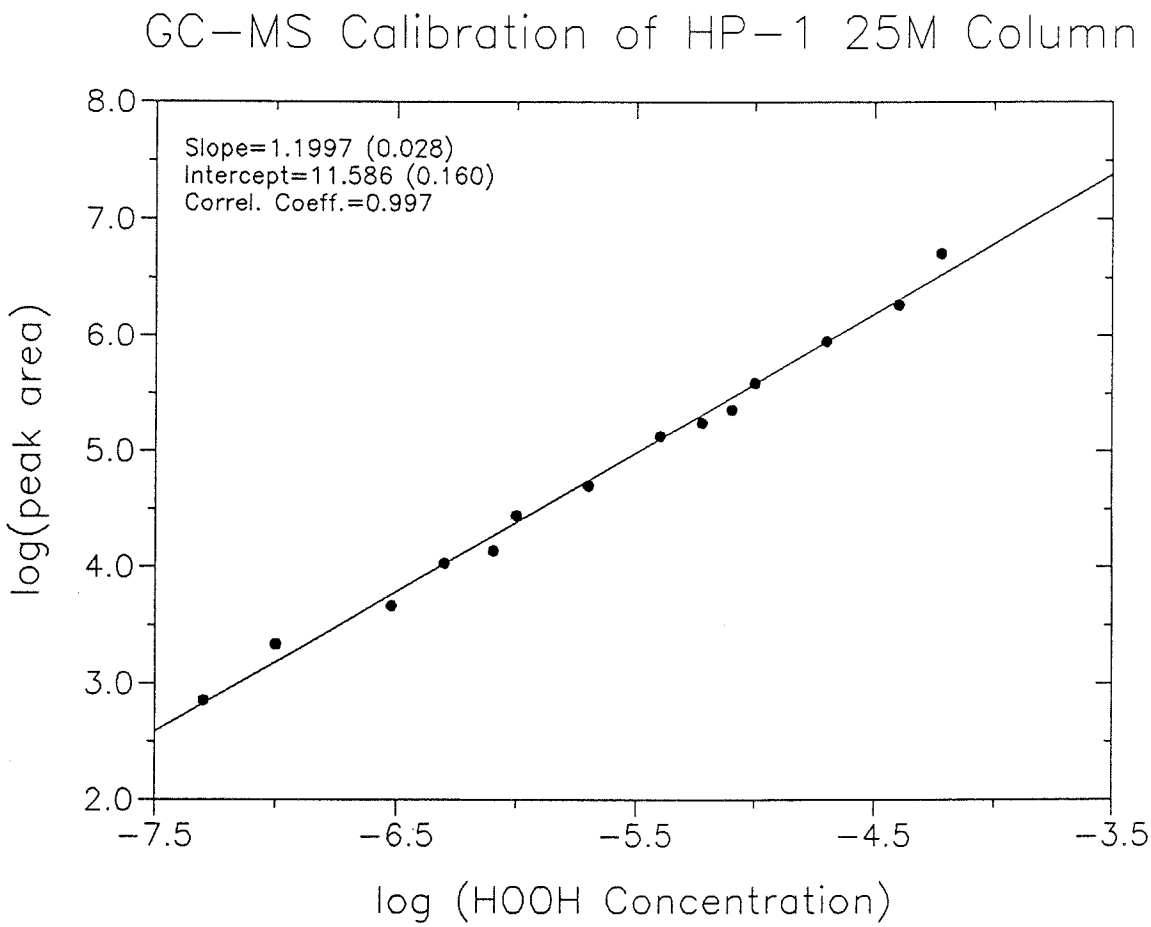

Figure 7: GC-MS hydrogen peroxide calibration curve using 25 meter HP-1 Column.

Oxygen Analysis	33/32*	34/32	35/32	36/32
$ZnO/^{18}O_2$ start	6.0598	10.4532	3.8567	0.4050
$ZnO/^{18}O_2$ end	6.0294	10.3919	3.9297	0.4248
$HOOH/^{18}O_2$ start	6.0122	10.3571	3.9696	0.4359
$HOOH/^{18}O_2$ end	6.0231	10.3791	3.9439	0.4288
$ZnO/H_2{}^{18}O$ start	.0040	.0008	0	0
$ZnO/H_2{}^{18}O$ end	.0041	.0008	0	0
$HOOH/H_2{}^{18}O$ start	.0040	.0008	0	0
$HOOH/H_2{}^{18}O$ end	.0040	.0008	0	0
HOOH Analysis	35/34	36/34	37/34	38/34
$ZnO/^{18}O_2$	6.1046	10.5447	3.7485	0.3770
$HOOH/^{18}O_2$	.0042	.0009	0	0
$ZnO/H_2{}^{18}O$	.0040	.0008	0	0
$HOOH/H_2{}^{18}O$	.0040	.0008	0	0

* Peak Area Ratio of Mass 33 to Mass 32 Ion Signals. H_2O_2 Peak Area Ratios are Corrected for fractionation of H_2O_2 to HO_2^+.

Table 2: Mass ratios from ^{18}O isotopic labelling experiments. 1mM Q-sized ZnO, 2mM formate.

irradiation. Comparison of the mass ratios from hydrogen peroxide and oxygen analysis of the runs without ZnO indicates no detectable oxygen isotope exchange between water and hydrogen peroxide in 120 minutes and a slight exchange between hydrogen peroxide and oxygen in 120 minutes. No isotopically enriched hydrogen peroxide product was detected in the runs containing isotopically enriched water: however, the enrichment factors were low, and it is possible that the higher masses were below detection limits. More importantly, isotopically enriched hydrogen peroxide product was detected only in the run containing ZnO and isotopically enriched oxygen gas, and each mass ratio from the peroxide analysis matched within 6% the corresponding mass ratio from the oxygen analysis. Thus, the oxygen in the photoproduced hydrogen peroxide originates entirely from the oxygen gas according to the reactions:

$$O_2 + e^- \rightarrow O_2^{-\bullet} \quad (13)$$

$$O_2^{-\bullet} + H_2O \rightarrow HO_2^{\bullet} + OH^- \quad (14)$$

$$2HO_2^{\bullet} \rightarrow H_2O_2 + O_2 \quad (15)$$

$$HO_2^{\bullet} + e^- + H_2O \rightarrow H_2O_2 + OH^- \quad (16)$$

Figure 8 presents the semiconductor concentration dependence of peroxide production. As the concentration of ZnO increased, the rate of H_2O_2 production also increased, as might be expected since increasing the semiconductor concentration also increases the number of surface sites available for reaction. An additional effect arises from differences in the absorbed light intensity with the variation in semiconductor concentration. The extinction coefficient of Q-sized ZnO is approximately 320 M^{-1} cm^{-1} at 350 nm. When the quantum yields are calculated, which correct for differences in absorbed light intensity, the variation with absorbed light intensity is in a manner opposite

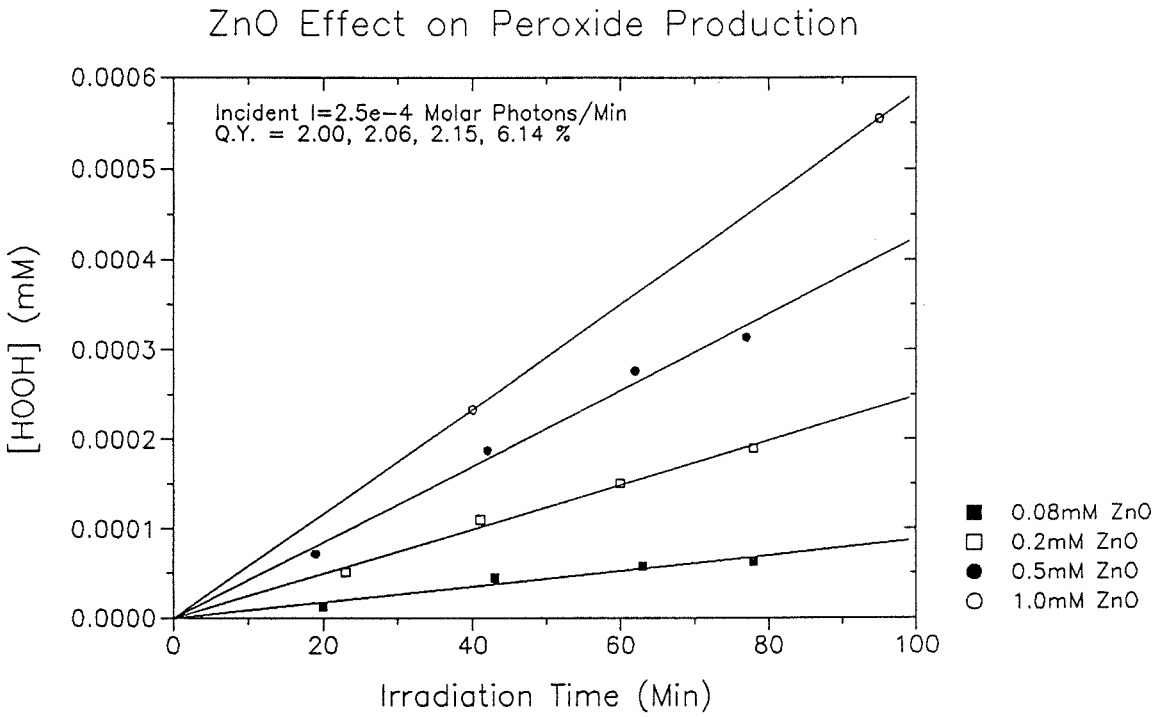

Figure 8: Effect of semiconductor concentration on hydrogen peroxide production.

to that of the rate of peroxide production. That is, the quantum yields of peroxide production decreased from 6.1% to 2.0% with increasing concentration of the semiconductor. This result led us to examine the effect of light intensity on the quantum yields of peroxide production.

By using a combination of neutral density filters and different wattage Xe arc lamps, we were able to vary the light intensity over three orders of magnitude. As exhibited in Figure 9, the quantum yield decreased rapidly as the light intensity increased. The solid line is a fit of the quantum yield to the inverse square root of light intensity. When the absorbed light intensity is varied by changing the ZnO concentration while keeping the incident light intensity constant, the values of the quantum yields fit to the same line. Thus, the controlling factor in this case is the difference in absorbed light intensity, not the change in concentration of surface sites. The quantum yield is expected to vary as the inverse square root of the absorbed light intensity under conditions in which second order recombination reactions compete with first order peroxide production. A simple model for this case is as follows:

$$\text{Excitation:} \quad ZnO \xrightarrow{h\nu} e^- + h^+ \tag{17}$$

$$\text{Adsorption:} \quad O_2 + \text{Site} \rightarrow O_{2\ ads} \tag{18}$$

$$\text{Recombination:} \quad e^- + h^+ \rightarrow \text{heat or light} \tag{19}$$

$$\text{Electron trapping:} \quad Zn(II)\text{-}H_2O + e^- \rightarrow Zn(I)\text{-}H_2O^{\bullet -} \tag{20}$$

$$\text{Oxygen Reduction:} \quad Zn(I)\text{-}H_2O^{\bullet -} + O_{2\ ads} \rightarrow Zn(II) + O_2{}^{\bullet -}{}_{ads} + H_2O \tag{21}$$

If the rate determining step is the reduction of the adsorbed oxygen with surface trapped electrons, the rate of reduction is given by:

$$R_{21} = k_{21}\,[Zn(I)\text{-}H_2O^{\bullet -}]\,[O_{2\ ads}] \tag{22}$$

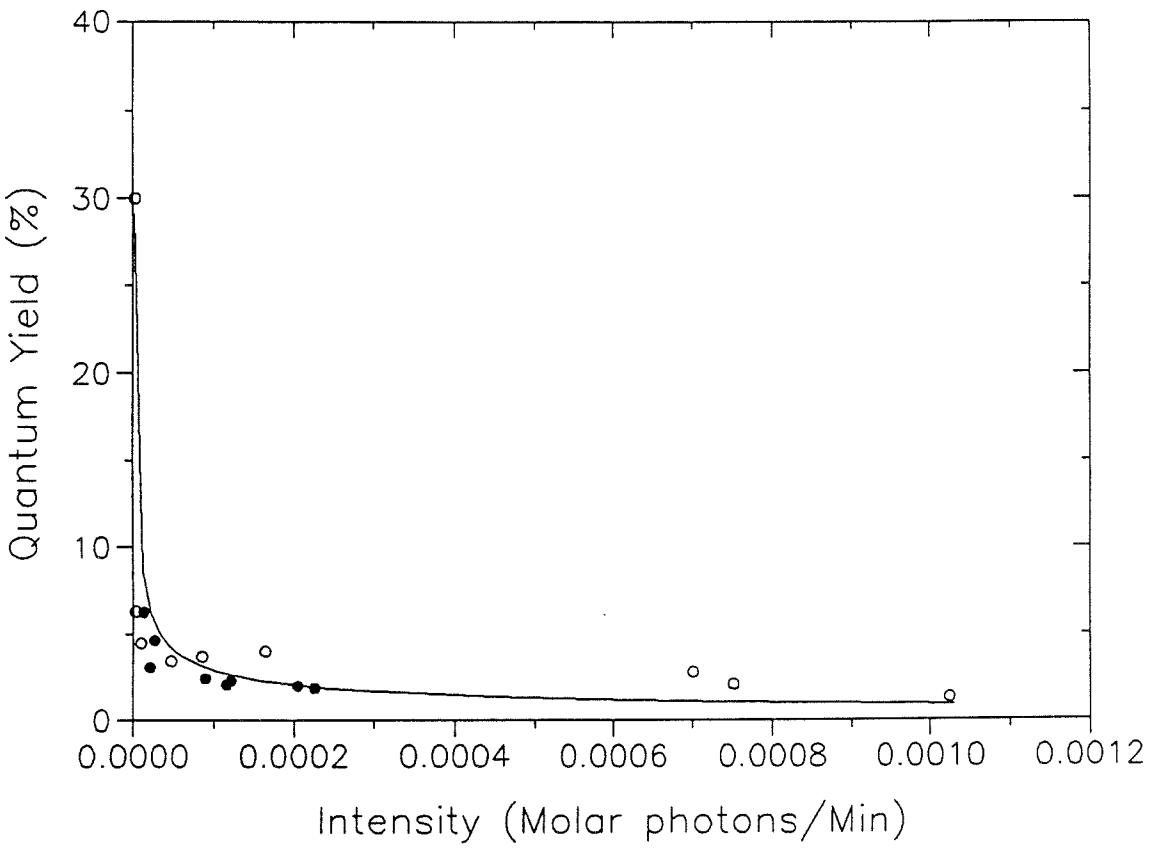

Figure 9: Light intensity dependence of quantum yields of hydrogen peroxide production. Open and closed circles represent different batches of colloid. 1mM Q-sized ZnO, 2mM acetate. Solid line is fit of data to inverse square root of intensity.

Using a steady state analysis on Zn(I)-$H_2O^{\bullet -}$ gives the expression:

$$[\mathrm{Zn(I)-H_2O^{\bullet -}}] = \frac{k_{20}[\mathrm{Zn(II)-H_2O}][e^-]}{k_{-20} + k_{21}[\mathrm{O_{2\ ads}}]} \tag{23}$$

Likewise the steady state analysis on e^- gives:

$$\frac{d[\mathrm{e^-}]}{dt} = \mathrm{I_{abs}} - k_{19}[\mathrm{e^-}][\mathrm{h^+}] - k_{20}[\mathrm{Zn(II)-H_2O}][\mathrm{e^-}] + k_{-20}[\mathrm{Zn(I)-H_2O^{\bullet -}}] \approx 0 \tag{24}$$

Since the photogeneration rates of h^+ and e^- are equal and the intrinsic carrier density is comparatively low, $[e^-] = [h^+]$, and the equation becomes:

$$\mathrm{I_{abs}} = k_{20}[\mathrm{Zn(II)-H_2O}][\mathrm{e^-}] - k_{-20}[\mathrm{Zn(I)-H_2O^{\bullet -}}] + k_{19}[\mathrm{e^-}]^2 \tag{25}$$

At high carrier concentrations, i.e., high light intensity, the third term in equation 25 is much larger than the other two terms and the equation simplifies to:

$$[\mathrm{e^-}] = \sqrt{\frac{I_{abs}}{k_{19}}} \qquad \{\text{at high intensity}\} \tag{26}$$

For very low light intensities, the third term in equation 25 is much less than the other two terms and the equation simplifies to:

$$[\mathrm{e^-}] = \frac{\mathrm{I_{abs}} + k_{-20}[\mathrm{Zn(I)-H_2O^{\bullet -}}]}{k_{20}[\mathrm{Zn(II)-H_2O}]} \qquad \{\text{at low intensity}\} \tag{27}$$

When back reaction rate of equation 16 is slow compared to the rate of light absorption, then the equation for the concentration of electrons simplifies further to give:

$$[e^-] = \frac{I_{abs}}{k_{20}[Zn(II) - H_2O]} \qquad \text{(at low intensity)} \qquad (24)$$

The rate of reduction of oxygen is then:

$$R_{21} = \frac{k_{21}k_{20}[Zn(II) - H_2O]I_{abs}^{1/2}k_{19}^{-1/2}[O_{2\,ads}]}{k_{-20} + k_{21}[O_{2\,ads}]} \qquad \text{(high intensity)} \qquad (28)$$

$$R_{21} = \frac{k_{21}I_{abs}[O_{2\,ads}]}{k_{-20} + k_{21}[O_{2\,ads}]} \qquad \text{(low intensity)} \qquad (29)$$

Rearranging equations 28 and 29 and collecting constants gives the result:

$$R_{21} = \frac{k_{obs}I_{abs}^{1/2}\kappa[O_{2\,ads}]}{1 + \kappa[O_{2\,ads}]} \qquad \text{(high intensity)} \qquad (30)$$

$$\text{with } k_{obs} = k_{20}k_{19}^{-1/2}[Zn(II) - H_2O] \text{ and } \kappa = \frac{k_{21}}{k_{-20}} \qquad (31)$$

$$R_{21} = \frac{I_{abs}\kappa[O_{2\,ads}]}{1 + \kappa[O_{2\,ads}]} \qquad \text{(low intensity)} \qquad (32)$$

$$\text{with } \kappa = \frac{k_{21}}{k_{-20}} \qquad (33)$$

The quantum yield is defined as the ratio of the rate of the reaction to the rate of photon absorption. Therefore, the final expressions for the quantum yields are as follows:

$$\Phi = \frac{k_{obs} I_{abs}^{-1/2} \kappa[O_{2\,ads}]}{1 + \kappa[O_{2\,ads}]} \quad \text{(high intensity)} \tag{34}$$

$$\Phi = \frac{\kappa[O_{2\,ads}]}{1 + \kappa[O_{2\,ads}]} \quad \text{(low intensity)} \tag{35}$$

This dependence has also been observed in this laboratory for the case of photodegradation of chloroform (35) and for the case of photoinduced polymerization of methyl methacrylate (36).

The semiconductor excitation wavelength dependence of the rate of peroxide production was also examined using acetate as the hole scavenger. Excitation wavelengths between 320 and 380 nm were selected using a Jarrell-Ash Monospec 27 triple grating monochromator with a resolution of 1.0 nm using a 0.5mm slit width. The results are shown in Figure 10. The production rate decreases as the wavelength increases, in a manner which loosely follows the absorption spectrum of the colloidal solution as shown in the inset to Figure 10. The quantum yields of peroxide production as a function of wavelength are listed in Table 3.

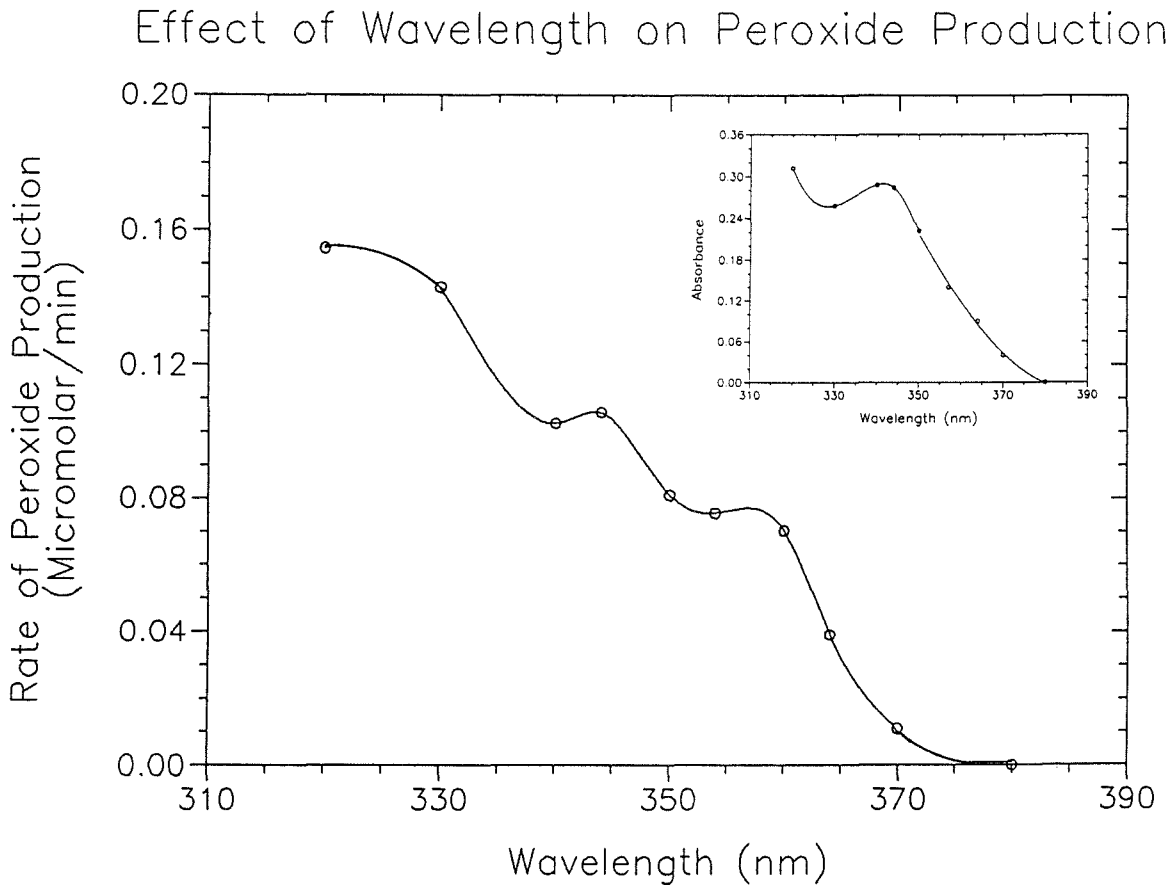

Figure 10: Effect of semiconductor excitation wavelength on rate of hydrogen peroxide production. 1mM Q-sized ZnO, 2mM acetate.

Wavelength (nm)	Quantum Yield (%)
320	9.15
330	16.32
340	3.99
344	4.08
350	3.86
354	4.23
360	6.86
364	4.35
370	1.45

Table 3: Wavelength dependence of quantum yields of hydrogen peroxide production. Corrected for differences in absorbed light intensity. 1mM Q-sized ZnO, 1mM acetate.

The effect of the size of the semiconductor particles and the type of semiconductor were also examined using 2.0 mM acetate as the hole scavenger. The initial rates of H_2O_2 production were 100 to 1000 times slower for bulk ZnO (diameter 1 μm, 1 mM) than for 1mM Q-sized ZnO. (We were unable to compare quantum yields due to the light scattering by the bulk ZnO.) When Q-sized ZnO and Q-sized TiO_2 (synthesized according to the method of Kormann et al. (37), diameter 2 nm) were compared, the quantum yields of both H_2O_2 and ROOH production were significantly higher for ZnO than for TiO_2 (i.e., 2.1% and 0.5% for ZnO vs. 0.1% and 0.1% for TiO_2). These results are complicated by the increased coagulation rate of TiO_2 in the presence of 2.0 mM acetate and the tendency of peroxides to adsorb to the TiO_2 surface (38). Peroxide adsorption is not a problem with ZnO because addition of the biphthalate buffer dissolves the colloid prior to iodometric analysis for peroxides. Under these conditions TiO_2 does not dissolve, thus the peroxide quantum yields may be artificially lower for TiO_2. This may be partially compensated by the decreased light absorption intensity of TiO_2 versus ZnO, which results in higher quantum yields as demonstrated in Figure 9. Kormann et al. have also observed lower quantum yields of peroxide formation for TiO_2 Vs ZnO (39), and have shown that the lower steady state concentration of peroxide for TiO_2 arises from a decreased quantum yield of peroxide formation combined with an enhanced degradative quantum yield.

Figure 11 illustrates in greater detail the dependence of the quantum yield of peroxide formation upon the semiconductor particle size. Different diameters of Q-sized ZnO in isopropanol were obtained by synthesis at 0 °C followed by slower aging at low temperatures. The absorption spectrum of each colloid was recorded before and after each irradiation, and the absorption onset was used to calculate the average particle diameter according the method of Brus (40). The absorption spectra were also used to integrate the colloid absorption as a function of wavelength over the light output of the

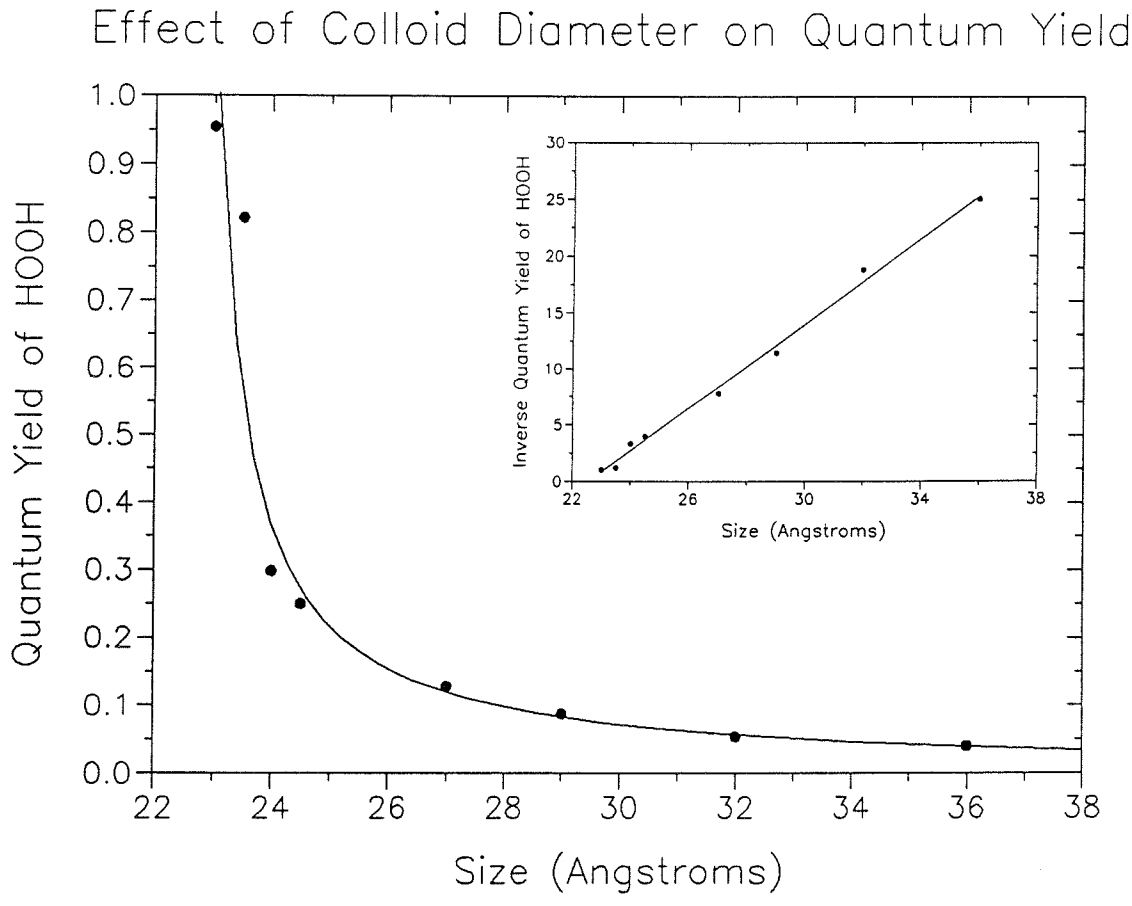

Figure 11: Particle size dependence of quantum yields. 1mM Q-sized ZnO, 2mM acetate, in isopropanol. Inset graph is fit of inverse quantum yield to particle diameter.

lamp/filter system as a function of wavelength. This was necessary to obtain the best value of the absorbed light intensity for each colloid since the absorption spectra change in intensity and red shift as a function of aging time. The quantum yields are much higher than before (approaching 1 at the lowest particle diameter) because isopropanol was used as the solvent. The quantum yields decrease rapidly as the Q-sized particle diameter increases. The data fits an inverse quantum yield versus particle diameter relationship, as shown in the inset to Figure 11. Decreasing quantum yields with increasing particle size has also been observed by Anpo et al. (41) for the photocatalytic hydrogenolysis of CH_3CCH with water using TiO_2 as a photocatalyst; however these quantum yields were calculated using incident light intensity instead of absorbed light intensity. The effect can be due to the increased surface area of the smaller diameter colloids or due to the enhanced redox potential of the conduction band electron.

Conclusions

We have demonstrated the production of H_2O_2 using oxygenated aqueous suspensions of semiconductors. Quantum yields as high as 30% have been obtained in the case of low light intensities with aqueous suspensions of ultrasmall particles, while quantum yields as high as 100% have been obtained using isopropanolic suspensions of ultrasmall particles. At high light intensities and long irradiation times, limiting steady state concentrations as high as 2mM have been observed. Using bulk ZnO, H_2O_2 was produced even in the absence of added hole scavengers; however, the concentrations were very low presumably due to back reactions of the peroxide with electrons or holes. Quantum yields increased as the concentration of the hole scavenger (e.g., acetate or isopropanol) increased. The hole scavenger competes with electron/hole recombination and increases the rate of peroxide production. The quantum yields depended on the type

of hole scavenger and increased in the order: citrate < no scavenger < acetate < oxalate < formate. The quantum yields for peroxide production depend strongly upon the absorbed light intensity and fit an inverse square root model. The dependence of the quantum yield on oxygen pressure was Langmuirian, suggesting that the primary formation of H_2O_2 occurs via the reduction of adsorbed oxygen by conduction band electrons. ^{18}O isotopic labeling experiments demonstrate that all the oxygen in the hydrogen peroxide product arises from dioxygen. The lack of scrambling of the higher mass ratios indicates that the O-O bond stays intact. The initial rates of peroxide production on bulk ZnO are 100 to 1000 times slower than those on Q-sized ZnO. Furthermore, the quantum yields decrease dramatically as the diameter of the Q-size ZnO increases. The observation of oxidized products of the hole scavenger, coupled with the increasing quantum yield for hydrogen peroxide formation with the concentration of the hole scavenger and the results of the isotopic labeling experiments strongly suggest that hydrogen peroxide is formed primarily as a product of reactions of the conduction band electron.

Acknowledgment. We are grateful to the US EPA (815041-01-0; 815170-01-0) for financial support, and we appreciate the assistance of Drs. Detlef Bahnemann, Claudius Kormann, and Peter Green in the early stages of this research.

References

1. Gunz, D. W.; Hoffmann, M. R. *Atmospheric Environment*, **1990**, *24A(7)*, 1601.

2. a) Hoffmann, M. R.; Boyce, S. D. in "Advances in Environmental Science and Technology;" Schwartz, S. E., Ed.; Wiley: New York, **1983**; Chapter 12, pp 147-189. b) Hoffmann, M. R.; Jacob, D. J. in "SO_2, NO, and NO_2 Oxidation Mechanisms: Atmospheric Considerations;" Calvert, J. G., Ed.; Acid Precipitation Series; Butterworth: Boston, MA, *1984*; Vol. III, pp 101-172. c) Jacob, D. J.; Hoffmann, M. R. *J. Geophys. Res. C: Oceans Atmos.* **1983**, *88*, 6611.

3. a) Kelly, T.J.; Daum, P. H.; Schwartz, S. E. *J. Geophys. Res. D: Atmos.* **1985**, *90*, 7861. b) Zika, R. G.; Saltzman, E.: Chameides, W. L.; Davis, D. D. *J. Geophys. Res. C: Oceans Atmos.* **1982**, *87*, 5015. c) Heikes, B. G.; Kok, G. L.; Walega, J. G.; Lazrus, A. L. *J. Geophys. Res. D: Atmos.* **1987**, *92*, 915.

4. Chameides, W.L.; Davis, D. D. *J. Geophys. Res. C: Oceans Atmos.* **1982**, *87*, 4863,

5. Zika, R. G.; Saltzman, E.; Chameides, W. L.; Davis, D. D. *J. Geophys. Res. C: Oceans Atmos.* **1982**, *87*, 5015.

6. a) Zika, R. G. *Elsevier Oceanogr. Ser.* (Amsterdam) **1981**, 31, 299. b) Cooper, W. J.; Zika, R. G. *Science* (Washington, D. C.) **1983**, *220*, 711. c) Moffett, J. W.; Zika, R. G. *Mar. Chem.* **1983**, *13*, 39.

7. a) Graedel, T. E.; Goldberg, K. I. *J. Geophys. Res. C: Oceans Atmos.* **1983**, *88*, 10865. b) Chameides, W. L. *J. Geophys. Res. D: Atmos.* **1984**, *89*, 4739.

8. Fendler, J. H. *J. Phys. Chem.* **1985**, *89*, 2730.

9. a) Schrauzer, G. N.; Strampach, N.; Hui, L. N.; Palmer, M. R.; Saleshi, J. *Proc. Natl. Acad. Sci. U.S.A.* **1983**, *80*, pp 3873-3876. b) Soria, J.; Conesa, J. C.; Augugliaro, V.; Palmisano, L.; Schiavello, M.; Sclafani, A. *J. Phys. Chem.* **1991**, *95*, 274.

10. Kormann, C.; Bahnemann, D. W.; Hoffmann, M. R.. *Environ. Sci. Technol.* **1988**, *22*, 798.

11. Ollis, D. F.; Pelizzetti, E.; Serpone, N. *Environ. Sci. Technol.* **1991**, *25(9)*, 1523.

12. a)Ollis, D. F.; Pelizzetti, E.; Serpone, N. in "Photocatalysis: Fundamentals and Applications;" Serpone, N.; Pelizzetti, E., Eds.; Wiley: New York, **1989**; pp. 604-637. b) Chemseddine, A.; Boehm, H. P. *J. Mol. Catal.* **1990**, *60*, 295. c) Kormann, C.; Bahnemann, D. W.; Hoffmann, M. R. *Environ. Sci. Technol.* **1991**, *25*, 494. d) Hidaka, H.; Zhao, J.; Pelizzetti, E.; Serpone, N. *J. Phys. Chem.* **1992**, *96*, 2226. e) D'Oliveira, J-

C.; Al-Sayyed, G.; Pichat, P. *Environ. Sci. Technol.* **1990**, *24*, 990. f) Kochany, J.; Bolton, J. R. *Environ. Sci. Technol.* **1992**, *26*, 262. g) Mills, G.; Chew, B.; Hoffmann, M. R., submitted to *Environ. Sci. Technol.*

13. a) Pruden, A. L.; Ollis, D. F. *J. Catal.* **1983**, *82*, 404. b) Serpone, N.; Pelizzetti, E., Eds. "Photocatalysis: Fundamentals and Applications," Wiley: New York, **1989**, 604.

14. Gerischer, H.; Heller, A. *J. Phys. Chem.* **1991**, *95*, 5261.

15. a) Henglein, A. *Chem. Rev.* **1989**, *89*, 1861. b) Brus, L. E. *J. Chem. Phys.*, **1984**, *80*, 4403. c) Brus, L. E. *J. Chem. Phys.*, **1983**, *79*, 5566.

16. Bahnemann, D. W.; Kormann, C.; Hoffmann, M. R. *J. Phys. Chem.* **1987**, *91*, 3789.

17. Heller, H. G.; Langan, J. R. *J. Chem. Soc., Perkin Trans.***1981**, *2* , 341.

18. Kormann, C.; Bahnemann, D. W.; Hoffmann, M. R. *Environ Sci. Technol.* **1988**, *22(7)*, 798.

19. Kormann, C.; Bahnemann, D. W.; Hoffmann, M. R. *Environ Sci. Technol.* **1988**, *22(7)*, 798.

20. Boer, K. W. "Survey of Semiconductor Physics," Van Nostrand Reinhold: New York, **1990**, 249.

21. Gratzel, M. "Heterogeneous Photochemical Electron Transfer," CRC Press: Boca Raton, FL, **1989**, p 101.

22. Memming, R. In "Topics in Current Chemistry;" Steckhan, E., Ed.; Springer-Verlag: Berlin, **1988**, Volume 143, pp 79-113.

23. Kormann, C.; Bahnemann, D. W.; Hoffmann, M. R. *Environ Sci. Technol.* **1988**, *22(7)*, 798.

24. a) Schumb, W. C.; Satterfield, C. N.; Wentworth, R. L. "Hydrogen Peroxide," Reinhold Publishing Corp.: New York, NY, **1955**, 291. b) Zellner, R.; Exner, M.; Hermann, H. *J. Atmos. Chem.* **1990**, *10*, 411.

25. Kormann, C.; Bahnemann, D. W.; Hoffmann, M. R. *Environ Sci. Technol.* **1988**, *22(7)*, 798.

26. Smith, R. M.; Martell, A. E. "Critical Stability Constants," Plenum Press: New York, **1977**, Vol. III, 1.

27. Buxton, G. V.; Greenstock, C. L.; Helman, W. P.; Ross, A. B. *J. Chem. Phys. Ref. Data* **1988**, *17(2)*, 513.

28. Gomes, W. P.; Freund, T.; Morrison, S. R. *J. Electrochem Soc.: Solid State Science* **1968**, *115(8)*, 818.

29. Okamoto, K-I; Yamamoto, Y.; Tanaka, H.; Itaya, A. *Bull. Chem. Soc. Jpn.* **1985**, *58*, 2023.

30. Turchi, C. S.; Ollis, D. F. *J. Catal.* **1990**, *122*, 178.

31. Calvert, J. G.; Theurer, K.; Rankin, G. T.; MacNevin, W. M. *J. Am. Chem. Soc.* **1954**, *76*, 2575.

32. Cahill, A. E.; Taube, H. *J. Am. Chem. Soc.* **1954**, *74*, 2312.

33. a) Foner, S. N.; Hudson, R. L. *J. Chem. Phys.*. **1962**, *36(10)*, 2676. b) Roberson, A. J. B. *Trans. Farad. Soc.* **1952**. *48*. 228. c) Lindemann, L. P.; Guffy, J. C. *J. Chem. Phys.*. **1958**, *29*, 246.

34. a) Lazrus, A. L.; Kok, G. L.; Gitlin, S. N.; Lind, J. A.; McLaren, S. E. *Anal. Chem.* **1985**, *57*, 917. b) McLaren, S. E.; Kok, G. L. submitted to *Anal. Chem.* c) Nyarady, S. T.; Barkley, R. M.; Sievers, R. E. *Anal. Chem.* **1985**, *57*, 2074.

35. Kormann, C.; Bahnemann, D. W.; Hoffmann, M. R. *Environ. Sci. Technol.* **1991**, *25*, 494.

36. Hoffman, A. J.; Mills, G.; Yee, H; Hoffmann, M. R. *J. Phys. Chem.*, **1992**, *96*, 5540.

37. Bahnemann, D. W.; Kormann, C.; Hoffmann, M. R. *J. Phys. Chem.*, **1987**, *91*, 3789.

38. Kiwi, J; Gratzel, M . *J. Mol. Catal.* **1987**, *39*, 63.

39. Kormann, C.; Bahnemann, D. W.; Hoffmann, M. R. *Environ Sci. Technol.* **1988**, *22(7)*, 798.

40. a) Henglein, A. *Chem. Rev.* **1989**, *89*, 1861. b) Brus, L. E. *J. Chem. Phys.*, **1984**, *80*, 4403. c) Brus, L. E. *J. Chem. Phys.*, **1983**, *79*, 5566.

41. Anpo, M; Shima, T.; Kodama, S.; Kubokawa, Y. *J. Phys. Chem.*, **1987**, *91*, 4305.

Chapter 6

Photocatalytic Oxidation of Organic Acids on Quantum-sized Zinc Oxide

[The text of this chapter has been submitted to *Env. Sci. Technol.* 1993.]

Abstract

A detailed analysis of products in the photocatalytic oxidation of acetate in the presence of quantum-sized ZnO particles is presented. The products observed were CO_2, HCO_2^-, HCHO, CH_3OOH, CH_3COOOH, and H_2O_2. The relative selectivity of electron donors by ZnO was HCO_2^- > HCHO > $CH_3CO_2^-$ > H_2O_2 > CH_3COOOH > CH_3OOH. Results are discussed in terms of reaction pathways involving direct oxidation of surface bound acetate by valence band holes or indirect oxidation of acetate by surficial hydroxyl radicals. The reaction rate stoichiometry (1:1 donor:H_2O_2) observed at a low rate of light absorption is not consistent with oxidation by free hydroxyl radicals. A mechanism involving the reaction of an intermediate carbon-centered radical with >ZnOH surface sites is proposed. Quantitative agreement with the array of products elucidated by von Sonntag and coworkers using homogeneous pulse radiolysis techniques is unlikely since in the heterogeneous system the hole scavengers are proposed to donate two electron equivalents. We have shown that while for acetate and formate there are differences in the rates of loss, the rates fail to correlate to the strength of the 1:1 Zn^{+2}-ligand stability constant (i.e., log K = 1.1 (acetate) vs. 0.7 (formate)). Since the differences in the degradation rates are small (i.e., -15 $\mu M\ min^{-1}$ (acetate) vs. -22 $\mu M\ min^{-1}$ (formate)), this implies that surface adsorption of the donor is not the limiting step. Thus, in this system in which the electron donors are strongly adsorbed, surface mediated reactions play a significant role in the stoichiometry and observed product distribution.

Introduction

The application of illuminated semiconductors for the destruction of contaminants has been used successfully for a wide variety of compounds such as PCBs, simple aromatics, halogenated alkanes and alkenes, surfactants, and pesticides (1-7). In many cases, complete mineralization has been reported, (i.e., the pollutant was oxidized fully to carbon dioxide and water)(8). Semiconductors are also excellent photocatalysts for the recovery of heavy metals (e.g., Pt^{4+}, Au^{4+}, Rh^{3+}) from aqueous solution (9). In addition, illuminated aqueous suspensions of semiconductors (CdS, CdSe, α-Fe_2O_3, TiO_2, and ZnO) have been shown to generate significant concentrations of hydrogen peroxide (10-15). Hoffman et al. have recently shown that ZnO produces H_2O_2 more efficiently than any other semiconductor (16).

Semiconductors with bandgap energies in the range of UV and visible light exhibit photocatalytic activity because light absorption produces a conduction band electron (a reductant) and a valence band hole (an oxidant). Even though the mechanistic details of the processes are not fully understood, hydrogen peroxide is known to be produced from dioxygen by reduction with conduction-band electrons while in contrast most organic compounds are degraded via oxidation by valence band holes or OH· radicals. Since the electron and hole are produced simultaneously, a suitable route of reaction for each reactant must be provided in order to compete with electron-hole recombination and thus increase the efficiency of the desired process. For example, the coating of TiO_2 with Pt "islands" which act as an "electron trap" increases the efficiency of the photo-oxidation of lactic acid presumably by short-circuiting the band-gap recombination process (17).

In the present study, the photo-oxidation of acetate, formate, and glyoxylate was investigated along with the concurrent production of hydrogen peroxide by quantum-sized

(Q-sized) ZnO. Acetate in particular was chosen as a hole scavenger, since it is already present as a by-product of the synthesis of Q-sized ZnO, and radiolysis studies of acetate oxidation have suggested that OH· and direct hole oxidation reactions would result in different products and product ratios (18,19). Q-sized ZnO particles (D_p = 40 Å) were selected as photocatalysts due to their negligible light scattering properties, higher specific surface areas, and larger bandgap energies relative to the bulk-sized semiconductor particles ($D_p \cong 0.1$ μm). Detailed product analyses for the oxidation of acetate and intermediate carboxylic acids are presented and discussed in terms of their mechanistic implications.

Experimental

Q-sized ZnO particles were synthesized in isopropanol according to procedures described previously (20). Zinc acetate (Fisher) and isopropanol (Fisher or Burdick & Jackson) were reagent grade and were used as received. Aqueous Q-sized ZnO suspensions were prepared by rotary evaporation to remove isopropanol followed by resuspension of the white residue in water purified by a Milli-Q/RO system to a resistivity of about 18 MΩ cm. The donors added to the suspensions were reagent grade and were used as received. These included sodium formate (Aldrich) and sodium glyoxylate (Sigma). The pH of the ZnO solutions was always approximately 7.8, due to the buffering by ZnO surface speciation.

Aqueous suspensions were irradiated with either a Kratos 450W xenon lamp or a Spindler and Hoyer 1000W xenon lamp. The ZnO suspensions were insulated from unnecessary heating by IR radiation and from degradation by higher energy UV radiation

through the use of a $CuSO_4$ water filter, a glass IR filter, and a Corning GS7601 filter (330-370 nm bandpass). Incident light intensity was measured using Aberchrome 540 according to procedures described by Heller and Langan (21). Absorbed light intensity was calculated from actinometer results by correcting for the absorbance of the solutions and the path length of the irradiation cell. The suspensions were continuously bubbled with oxygen for 30 minutes before and during irradiation in quartz-glass vessels at a temperature of 24 $^{o}C \pm 1\ ^{o}C$. Reaction volumes varied from 3 ml to 50 ml. In some cases, aliquots of the irradiation mixture were withdrawn at various times for composition analysis. However, in most experiments, separate solutions were prepared for each data point in concentration-time space. This facilitated multiple and duplicate chemical analyses on identical solutions in addition to the trapping of CO_2 released during complete oxidation.

Hydrogen peroxide and organic hydroperoxides were determined by several independent methods. Calibration curves for the various methods were constructed using standards prepared by dilution of a hydrogen peroxide stock solution which had been standardized by titration with potassium permanganate. The first method, which is sensitive to 1 μM H_2O_2, involved oxidation of I^- to I_3^- by peroxides as catalyzed by ammonium molybdate (22). The I_3^- product is quantified spectrophotometrically by absorbance at 352 nm ($\varepsilon = 26{,}400\ M^{-1}\ cm^{-1}$). Organic hydroperoxides have been found to react more slowly with I^- than hydrogen peroxide; thus H_2O_2 and ROOH are distinguished by measuring the absorbance after 2 minutes (for H_2O_2) and after 1 hour (for total peroxide). The absorbance measurements were made using a Hewlett-Packard 8451A Diode Array Spectrophotometer or a Shimadzu MPS-2000 Recording Spectrophotometer. With the Hewlett-Packard instrument, we found that the stability of the I_3^- absorbance was improved by using the 300 nm cut-off filter on the Hewlett-

Packard filter wheel to absorb excess UV light.

A second method for peroxide analysis, which is sensitive to 0.01 μM H_2O_2, involved the formation of a fluorescent dimer of p-hydroxyphenylacetic acid produced by the reaction of p-hydroxyphenylacetic acid (PHOPA) with peroxides as catalyzed by horseradish peroxidase (23). Fluorescence measurements were made using a Shimadzu RF-540 Spectrofluorimeter using excitation and emission wavelengths of 315 and 406 nm, respectively, and bandpasses of ≤10 nm. In this method, hydrogen peroxide and organic hydroperoxides can be distinguished by reacting the samples with catalase (Sigma) to destroy the H_2O_2 before the treatment with peroxidase to determine ROOH.

Hydrogen peroxide was also quantified by ion-exchange chromatography using a Dionex Bio-LC system equipped with the pulsed electrochemical detector and gold electrode. A Dionex OmniPac PAX-500 column and aqueous sodium hydroxide at pH 10 were used to separate hydrogen peroxide and organic hydroperoxides. The electrochemical program giving optimal sensitivity is shown in Table 1. The electrochemical approach used was modified from a procedure developed for hydroxy-compounds (24). Due to peroxide degradation in the mobile phase and on the column, the detection limits were only 40 μM for hydrogen peroxide and peracetic acid.

Peroxides were also analyzed chromatographically (25) with a Dionex Bio-LC fitted with an Alltech Econosphere C18 column (5 μm, 4.6 x 250 mm). 1 mN H_2SO_4 with 0.1 mM EDTA was used as the mobile phase. Post-column derivatization was performed using an Alpkem RFA-300 autoanalyzer and fluorescence was measured with the Shimadzu RF-540 Spectrofluorimeter using a quartz flow cell. The detection limits were 10 μM for hydrogen peroxide. The retention times were 10.0 min., 10.4 min., and 12.0 min. for H_2O_2, CH_3OOH, and CH_3COOOH respectively.

Table 1. Electrochemical Program
(Integrated Amperometry)

Time (sec)	Potential (V vs. pH)
0.00	+0.20
0.15	0.20
0.17	0.20
0.22	1.00
0.23	1.00
0.61	0.20
0.69	0.20
0.74	0.20
0.75	-0.33
0.80	-0.30
0.81	+0.10
Integration Time: 0.15 to 0.69 sec	

Table 1: Electrochemical program used to detect hydrogen peroxide by ion-exchange chromatography.

Carboxylic acid concentrations ($\geq$ 5 μM) were determined on a Dionex Bio-LC with a Dionex OmniPac PAX-500 column (8 μm, 5 x 250 mm) using a NaOH gradient coupled with conductivity detection. 100 μL of 0.01M HF was added to each 5 ml aliquot of illuminated solution before treatment with a Dionex OnGuard-H filter to remove excess Zn^{+2} which would otherwise precipitate at the high pH of the eluant. Formaldehyde ($\geq$ 5 μM) was detected using the Nash method (26). Carbon dioxide was analyzed by scrubbing the oxygen gas used for bubbling in a NaOH solution. The amount of CO_2 absorbed was calculated from the drop in pH.

Results and Discussion

Background

Previous radiolysis studies by von Sonntag and coworkers (18,19) indicated that the oxidation of acetate should produce different product state distributions depending on whether the oxidation proceeds via hydroxyl radicals (either adsorbed at the surface or free in solution) to abstract an H atom followed by oxygen addition and disproportion reactions, or whether the oxidation proceeds via direct oxidation with valence band holes followed by CO_2 loss in a photo-Kolbe type reaction. The two pathways are outlined in Figure 1. Von Sonntag and coworkers found the final products of the radiolysis of acetate ($OH\cdot$ pathway) at pH 7.8 to be glyoxylic acid (2.7), glycolic acid (0.7), formaldehyde (1.4), carbon dioxide (1.4), hydroperoxide (0.7), and hydrogen peroxide (2.5). The G values, which are given in parentheses, are defined as the number of molecules of each product formed per 100 eV of absorbed energy. The products from the direct oxidation of acetate by valence band holes are expected to correspond to those observed for the aqueous-phase radiolysis of CH_4 and N_2O. These products at pH 8 are (G values in

Proposed Reaction Mechanisms

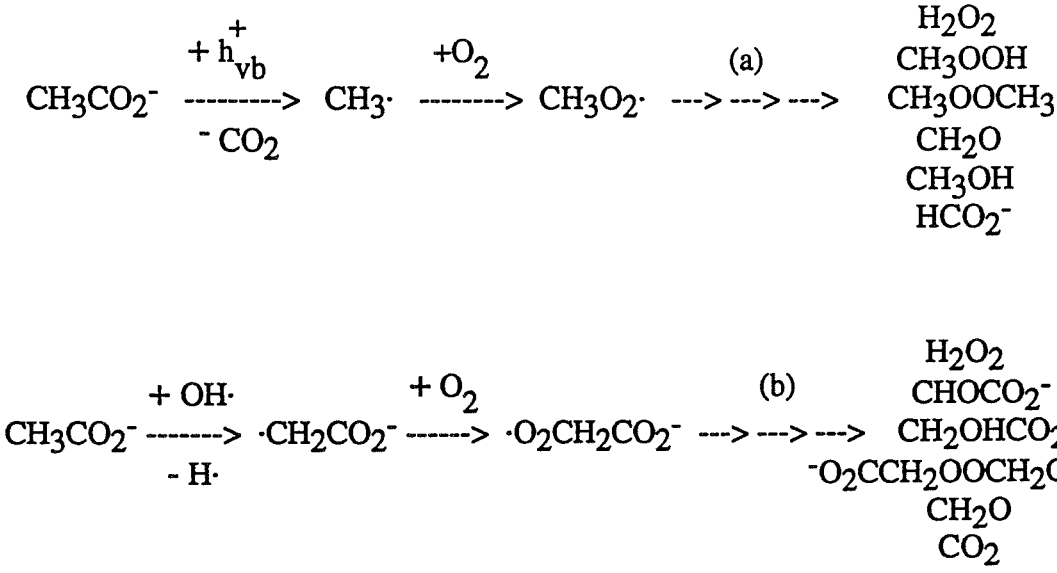

Figure 1: Two possible pathways for the oxidation of acetate in aqueous semiconductor colloids. Pathway ***a*** is the direct oxidation via the valence band holes. Pathway ***b*** is the indirect oxidation via hydroxyl radicals.

parentheses) formaldehyde (2.8), hydrogen peroxide (2.1), methanol (1.5), methylhydroperoxide (0.8), formic acid (0.3), and dimethyl peroxide (0.1).

Convincing evidence for both pathways exists in the literature. For example, intermediates detected during the photocatalytic degradation of halogenated aromatic compounds are typically hydroxylated structures (27). These intermediates are consistent with those found when similar aromatics are reacted with a known source of hydroxyl radicals. In addition, ESR studies have verified the existence of hydroxyl and hydroperoxyl radicals in aqueous solutions of illuminated TiO_2 (28). Mao et al. (29) have found that the rate of oxidation of chlorinated ethanes correlates with the C-H bond strengths of the organics, which indicates that H atom abstraction by OH· is an important factor in the rate-determining step for oxidation. The strong correlation between degradation rates and concentration of the organic pollutant adsorbed to the surface (30) also implies that the hydroxyl radicals are adsorbed at the surface; however, evidence has also been presented for the homogeneous phase hydroxylation of furfuryl alcohol in aqueous ZnO suspensions (31). On the other hand, Mao et al. (29) have observed that trichloroacetic acid and oxalic acid, with TiO_2 as photocatalyst, are oxidized primarily by valence band holes via a photo-Kolbe process. (These compounds also have no hydrogen atoms available for abstraction by OH·.) Likewise, Draper and Fox (32) were unable to find evidence of any hydroxyl radical adducts for the TiO_2 sensitized reactions of potassium iodide, 2,4,5 trichlorophenol, tris(1,10-phenanthroline)-iron(II) perchlorate, N,N,N',N'-tetramethyl-p-phenylenediamine, and thianthrene. They used the technique of diffuse reflectance flash photolysis with a time resolution of 15 ns. In each case where the product of hydroxyl radical mediated oxidation was known from pulse radiolysis studies to be different from that of direct electron transfer oxidation, Draper and Fox observed only the products of the direct electron transfer oxidation.

Products of Acetate Oxidation

Loss of acetate and yields of several of the predicted stable products from the photooxidation of acetate by Q-sized ZnO were measured as a function of irradiation time. Figure 2 shows the results obtained for a suspension of ZnO in which the electron donor is the native 2.0 mM acetate ion. The H_2O_2 and ROOH analyses were performed using the iodide colorimetric method. The production of carbon dioxide was also measured; however, the pH changes were too small at early times to accurately determine the carbon dioxide concentration. Instead, the carbon dioxide concentrations were determined from longer irradiations (1 hour). The results obtained when additional donors, formate and glyoxylate at 2 mM, were added are shown in Figures 3 and 4, respectively. As described in the experimental section, each point is derived from an independently irradiated solution. Variations in absorbance from solution to solution and in incident light intensity would affect the rate of light absorption and thus the rate of change in concentration of these compounds. The data shown in Figures 2-4 have not been corrected or normalized for these variations because the effects have been determined to be small. Adjusting for the 5 cm path length in the irradiation cell yields transmittances of less than 2% for all of the colloid suspensions. Actinometry results have shown the variation in lamp intensity over approximately 12 hours of continuous operation is about 5%. Initial rates of loss or formation of these species have been calculated from the data in Figures 2-4 and are given in Table 2. The use of initial rates is important because of the potential for products of the donor-hole reaction to participate in subsequent donor-hole reactions.

Several conclusions can be drawn from Figures 2-4 and Table 2. First of all, the presence of acetate at a concentration of about 2 mM does not affect the ability of other electron donors to interact with the colloid. In fact, any other added donor species appears to be preferentially oxidized. This is evidenced by the net change in acetate

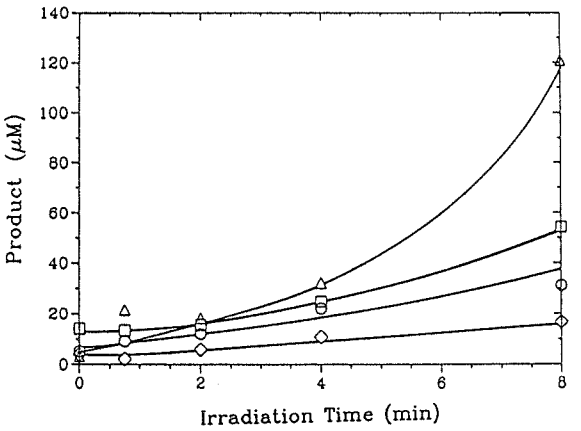

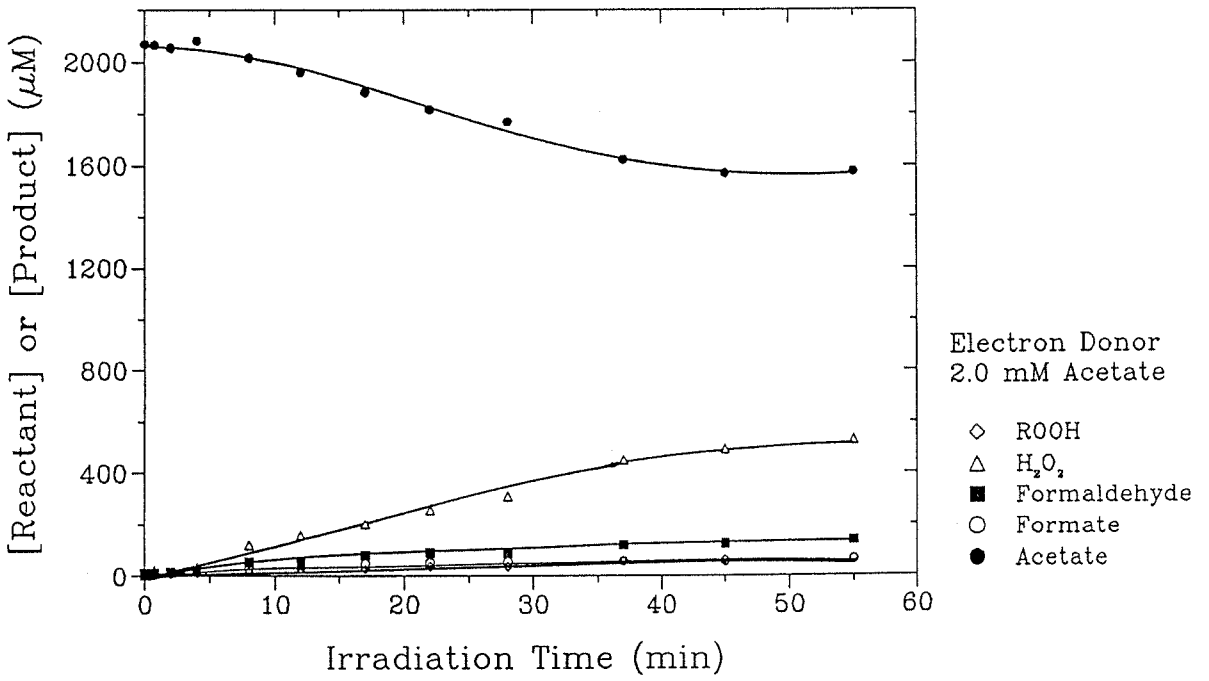

Figure 2: Photooxidation of 2.0 mM acetate using 1 mM Q-sized ZnO as photocatalyst.

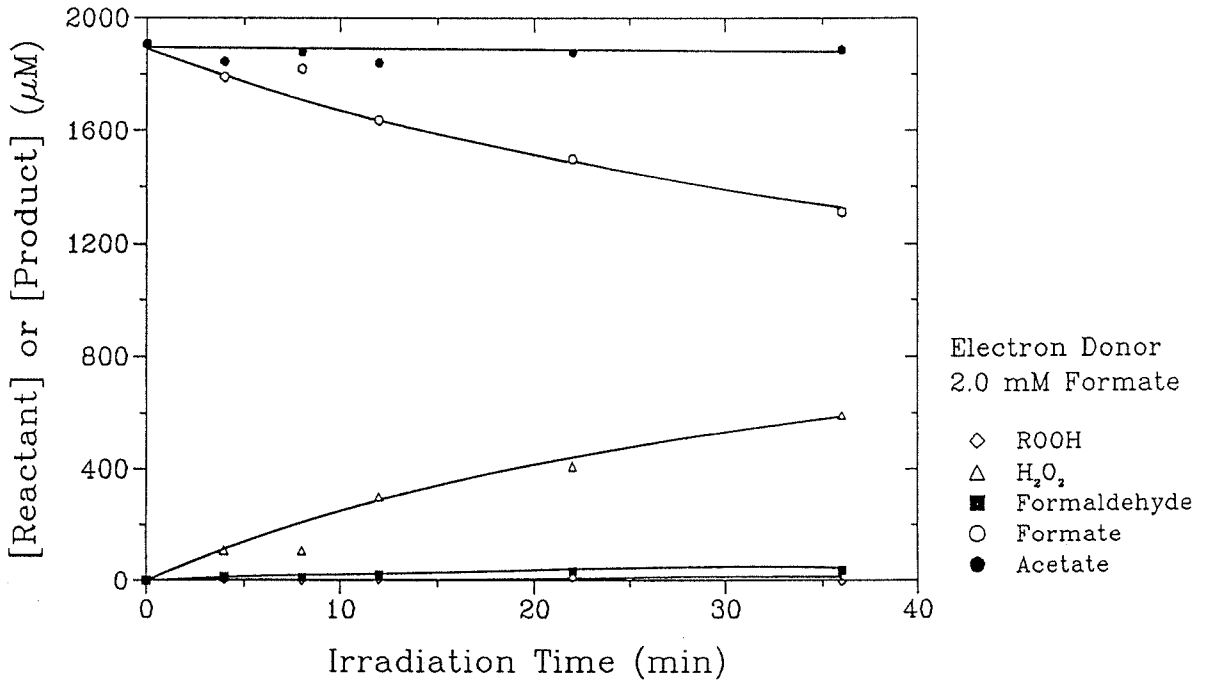

Figure 3: Photooxidation of 2.0 mM formate using 1 mM Q-sized ZnO as photocatalyst.

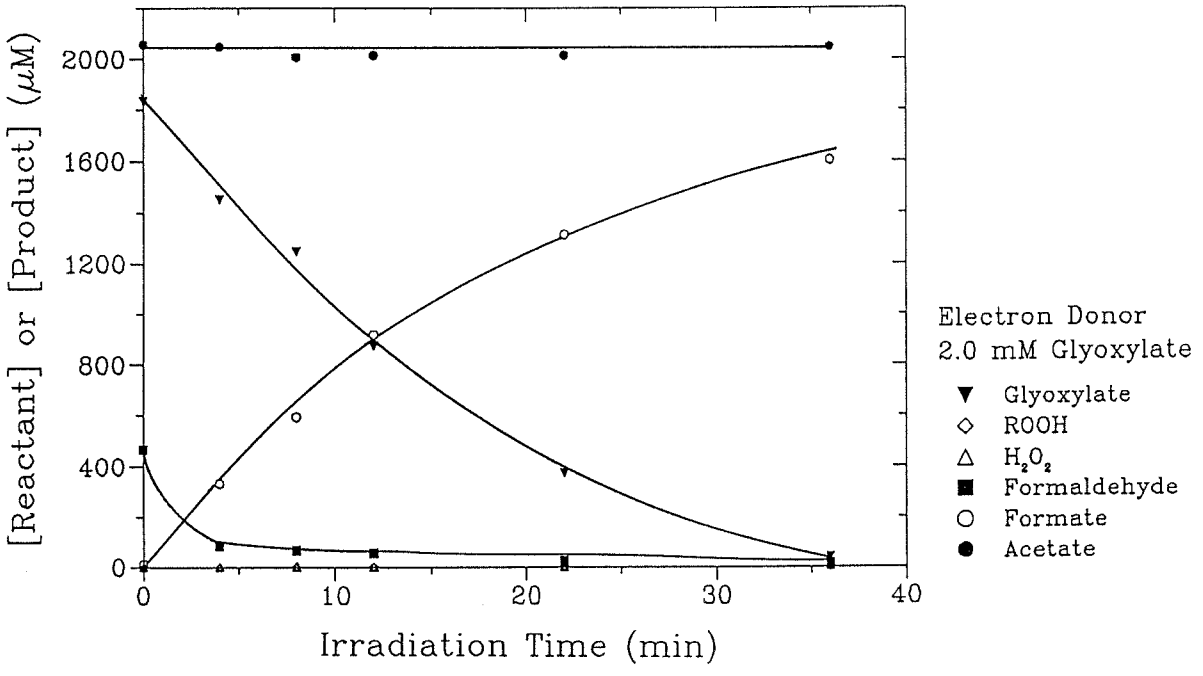

Figure 4: Photooxidation of 2.0 mM glyoxylate using 1 mM Q-sized ZnO as photocatalyst.

Table 2. Initial Rates of Formation or Loss (in μM/min)

Species→ Donors ↓	$CH_3CO_2^-$	CH_2O	HCO_2^-	$CHOCO_2^-$	H_2O_2	RO_2H
$CH_3CO_2^-$	-14.7 ± 0.5	+6.6 ± 0.7	+4.2 ± 0.4	N/O	+17.8 ± 3.8	+2.6 ± 0.1
HCO_2^-	-1.9 ± 0.7	+1.5 ± 0.5	-22.3 ± 1.7	N/O	+25 ± 0.8	+0.03 ± 0.1
$CHOCO_2^-$	-0.1 ± 0.8	-96 (initial) -3.3 ± 0.2 (2nd region)	+74 ± 2.0	-79 ± 6.0	+0.2 ± 0.02	+0.03 ± 0.04

N/O=Not Observed; Uncertainty in slope linear regression indicated by ± values.

Table 2: Initial rates of reactant loss and product formation in the photooxidation of organic acids by Q-sized ZnO. (The quantum yields equal these rates divided by the absorbed light intensity: 440 μM einsteins min^{-1} l^{-1}.)

concentration of nearly zero in irradiations with added formate and glyoxylate (Figures 3-4). A reasonable explanation for the small loss observed is that some acetate is closely associated with the ZnO matrix during the synthesis and this acetate is quickly reacted. The decreases in acetate concentration are on the order of the experimental uncertainty and are less than 200 μM, which is the amount of acetate which was found to be non-dialyzable at pH 7.8.

A comparison of initial rates of degradation of the donors combined with a knowledge of their chemistry allows one to deduce a relative selectivity of electron donors by ZnO:

$$HCO_2^- > HCHO > CH_3CO_2^- > H_2O_2 > CH_3COOOH > CH_3OOH$$

This ordering primarily reflects the observation that acetate performs only moderately well as an electron donor in this system. Formate is the most effective donor studied. In another study, the rate of hydrogen peroxide formation decreased in the following order of electron donors: $HCO_2^- > C_2O_4^{2-} > CH_3CO_2^-$. The redox potentials (vs. NHE) of formate, formaldehyde, oxalate, acetate, and hydrogen peroxide are 2.16, -1.22, 2.43, 2.33, and 1.78 V respectively (33). For comparison, at pH 8, the redox potentials (vs. NHE) of the electron and hole in ZnO are approximately -0.33 and 2.87 V respectively (34).

Formaldehyde is difficult to place in this order, because it is observed in low concentrations compared to acetate and added formate. In the glyoxylate experiments, the initial rate of formaldehyde degradation appears to be the highest observed in all the experiments. However, in irradiations with acetate, the concentration of formaldehyde builds up to a higher level than formate, indicating a higher rate of formation and/or a

slower rate of degradation. Formaldehyde has been shown to be a major product, formed in large excess over formate, in both studies by von Sonntag and coworkers (18,19). This supports a higher rate of formation of formaldehyde in the ZnO system. When acetate is the only electron donor present initially, the formate concentration levels off more quickly than does formaldehyde. This is consistent with a higher rate of oxidation of formate. At pH 7.7, formate would be expected to be attracted to the net positively charged ZnO surface (pH_{zpc} = 9.3) and therefore exhibit a higher rate of degradation. Based on these electrostatic considerations, formate is ranked above formaldehyde as an electron donor. The initially high level of formaldehyde in the experiments with added glyoxylate is artificially elevated due to interference by glyoxylate. At high concentrations, glyoxylate exhibits a positive response to the Nash method. This response equals 1/10 of the response observed with an equivalent concentration of formaldehyde.

Based upon the results in Table 2, glyoxylate appears to exhibit the fastest rate of degradation of all the added donors; however, the very low production rate of H_2O_2 in the presence of glyoxylate suggests that either glyoxylate interferes with the reduction of dioxygen by conduction band electrons or glyoxylate rapidly degrades H_2O_2. Yokota et al. (35) investigated the homogeneous reaction of radioactively labeled $HCOCO_2^-$ and H_2O_2:

$$H^{14}COCO_2^- + H_2O_2 \rightarrow H^{14}CO_2^- + CO_2 + H_2O \qquad (1)$$

The reaction was found to be second order, with a rate constant of 2.27 $M^{-1}s^{-1}$ at pH 8.0 and 25 °C. Using this rate constant, the initial concentration of H_2O_2 necessary to give the observed rate of glyoxylate loss is 313 μM. Since initial hydrogen peroxide concentrations in the other runs with acetate and formate were below detection limits, this value appears to be unreasonable; however, in this heterogeneous system, the H_2O_2

produced at the semiconductor surface experiences a high local concentration of adsorbed glyoxylate which increases the rate of glyoxylate degradation by H_2O_2. The observation that the rate of glyoxylate degradation equals the rate of formate production suggests that formate is a direct product of glyoxylate degradation. Furthermore, the observation that glyoxylate loss continues at longer irradiation times in the presence of a high concentration of formate indicates that glyoxylate is a better hole scavenger that formate. A reaction mechanism consistent with these observations is as follows:

$$HCOCO_2^- + H_2O \Leftrightarrow HC(OH)_2CO_2^- \quad (2)$$

$$HC(OH)_2CO_2^- + h^+_{vb} \rightarrow HC(OH)_2CO_2\cdot \quad (3)$$

$$HC(OH)_2CO_2\cdot \rightarrow HC(OH)_2\cdot + CO_2 \quad (4)$$

$$HC(OH)_2\cdot + h^+_{vb} \rightarrow HCO_2^- + 2H^+ \quad (5)$$

$$O_2 + e^-_{cb} \rightarrow O_2\cdot^- \quad (6)$$

$$O_2\cdot^- + H^+ \rightarrow HO_2\cdot \quad (7)$$

$$2HO_2\cdot \rightarrow H_2O_2 + O_2 \quad (8)$$

$$HO_2\cdot + e^-_{cb} \rightarrow HO_2\cdot^- \quad (9)$$

$$HO_2\cdot^- + H^+ \rightarrow H_2O_2 \quad (10)$$

$$HCOCO_2^- + H_2O_2 \rightarrow HCO_2^- + CO_2 + H_2O \quad (11)$$

With the net result,

$$2HCOCO_2^- + O_2 \rightarrow 2HCO_2^- + 2CO_2 \quad (12)$$

With this stoichiometry, the corrected rate of glyoxylate loss via hole scavenging equals 39.5 $\mu M\ min^{-1}$.

Hydrogen peroxide is apparently a poor electron-donating agent. The build up of hydrogen peroxide to over 500 μM does not prevent acetate degradation and hydrogen

peroxide is observed to reach the highest concentrations of any products detected. It is difficult to assess the position of CH_3OOH and CH_3COOOH in this scheme because they are always observed in very small amounts. This is at least partially because they are formed in such small amounts, but could also be because of significant reactivity as an electron donor. However, hydroperoxides are less reactive than hydrogen peroxide and peracetic acid as oxidizing agents in reactions with catalase (25). As reducing agents in the iodide/molybdenum reaction, hydrogen peroxide is again more reactive (36). Therefore, CH_3OOH is placed as the poorest electron donating agent observed. Significant concentrations of organic peroxides are produced only when acetate is used as the hole scavenger. Essentially no organic peroxides are produced when formate, oxalate, or citrate are used as hole scavengers. The organic peroxides from acetate oxidation were identified via LC retention times to be methylhydroperoxide and peracetic acid. Figure 5 shows the time evolution of peroxides produced upon illumination of a Q-sized ZnO suspension containing 2 mM acetate as the hole scavenger. Formation of these peroxide products is consistent with the following mechanism:

$$CH_3COO^- + h_{vb}^+ \rightarrow \cdot CH_3 + CO_2 \quad (13)$$

$$\cdot CH_3 + HO_2\cdot \rightarrow CH_3OOH \quad (14)$$

$$\cdot CH_3 + O_2 \rightarrow CH_3O_2\cdot \quad (15)$$

$$2CH_3O_2\cdot \rightarrow CH_3OOH + CH_2O_2 \quad (16)$$

$$CH_3COO^- + H_2O_2 \rightarrow CH_3COOOH + OH^- \quad (17)$$

In the case of formate, no organic peroxides would be expected since oxidation of formate leads to the formyl radical which rapidly oxidizes to CO_2:

$$HCOO^- + h_{vb}^+ \rightarrow HCOO\cdot \quad (18)$$

$$HCOO\cdot \rightarrow CO_2 + H^+ + e^- \quad (19)$$

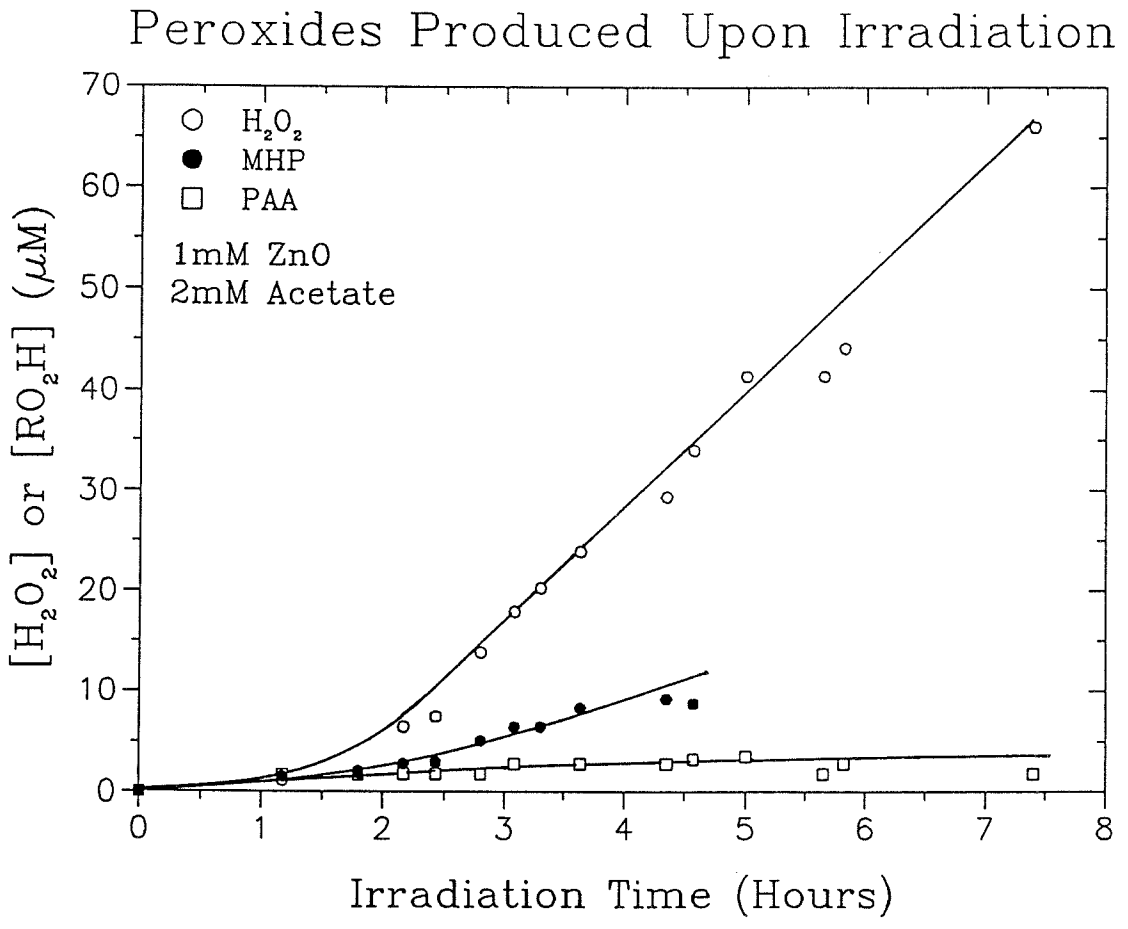

Figure 5: Peroxide production in an irradiated Q-sized ZnO suspension. 1 mM ZnO, 2 mM acetate

Mass Balance Analysis

The absence of sufficiently sensitive carbon dioxide measurements at short illumination times precludes an exact time-resolved mass balance in systems investigated here. In the acetate donor case, comparing the initial rate of loss of acetate to rates of formation of all the observed products gives 46% recovery on the basis of carbon (assuming hydroperoxides contain a single carbon). The G values reported by von Sonntag and coworkers[18,19] can be used to predict how much carbon dioxide should be produced for a given rate of acetate degradation for each mechanism. For indirect oxidation of acetate by hydroxyl radical, this correction brings the carbon mass balance to 59%. For direct oxidation or the photo-Kolbe mechanism, the rate of CO_2 production should be equal to acetate loss at early irradiation times. This correction brings the mass balance to 96%. The validity of this correction is demonstrated in another one hour irradiation experiment, in which the rate of loss of acetate was observed to be equal to the rate of production of CO_2 and to the rate of production of hydrogen peroxide. The irradiations with added formate and glyoxylate also achieve carbon balance if one assumes that formate and formaldehyde are oxidized to CO_2.

Implications for mechanism

Hydrogen peroxide may be produced by either the reduction of molecular oxygen and/or the oxidation of water. We have shown by ^{18}O isotopic labeling experiments (Chapter 5) that the production of H_2O_2 by photo-excited ZnO results from the two electron reduction of dissolved molecular oxygen (37). The concurrent one electron oxidation of a donor results in the formation of a radical species which can give an array of stable products via subsequent one electron reduction or oxidation reactions or by radical-radical combinations. The experimental results and mechanisms proposed by von

Sonntag and coworkers are under conditions in which the former is minimized and his mechanisms predict that products arise almost solely through dimerized radical precursors. Thus, for the radiolysis product yields to be quantitatively applicable here, the stoichiometry of $CH_3CO_2^-$:H_2O_2 should be 2:1. In the case of acetate and formate as donors, the initial rate of loss of these donors is 10 to 20% less than the initial rate of hydrogen peroxide formation.

To explain the observed stoichiometry of nearly 1:1, it is necessary to postulate a mechanism in which the donor is doubly oxidized. Two such possibilities will be considered here. In the first scheme, a donor undergoes a one electron oxidation and the resulting radical is trapped until a second reactive site is formed, i.e., a photon is absorbed and results in the formation of an electron-hole pair. Thus, the original donor undergoes two sequential one electron oxidations. In the second pathway, the radical species formed is oxidized by reaction with the ZnO particle via electron injection, producing a second conduction band electron which can further reduce oxygen. The net result is that one photon produces a two-electron reduction of O_2 and a two-hole oxidation of the donor, or, equivalently, current doubling. (This effect would cause the maximum quantum yield for hydrogen peroxide formation to be 1.0 instead of 0.5 as seen in Figure 11 of Chapter 5.)

In the first scheme, the amount of time between excitation events could be crucial in limiting the distance the radical diffuses, assuming that the oxidation steps must occur on or very near the semiconductor particle surface. Calculations by Turchi and Ollis (38) have indicated that the hydroxyl radical formed at the TiO_2 surface could diffuse 100 Å or more before reaction with some solution species. In the present experiments, the irradiation rate (≈440 μM photons/min) and concentration of particles (1 mM ZnO and ≈ 3000 molecules/particle (20)) give that the rate of photon absorption is 22

photons/particle/sec. This flux then gives the maximum possible rate of valence band hole formation. (The actual rate is probably much lower because of electron-hole recombination.) However, this maximum rate would allow the acetate or other radical species a minimum of 45 milliseconds to diffuse from the ZnO surface. Assuming a diffusion coefficient of 10^{-9} m^2/sec, the radical could diffuse a maximum distance of 13 μm between successive photon hits. Thus, the singly oxidized donor must be trapped on or bound to the surface in order to explain two successive one-electron oxidations of acetate.

Lawless et al. (39) studied the reaction of Q-sized TiO_2 and ·OH generated using pulse radiolysis. They determined the rate constant of this reaction to be 6.0×10^{11} $M^{-1}s^{-1}$, near the diffusion-controlled limit, and point out that hydroxyl radical desorption is unlikely. The product of the reaction was found to be an oxidant, not a reductant, and the authors argue that it is indistinguishable from a trapped hole. Oxygen had no effect on the reaction. Radicals other than the hydroxyl radical could be expected to exhibit high reactivities, generating a surface trapped species which may exist until another valence band hole is produced. A surface trapped acetate or other carbon-centered radical, however, should be distinguishable from a trapped hole, minimally in its function as a reductant rather than an oxidant. The surface trap for the carbon-centered radical could be reaction with surface adsorbed oxygen, which may be present in abundance. This idea is analogous to homogeneous radiolysis reactions in oxygenated solutions in which carbon-centered radicals immediately add dissolved oxygen.

The following example illustrates both the precedent of postulating a surface carbon radical species and electron injection. A surface carbon radical intermediate was postulated by Morrison and Freund (40) to explain a "current-doubling" effect observed in photocatalytic studies using single-crystal ZnO electrodes and formate. They proposed the

following steps:

$$h_{vb}^{+} + HCOO^{-} \rightarrow HCOO\cdot \quad (20)$$

$$HCOO\cdot \rightarrow CO_2 + H^{+} + e_{cb}^{-} \quad (21)$$

This scheme accomplishes two electron oxidation of the donor by reaction with a valence band hole and injection of an electron into the conduction band, resulting in electron-paired products. Morrison and Freund found O_2 to quench current-doubling in the external circuit, presumably by the reaction:

$$HCOO\cdot + O_2 \rightarrow CO_2 + H^{+} + O_2^{-}\cdot \quad (11)$$

Thus, the electron may be either injected into the semiconductor and then transferred to adsorbed oxygen, or the electron may be transferred directly to oxygen. Either pathway produces a net two-hole oxidation of the electron donor and two electron reduction of oxygen per photon absorbed. Additional evidence for this electron injection scheme is seen in the observation that the quantum yields of peroxide production approach 1.0 in concentrated isopropanol solution (Chapter 5). Pulse radiolysis studies of Q-sized TiO_2 in isopropanol have demonstrated that the isopropyl radicals, $(CH_3)_2COH\cdot$, initially produced by the reaction of $OH\cdot$, are strong reductants (-1.23V vs. NHE) and rapidly inject electrons into the conduction band of TiO_2 (41). Glyoxylate, formate, and oxalate have exhibited current-doubling effects in semiconductor electrode systems; however, acetate has not previously exhibited this effect.

Returning to the original question, are the oxidation products observed more like oxidation of acetate by hydroxyl radical or by a direct, photo-Kolbe mechanism? The direct decarboxylation of acetate and other carboxylic acid donors is supported by the

following: 1) no glycolic acid was observed by anion chromatography even though radiolysis G values indicate it should be formed at half the rate of formaldehyde; 2) the assumption of one CO_2 per acetate lost closes the carbon mass balance; 3) the 1:1 donor:H_2O_2 stoichiometry observed cannot be explained without invoking surface reactions. Quantitative agreement with the array of products elucidated by von Sonntag and coworkers is unlikely since the hole scavengers are proposed to donate two electron equivalents. The major argument against direct or surface oxidation is that differences in adsorption capacity and kinetics should be reflected in rates of disappearance of the donors. We have shown that while for acetate and formate there are differences in the rates of loss, the rates fail to correlate to the strength of the Zn^{+2} binding constant (log k = 1.1 (acetate) vs. 0.7 (formate). In the previous study, we have shown that the quantum yields of H_2O_2 production are relatively insensitive to the nature of the hole scavenger (i.e., the quantum yield decreased from 5.4% to 4.2% as the strength of the Zn^{+2} binding constant increased from 0.7 (formate) to 3.9 (oxalate). Furthermore, if the differences between many types of donors are relatively small, it implies that surface adsorption of the donor is not the limiting step. Thus, in this system in which the electron donors are strongly adsorbed, surface mediated reactions play a significant role in the stoichiometry and observed product distribution; however, in other systems such as alkane oxidations in which adsorption is weak, homogeneous $OH\cdot$ reactions in the bulk solution may play a greater role.

Conclusions

We have shown that while the results of homogeneous radiolysis of acetate give invaluable information in planning experiments and understanding radical reactions, the details of the product array in the heterogeneous system studied here did not agree with either of two comparable homogeneous systems. The proposed source of the differences

is that donor radicals react with the semiconductor surface, forming trapped intermediates which are further oxidized via semiconductor holes or injecting a second electron into the conduction band. The mechanisms presented here, along with supporting evidence, should lead to studies in which direct evidence of more types of surface intermediates is sought, rather than free hydroxyl radical-donor adducts. In the future, experiments measuring rf conductivity of illuminated Q-sized semiconductor colloids containing hole scavengers may provide more insight into electron injection by the initially formed radicals.

References

1. Serpone, N.; Pelizzetti, E., Eds. "Photocatalysis: Fundamentals and Applications," John Wiley and Sons: New York, **1989**; 604.

2. Chemseddine, A.; Boehm, H. P. *J. Mol. Catal.* **1990**, *60*, 295.

3. Kormann, C.; Bahnemann, D. W.; Hoffmann, M. R. *Environ. Sci. Technol.* **1991**, *25*, 494.

4. Hidaka, H.; Zhao, J.; Pelizzetti, E.; Serpone, N. *J. Phys. Chem.* **1992**, *96*, 2226.

5. D'Oliveira, J-C.; Al-Sayyed, G.; Pichat, P. *Environ. Sci. Technol.* **1990**, *24*, 990.

6. Kochany, J.; Bolton, J. R. *Environ. Sci. Technol.* **1992**, *26*, 262.

7. Mills, G.; Chew, B.; Hoffmann, M. R., submitted to *Environ. Sci. Technol.*

8. Borgarello, E. *Inorg. Chem.* **1986**, *24*, 4999.

9. Ollis, D. F.; Pelizzetti, E.; Serpone, N. *Environ. Sci. Technol.* **1991**, *25*, 1523.

10. Stephens, R. E.; Ke, B.; Trivich, D. *J. Phys. Chem.* **1955**, *59*, 966.

11. Harbour, J. R.; Hair, M. L. *J. Phys. Chem.* **1977**, *81*, 1791.

12. Pappas, S. P.; Fischer, R. M. *J. Paint Technol.* **1974**, *46*, 65.

13. Cundall, R. B.; Rudham, R.; Salim, M. S. *J. Chem. Soc., Faraday Trans. 1* **1976**, *72*, 1642.

14. Fraissard, J. P.; Resing, H. A., Eds "Magnetic Resonance in Colloid and Interface Science"; Riedel Publ. Co.: Boston, MA. **1980**, 431.

15. Kormann, C.; Bahnemann, D. W.; Hoffmann, M. R. *Environ. Sci. Technol.* **1988**, *22*, 798.

16. Hoffman, A. J.; Carraway, E. R.; Hoffmann, M. R. submitted to *Environ. Sci. Technol.* **1993**.

17. Pelizzetti, E.; Serpone, N. Eds. "Homogeneous and Heterogeneous Photocatalysis," D. Reidel Publishing Co.: Boston, MA. **1986**, 404.

18. Schuchmann, M. N.; Zegota, H.; von Sonntag, C. *Z. Naturforsch.* **1984**, *40b*, 215.

19. Schuchmann, H-P.; von Sonntag, C. *Z. Naturforsch.* **1984**, *39b*, 217.

20. Bahnemann, D. W.; Kormann, C.; Hoffmann, M. R. *J. Phys. Chem.* **1987**, *91*, 3789.

21. Heller, H. G.; Langan, J. R. *J. Chem. Soc., Perkin Trans.* **1981**, *2*, 341.

22. Allen, A. O.; Hochmanadel, C. J.; Ghormley, J. A.; Davis, T. W. *J. Phys. Chem.* **1952**, *56*, 575.

23. Guilbault, G. G.; Brignac, P. J.; Juneau, M. *Anal. Chem.* **1968**, *40*, 1256.

24. a) Welch, L. E.; LaCourse, W. R.; Mead, D. A., Jr.; Johnson, D. C. *Anal. Chem.* **1989**, *61*, 555. b) Neuburger, G. G.; Johnson, D. C. *Anal. Chem.* **1988**, *60*, 2288. c) Johnson, D. C. *Nature* **1986**, *321*, 451. d) Rocklin, R. D.; Pohl, C. A. *J. Liquid Chromatog.* **1983**, *6*, 1577.

25. a) McLaren, S. E.; Kok, G. L., personal communication. b) Kok, G. L.; Thompson, K.; Lazrus, A. L.; McLaren, S. E. *Anal. Chem.* **1986**, *58*, 1192. c) Lazrus, A. L.; Kok, G. L.; Gitlin, S. N.; Lind, J. A.; McLaren, S. E. *Anal. Chem.* **1985**, *57*, 917.

26. a) Nash, T. *Biochem. J.* **1953**, *55*, 416. b) Reitz, E. B. *Analyt. Lett.* **1980**, *13*, 1073.

27. a) Augugliaro, V.; Palmisano, L; Sclafani, A.; Minero, C.; Pelizzetti, E. *Toxicol. Environ. Chem.* **1988**, *16*, 89. b) Al-Ekabi, H.; Serpone, N.; Pelizzetti, E.; Minero, C.; Fox, M. A.; Draper, R. B. *Langmuir* **1989**, *5*, 250. c) Ollis, D. F.; Hsiao, C.; Budiman, L.; Lee, C. *J. Catal.* **1984**, *88*, 89. d) Turchi, C. S.; Ollis, D. F. *J. Catal* **1989**, *119*, 480. e) Mills, G.; Chew, B.; Hoffmann, M. R. , submitted to *Environ. Sci. Technol.*

28. Jaeger, C. D.; Bard, A. *J. Phys. Chem.* **1979**, *83*, 3146.

29. Mao, Y; Schoneich, C.; Asmus K.-D. *J. Phys. Chem.* **1991**, *95*, 10080.

30. a) Hong, A. P.; Bahnemann, D. W.; Hoffmann, M. R. *J. Phys. Chem.* **1987**, *91(24)*, 6245. b) Bockelmann, D.; Goslich, R.; Bahnemann, D. in "Proceedings of the Fifth IEA Symposium on Solar High Temperature Technologies," Kesselring, P; Smerker, O.,Eds. Davos, **1990,** 127.

31. Richard, C.; Lemaire, J. *J. Photochem. Photobiol. A: Chem.* **1990**, *55*, 127.

32. Draper, R. B.; Fox, M. A. *Langmuir*, **1990**, *6*, 1396.

33. Bard, A. J.; Lund, H. "Encyclopedia of Electrochemistry of the Elements, Vol. XII," Marcel Dekker: NY **1978**, 252.

34. Serpone, N.; Pelizzetti, E., Eds. "Photocatalysis," John Wiley and Sons: New York, **1989**, 136.

35. Yokota, A.; Kitaoka, S.; Miura, K.; Wadano, A. *Planta* **1985**, *165*, 59.

36. Kormann, C.; Bahnemann, D. W.; Hoffmann, M. R. *Environ. Sci. Technol.* **1988**, *22*, 798.

37. a) Hoffman, A. J.; Carraway, E. R.; Hoffmann, M. R. submitted to *Environ. Sci. Technol.* **1993** b) Calvert, J. G.; Theurer, K.; Rankin, G. T.; MacNevin, W. *J. Am. Chem. Soc.* **1954**, **76**, 2575.

38. Turchi, C. S.; Ollis, D. F. *J. Catal.* **1990**, *122*, 178.

39. Lawless, D.; Serpone, N.; Meisel, D. *J. Phys. Chem.* **1991**, *95*, 5166.

40. a) Morrison, S. R.; Freund, T. *J. Chem. Phys.* **1967**, *47*, 1543. b) Gomes, R.; Freund, T.; Morrison, S. R. *J. Electrochem. Soc.* **1968**, *115*, 818.

41. Pelizzetti, E.; Serpone, N. Eds. "Homogeneous and Heterogeneous Photocatalysis," D. Reidel Publishing Co.: Boston, MA. **1986**, 218.

Chapter 7

Formation of Humic-like Substances in Q-sized Semiconductor Colloids

Humic substances comprise a general class of biogenic, yellow-black organic substances that are ubiquitous in terrestrial and aquatic environments. These humic substances constitute the major fraction of organic compounds in soils. They are described as amorphous polymers (300 to 30,000 molecular weight) containing primarily phenolic OH and carboxylic groups with a lower number of aliphatic OH groups. Based on their solubility in alkaline and acid solutions, humic acids are ususally divided into three fractions (1): humic acid, which is soluble in alkaline solution but is precipitated by acidification below pH 2; fulvic acid, which is the humic fraction that is soluble over the entire pH range; and humin, the fraction that cannot be extracted by acid or base. Structurally, the three fractions are believed to be similar, although they differ somewhat in molecular weight and functional group content. For example, fulvic acid has probably a lower molecular weight but more hydrophilic functional groups than humic acid and humin. Humic substances do not correspond to a unique chemical entity and cannot be described in unambiguous structural terms. The structure (2) varies depending upon the source environment (i.e., whether the sample is from a river, peat bog, ocean, estuary, or lake). Several proposed structures are shown in Figure 1.

Humic substances are important in the global carbon cycle because they serve as a major reservoir of organic carbon in soils and in marine waters. Humic and fulvic acids also contribute to the cation-exchange capacity of the soil, due largely to the ionization of the carboxylate groups. Humic acids form stable complexes with polyvalent cations, which facilitates the mobilization, transport, segregation, and deposition of trace metals in soils, sediments, and water columns. In addition, humic substances also sorb compounds introduced into soils and sediments as pesticides or noxious waste organic chemicals. Bioactivity, persistence, biodegradability, leachability, and volatility of organic chemicals are all affected by this sorption phenomenon. For all of these reasons, humic substances play a very important role in the environment.

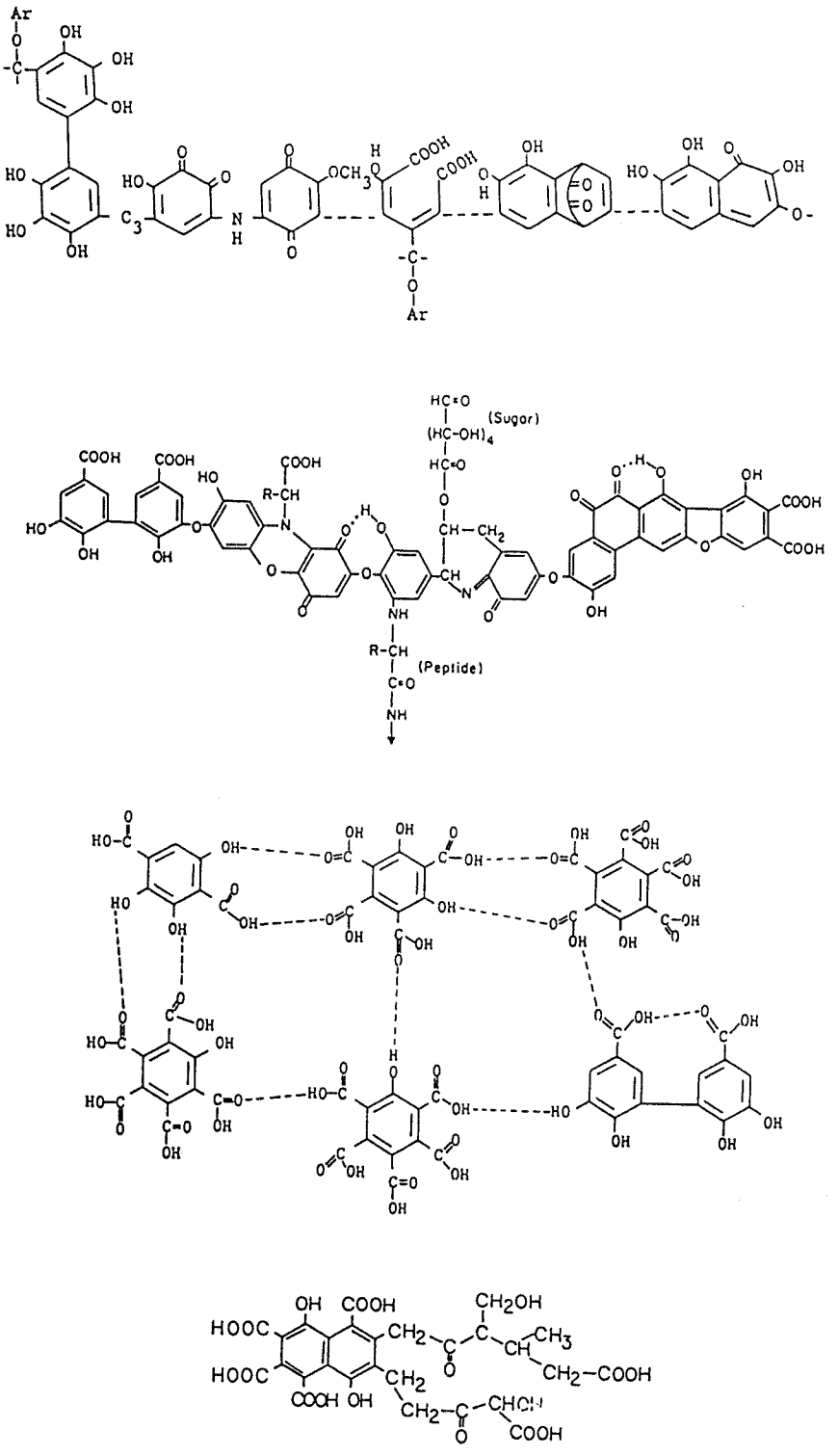

Figure 1: Several proposed structures for humic and fulvic acids.

The biochemical processes by which humic substances form are not fully understood. Generally, four stages of development occur in the transformation of soil biomass to humic substances (3). They are as follows: (1) decomposition of the biomass components, including lignin, into simple organic compounds, (2) microbial metabolism of the simple compounds, (3) cycling of C,H, N, and O between soil organic matter and the microbial biomass, and finally (4) microbially mediated polymerization of the cycled organic compounds.

Recent studies in this laboratory indicated that Q-sized semiconductors are efficient photoinitiators for the polymerization of vinylic monomers (4). These results lead to the proposal that humic substances could also be formed by semiconductor photoinduced polymerization of simple organic compounds. Early work by Markham, Hannan, and Evans (5) on the oxidation of phenols catalyzed by ZnO and light provided support for this theory. They observed under certain conditions the precipitation of dark amorphous powders which exhibited general absorption throughout the ultraviolet and blue regions of the spectrum when in acidic or basic solution. This communication details an investigation of polymerization of phenolic compounds using Q-sized ZnO as photocatalyst.

Colloidal suspensions of ZnO with a mean diameter of 5 nm were synthesized via the controlled hydrolysis of $Zn(CH_3COO)_2$ in isopropanol (6). The photolysis apparatus consisted of a Spindler and Hoyer 1000W Xe arc lamp. A combination of a $CuSO_4$ water filter, a glass IR filter, and a Corning GS7601 filter (bandpass 330-370 nm) was employed. Light intensities during photolysis were 1.0 X 10^{-4} einsteins l^{-1} min^{-1} .

In a typical experiment, 25 ml samples of 1mM ZnO colloid in isopropanol were evaporated in a rotoevaporator to yield thin films of ZnO which were immediately resuspended into an equal volume of water containing the 2mM phenolic compound. The pH of each stock solution of the phenolic compound was adjusted to 7.5 prior to resuspension. The suspension was transferred to a quartz-windowed reactor, and bubbled with oxygen for 10 minutes before and during irradiation. After irradiation, samples were filtered to obtain the product. UV/Vis absorption spectra were measured using a Hewlett Packard 8451A diode array spectrophotometer.

Colloidal suspensions containing Q-sized ZnO and either phenol, catechol or gallic acid were irradiated for two hours. Phenol irradiation produced no observable change other than precipitation of the colloid. Gallic acid irradiation produced a slight yellow coloration in two hours. The absorption spectrum indicated a weak absorbance tailing off to 600 nm. Catechol irradiation produced a faint yellow color in less than ten minutes of irradiation, which deepened to a dark brown colored solid with continuing illumination. A blank solution containing catechol and ZnO in the dark demonstrated no color change in two hours; however, measuring the absorbance of the blank solution in the HP diode array spectrophotometer caused a slight yellow color change. The spectra of the ZnO/catechol solution before and after irradiation is shown in Figure 2. The featureless absorption tail to 800 nm is typical of humic acids (7). The brown solid, when separated by filtration and acidified to pH 1, dissolved and produced a similar, but weaker absorbance spectrum. Some of the dark coloration may also be due to Zn(0) formation, which would dissolve upon acidification.

The products formed in illuminated Q-sized ZnO suspensions containing catechol should be further characterized by FT-IR or elemental analysis; however, these preliminary results suggest that humic-like substances are formed. The mechanism probably involves

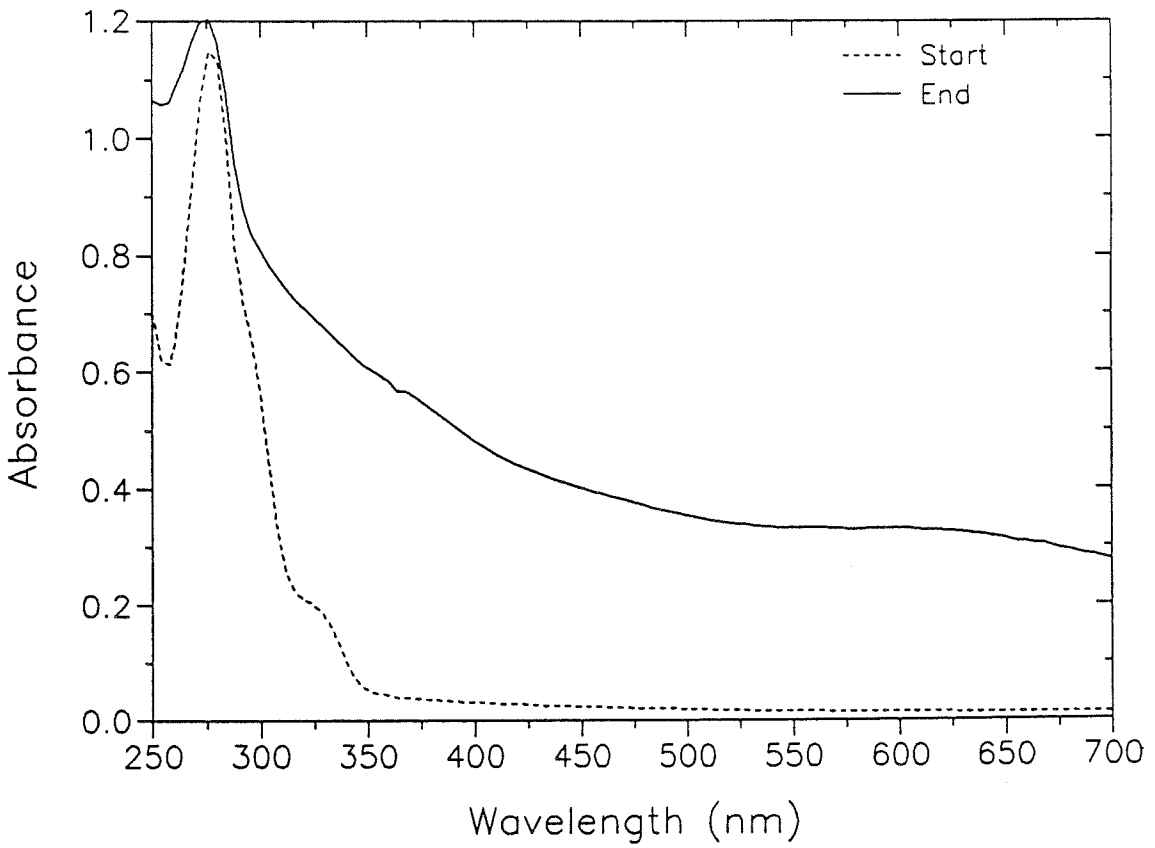

Figure 2: UV-Vis absorption spectra of 1mM Q-sized ZnO solutions containing 2.0mM catechol, before and after illumination at 330-370 nm.

initiation by OH· radicals, followed by polymerization. This reaction may provide an additional pathway for the formation of humic-like substances in polluted surface waters.

References

1. Stumm, W.; Morgan, J. J. "Aquatic Chemistry," John Wiley and Sons: New York, **1981**, 514.

2. Aiken, G. R.; McKnight, D. M.; Wershaw, R. L., MacCarthy, P., Eds. "Humic Substances in Soil, Sediment, and Water," John Wiley and Sons: New York, **1985**, 23.

3. Aiken, G. R.; McKnight, D. M.; Wershaw, R. L., MacCarthy, P., Eds. "Humic Substances in Soil, Sediment, and Water," John Wiley and Sons: New York, **1985**, 21.

4. a) Hoffman, A. J.; Mills, G.; Yee, H.; Hoffmann, M. R. *J. Phys. Chem.* **1992**, *96*, 5546. b) Hoffman, A. J.; Mills, G.; Yee, H.; Hoffmann, M. R. *J. Phys. Chem.* **1992**, *96*, 5540.

5. Markham, M. C.; Hannan, M. C.; Evans, S. W. *J. Am. Chem. Soc.* **1954**, *76*, 820.

6. Bahnemann, D. W.; Kormann, C.; Hoffmann, M. R. *J. Phys. Chem.* **1987**, *91*, 3789.

7. Aiken, G. R.; McKnight, D. M.; Wershaw, R. L., MacCarthy, P., Eds. "Humic Substances in Soil, Sediment, and Water," John Wiley and Sons: New York, **1985**, 550.

Chapter 8

Epilogue

In the preceding chapters, research was presented which demonstrates that semiconductors can efficiently photoinitiate a wide variety of chemical reactions, including polymerization of vinylic monomers, production of peroxides, oxidation of carboxylic acids, and formation of humic-like substances. Oxidation reactions caused by the valence band hole and reduction reactions caused by the conduction band electron occur simultaneously. At least one reactant species must be adsorbed at the semiconductor surface to act as a trap, so that the electron transfer to the adsorbate can compete with electron-hole recombination. The rates of reactions catalyzed by Q-sized semiconductors were found to be higher than those catalyzed by bulk-sized semiconductors. Quantum yields exhibited an inverse square root dependence on absorbed light intensity. Thus, increasing the light intensity increases the reaction rate and at the same time decreases the overall efficiency of the reaction.

The fundamental question which remains to be answered is what causes the Q-sized semiconductors to exhibit enhanced reactivity over their bulk-sized counterparts? Since results indicate that reactants are adsorbed prior to reaction, one explanation for the enhanced reactivity may lie in the larger surface areas of Q-sized semiconductors. With the exception of a BET analysis of a powder sample (1), measurements of the surface area of Q-sized semiconductors have not been performed. The surface area could be measured *in situ* via the change in the optical absorption spectrum of phenylfluorone upon binding to the metal oxide surface (2). Another explanation of the enhanced reactivity of Q-sized semiconductors may lie in their increased bandgap energy relative to bulk-sized semiconductors. For example, in the case of 40 Å diameter ZnO, the bandgap energy is 3.8 eV versus 3.4 eV for the bulk-sized ZnO. Assuming the increased bandgap energy translates into a 0.2 eV increase in the potential of the valence band hole, the change in rate of electron transfer with increased driving force can be calculated from the Marcus equation (3). Using a potential of 2.75 V at pH 7 for the valence band hole in the bulk

sized ZnO and a potential of 2.00 V at pH 7 for acetate and assuming other factors such as solvent reorganization energy are equal, gives the result that the rate of electron transfer is approximately 30% slower in the bulk-sized ZnO than in Q-sized ZnO. We observed reaction rates that were 100 to 1000 times slower in the bulk phase. Clearly, a better estimate of the oxidation potential of the valence band hole in Q-sized semiconductors is needed. The oxidation potential could be bracketed by reaction with a series of oxidants of known electrochemical potential; however, analysis will be complicated by the shifts in potential with surface speciation and with the changing density of charge carriers. Another explanation for the enhanced reactivity of Q-sized semiconductors may lie in an increased concentration of surface defects responsible for either specific adsorption of the substrate or decreased efficiency of electron-hole recombination due to trapping at surface sites. In the future, rf experiments may follow the decay of transients produced upon illumination and provide rate measurements of surface-trapping reactions (4).

Several other factors still need to be addressed with regard to the industrial application of Q-sized semiconductors to degrade organic pollutants. The first of these factors is the efficiency of UV-light generation. With high pressure zenon-arc lamps, the manufacturers' reported conversion efficiency of electricity to UV light ranges from 10-20% (5). In our experiments, with the addition of filters to select wavelengths between 330-370 nm, the efficiency drops to <1%. This low power conversion compares unfavorably with other methods of generation of OH· radicals such as sonolytic or pulsed-plasma discharge systems. However, when the source of UV light is "free" photons from the sun, semiconductor-assisted photodegradation can compete with the other methods. In our experiments, the incident light flux between 330 and 370 nm using the 1000W lamp is about 2.5 X 10^{15} photons cm^{-2} sec^{-1}. The incident flux of solar light reaching the surface depends upon the cloud cover, the season, and the azimuthal angle of the sun. A

typical value for light between 350 and 400 nm in midsummer at latitude 41° N is 5 X 10^{15} photons cm^{-2} sec^{-1} (6). Thus the light intensities used in the laboratory experiments are on the same order of magnitude as the solar light intensities.

Another serious issue which must be addressed in order for Q-sized semiconductor systems to become commercially viable is that of a catalyst support. Current methods of removal of the Q-sized semiconductor from the reaction mixture are either dissolution of the colloid by acidification to pH 1-3 or coagulation of the colloid at the pH_{zpc} followed by filtration. Neither of these methods are recommended in an industrial setting. Possible catalyst supports include glass beads, ceramics, activated carbon, and polymer films (7). The problem with glass beads or ceramics is that at the high temperatures used for sintering, the Q-sized semiconductors grow in size and change morphology. The disadvantage of activated carbon and polymer film supports is light absorption by the support. Also, in the case of polymer film supports, the OH· radicals which are generated upon illumination may oxidize the polymer instead of the pollutant. The use of perfluorinated polymers such as Nafion may avoid this complication. Q-sized semiconductors could also be synthesized in zeolites (which could also provide a method to control particle size) and then tethered to a glass surface using siloxanes.

Finally, research efforts to increase the efficiency of semiconductor assisted photodegradation are necessary. Currently quantum yields are on the order of 1-20%. Different reactor designs such as the thin film reactor (8) may improve mass transfer and light absorption and increase the efficiency. In addition, doping of the semiconductor to aid in electron/hole separation may increase the overall efficiency of the reaction (9). Preparation of mixed-type semiconductors (10) may increase light absorption further into the visible area; however, this occurs at the cost of reduced oxidizing power of the valence band hole.

The future of Q-sized semiconductor research looks promising. Q-sized semiconductors are interesting from several standpoints. Fundamentally, they represent the transition regime between molecular and bulk properties. Experimentally, their small size facilitates the accurate measurement of quantum yields and aids in the elucidation of reaction mechanisms by allowing optical detection of transient intermediates and energetic states. Commercially, their enhanced reactivity over bulk-sized semiconductors may increase their role in the development of practical photocatalytic systems that can be utilized for the degradation of organic pollutants in industrial and domestic applications.

References

1. Sclafani, A.; Palmisano, L; Schiavello, M. *J. Phys. Chem.* **1990**, *94*, 829.

2. Hoffman, A. J. *Research Proposition # 1*, California Institute of Technology, **1993**, 3.

3. a) Marcus, R. A. *J. Chem. Phys.* **1956**, *24*, 1966. b) Sutin, N. *Progr. Inorg. Chem.* **1983**, *30*, 441. c) Gerischer, H. *J. Phys. Chem.* **1991**, *95*, 1356.

4. Martin, S.; Hermann, H.; Hoffmann, M. R., personal communication, 1993.

5. Calvert, J. G.; Pitts, J. N. "Photochemistry," J. Wiley and Sons, Inc: New York, **1966**, 691.

6. a) Serpone, N.; Pelizzetti, E; Eds. "Photocatalysis," J. Wiley and Sons: New York, **1989**, 572. b) Calvert, J. G.; Pitts, J. N. "Photochemistry," J. Wiley and Sons, Inc: New York, **1966**, 722.

7. a) Serpone, N. *Solar Energy* **1986**, *14*, 121. b) O'Regan, B.; Gratzel, M.; Fitzmaurice, D. *J. Phys. Chem.* **1991**, *95*, 10525. c) Rosenberg, I.; Brock, J. R.; Heller, A. *J. Phys. Chem.* **1992**, *96*, 3423. d) Sabate, J.; Anderson, M. A.; Aguado, M. A.; Gimenez, J.; Cervera-March, S.; Hill, C. G. Jr. *J. Molec.Catal.* **1992**, *71*, 57. e) Smotkin, E. S.; Brown, R. M. Jr.; Rabenberg, L. K.; Salomon, K.; Bard, A. J.; Campion, A.; Fox, M. A.; Mallouk, T. E.; Webber, S. E.; White, J. M. *J. Phys. Chem.* **1990**, *94*, 7543.

8. Herron, N.; Wang, Y.; Eddy, M. M.; Stucky, G. D.; Cox, D. E.; Moller, K.; Bein, T. *J. Am. Chem. Soc.* **1989**, *111*, 530.

9. a) Kormann, C.; Bahnemann, D. W.; Hoffmann, M. R. *Env. Sci. Technol.* **1991**, *25*, 494. b) Mills, G.; Chew, B.; Hoffmann, M. R. submitted to *Env. Sci. Technol.*, **1993**.

10. Matthews, R. W. *J. Phys. Chem.* **1987**, *91*, 3328.

11. Pelizzetti, E.; Serpone, N., Eds. "Homogeneous and Heterogeneous Photocatalysis," D. Reidel Publishing Co.: Boston, **1986**, 275.

12. Spanhel, L.; Weller, H.; Henglein, A. *J. Am. Chem. Soc.* **1987**, *109*, 6632.